UCLouvain

AGRO LOUVAIN

Faculté des bioingénieurs

Transaminases immobilized on a membrane reactor for the production of chiral amines

Auteur : Basile Bredun

Promoteur : Prof. Damien Debecker (UCLouvain/IMCN/MOST)

Lecteurs : Prof. Patricia Luis Alconero (UCLouvain/IMMC)
Prof. Johan Wouters (UNamur/CBS/NISM/NARILIS)

Année académique 2024-2025

Mémoire de fin d'études présenté en vue de l'obtention du diplôme de Bioingénieur : Chimie et bio-industries

Acknowledgments

Tout d'abord, je souhaite exprimer ma profonde gratitude à mon promoteur, le Professeur Damien Debecker, pour la confiance qu'il m'a accordée et pour m'avoir intégré dans son équipe. Merci pour son accessibilité constante, son écoute attentive et le temps précieux qu'il a consacré à mon accompagnement tout au long de ce mémoire. Par son humilité en tant que professeur et surtout par son humanité, il a été le seul enseignant que j'aurais osé tutoyer. Même si ce travail n'était pas de la thermostatistique, j'ai bien failli me noyer dans tous ces flux… Heureusement, grâce à lui, j'ai pu garder la tête hors de l'eau. Merci à toi, Damien !

Je tiens ensuite à remercier sincèrement le Docteur Hippolyte Meersseman Arango de m'avoir formé et encadré durant les derniers mois de sa thèse. Son accompagnement et ses conseils, qu'il a continué à m'apporter même après la soutenance de sa propre thèse, ont été d'une grande valeur. Merci également pour ses révisions de mon manuscrit entre deux entretiens d'embauche. Si les transaminases n'ont aujourd'hui presque plus de secrets pour moi, c'est en grande partie grâce à lui. Un immense merci, Hippo !

Ma gratitude s'adresse également aux Professeurs Patricia Luis et Johan Wouters d'avoir accepté d'être les lecteurs de ce mémoire, qui, je l'espère, ne leur sera pas trop pénible à parcourir. Je remercie tout particulièrement Patricia de m'avoir permis d'accéder à ses laboratoires et de découvrir les joies du flux tangentiel. Que vos futures expériences « overnight » soient des plus fructueuses ! Je souhaite également remercier le Docteur Mar Garcia Alvarez, toujours disponible, pour son aide précieuse et sa supervision lors de l'installation des espaces.

Je tiens à remercier chaleureusement tous les membres du C3 pour leur accueil. Plus spécialement, je suis reconnaissant envers l'équipe de biocatalyse, pour leur expérience, leurs conseils avisés partagés lors de nos réunions, ainsi que leur bonne humeur inépuisable. Merci à vous deux, Aurélien et Marty ! Un grand merci à François, « The Best », qui m'a initié au langage des machines et à l'art du déchiffrage des mots de passe. Merci à Nathalie, souvent sollicitée pour mes incessantes commandes de seringues, ainsi qu'à Jean-Charles pour son aide précieuse (et ses outils) dans mes bricolages improbables. Enfin, un merci à tous les autres membres du C3 avec qui j'ai eu le plaisir de partager des moments festifs.

En dehors du laboratoire, je souhaite remercier mon ami et frère de cœur, Ismaël Peeters, pour nos conversations, qu'elles soient autour d'un café ou entre deux séances de fentes. Elles enrichissent ma vie et m'inspirent à repousser mes limites. J'espère que cette année n'est que le début d'une longue série ! Merci également à toi, Tom Baussart, d'être mon ami et de m'entraîner dans toutes ces aventures sportives qui me permettent de m'évader.

Enfin, mes remerciements vont à ma famille, particulièrement à mes parents et mes grands-parents, qui, en partageant leur expérience et leur sagesse, m'ont permis de devenir l'homme que je suis aujourd'hui. Sans eux, rien de tout ceci n'aurait été possible. Merci aussi à toi, Anatole, futur grand maître des échecs, d'être ce frère qui, sans même le savoir, me pousse à me dépasser. Enfin, un tout grand merci à toi, Alexandra Bredun, ma cousine, ma co-kotteuse et aussi mon chauffeur, sans qui mes retours épuisés de Louvain-la-Neuve auraient certainement été beaucoup plus pénibles.

Summary of the Master's Thesis

Compared to conventional chemical routes, biocatalysis appears to be a more sustainable approach for producing enantiopure chiral amines, essential components of active pharmaceutical ingredients (APIs). Enzymes, particularly transaminases (TAs), are attractive catalysts as they offer several promising pathways for the synthesis of chiral amines with excellent enantioselectivity under mild conditions. Asymmetric synthesis is especially relevant, enabling the production of chiral amines from keto precursors using inexpensive and readily available amino donors. However, challenges such as unfavorable reaction equilibria and poor enzyme stability still limit the development of this strategy into a truly productive industrial alternative. Thus, strategies are required to mitigate these two major issues. Among them, TA immobilization on membranes appears promising, as it can enhance enzyme stability while simultaneously allowing the membrane to act as a one-pot biocatalytic and separation unit—a powerful approach to address thermodynamic limitations. In particular, integrating such biocatalytic membranes with continuous flow processes has the potential to intensify the process and thereby improve chiral amine production. Continuous substrate feeding and product removal can further enhance enzymatic performance. In this context, this work aims to demonstrate the influence of flow process implementation on (i) biocatalytic membrane preparation, (ii) catalytic performance, and (iii) membrane robustness compared to a conventional batch reactor, as a first step toward more advanced processes involving membrane-based separations. Specifically, the effect of flow rate on membrane preparation and enzymatic performance was investigated.

Dead-end flow mode was employed to optimize biocatalytic membrane preparation via covalent immobilization on functionalized polypropylene membranes. Dead-end flow demonstrated improved TA immobilization compared to batch methods, particularly at lower flow rates. Following membrane preparation, asymmetric synthesis targeting the conversion of 2'-fluoroacetophenone (FAP) into (R)-fluoromethylbenzylamine (R-FMBA) using isopropylamine as the amino donor was evaluated under both dead-end and recirculating tangential-flow conditions. In dead-end mode, FMBA production was improved relative to batch when high enzyme loadings were immobilized. Catalytic tests under tangential flow showed similar performance to batch, confirming the relevance of this configuration for integration with membrane separation processes. Finally, the robustness of TA-immobilized membranes under both dead-end and tangential flow conditions was successfully demonstrated through leaching tests.

Building on these results, the successful implementation of flow processes paves the way for more sophisticated membrane–separator systems, which could further enhance chiral amine production.

Table of contents

List of acronyms

API - Active Pharmaceutical Ingredient

APTES - 3-AminoPropylTriEthoxySilane

AS - Asymmetric Synthesis

ATA - Amine TransAminase

BMBA - Bromo-α-MethylBenzylAmine

BMR - Biocatalytic Membrane Reactor

CLEA - Cross-Linked Enzyme Aggregate

CLEC - Cross-Linked Enzyme Crystal

CSTR - Continuous Stirred-Tank Reactor

DF - Dead-end Flow

DPPA - DiPhenylPropionic Acid

EDA – EthyleneDiAmine

ee - enantiomeric excesses

EMA - European Medicine Agency

EMR - Enzyme Membrane Reactor

EPC - Enzyme–Polyelectrolyte Complexe

FAP - 2'-FluoroAcetoPhenone

FDA - Food and Drug Administration

FMBA - (R)-2-Fluoro-α-MethylBenzylAmine

GDE - Glycidyl DiEther

GLU – GLUtaraldehyde

ISO – ISOpropylamine

KR - Kinetic Resolution

MF – MicroFiltration

MWCO - Molecular Weight Cut-Off

NF – NanoFiltration

PAH - PolyAllylamine Hydrochloride

PBR - Packed-Bed Reactor

PCADE - PolyCarvone Acrylate Di-Epoxide TA – TransAminase

PDA – PolyDopAmine

PDMS - PolyDimethylSiloxane

PE - PolyEthylene

PEI – PolyEthyleneImine

PFR - Plug Flow Reactor

PLP - PyridoxaL-5-Phosphate

PP - PolyPropylene

PVDF - PolyVinyliDene Fluoride

RO – Reverse Osmosis

RTA – R-selective TransAminase

STA – S-selective TransAminase

TA – TransAminase

TF - Tangential Flow

TsRTA – *Thermomyces stellatus* R-selective TransAminase

UF – UltraFiltration

α-TA - α-TransAminase

ω-TAs- ω-TransAminase

I. Introduction

I.1 Context

Since the dawn of time, humans have continually discovered, learned, and invented. Initially, these endeavors aimed solely at ensuring survival. However, this formidable force—human intelligence—quickly enabled humankind to achieve supremacy over other living species. The relentless pursuit of comfort and luxury reached its peak during the Industrial Age, when mass production and mass consumption became the norm. Despite the undeniable benefits of this period—particularly improvements in quality of life—this productivity-driven system has revealed its limitations. Decades of unrestrained production have generated an environmental debt, which continues to grow and now threatens the resilience of our planetary systems [1,2]. Only recently—on the scale of human existence—have we become aware of the magnitude of our activities' impact on the Earth [3], whose systems are now showing signs of distress [4]. These early warning signals have disrupted our self-centered perspective, revealing that the world of tomorrow must not only ensure human well-being but also safeguard the environment in which we live. If we are to maintain our current quality of life and secure a decent standard of living for future generations, it is imperative to rethink our production systems and mitigate their harmful environmental effects through more sustainable approaches.

The healthcare sector—and particularly the pharmaceutical industry—is no exception. The large-scale production of active pharmaceutical ingredients (APIs), essential building blocks of numerous therapeutic molecules, often relies on energy-intensive processes and hazardous reagents that are not environmentally sustainable, generating significant amounts of poorly valorized waste [5–8]. This is particularly critical in APIs manufacturing, which produces approximately 10 billion kilograms of waste annually [9]. While the concept of "production sobriety" may be viable in certain industries, slowing or reducing pharmaceutical output is not an option, given its critical role in safeguarding human health. In this context, the development of production processes that are both environmentally and economically sustainable is urgent and essential.

Among all pre-therapeutic molecules, chiral amine compounds are particularly important, as it is estimated that nearly half of all current APIs contain a chiral amine moiety in their structure [10,11]. Like other chiral chemicals, chiral amines remain challenging to produce due to their stereochemistry. These compounds are typically synthesized through chemo-catalytic processes [12–14] requiring organometallic catalysts—often containing heavy metals—and harsh reaction conditions such as toxic solvents and high temperatures [14,15]. In contrast, green chemistry approaches, particularly biocatalytic processes, offer a promising alternative for producing chiral amines more sustainably, by

minimizing waste generation, reducing energy consumption, and lowering the use of hazardous reagents [16,17].

Thanks to their exceptional diversity, enantioselectivity, and activity under mild operating conditions (e.g., aqueous media, low temperature), enzymes have emerged as a prominent focus of research for greener production of pharmaceutical molecules [18]. Among them, amine transaminases (ATAs)—a class of enantioselective enzymes—enable the direct synthesis of chiral amines from prochiral ketones using inexpensive and readily available amino donors (e.g., isopropylamine, amino acids) via transamination. As ATAs can significantly improve overall production efficiency, these enzymes have been intensively studied in recent years [19] and have already shown promising results for chiral amine synthesis at the pilot scale [20–22].

However, enzymatic processes—often constrained by thermodynamic limitations and typically applied in suboptimal configurations such as "free" enzymes in batch reactors—remain less productive and economically competitive than conventional chemical production methods [23]. Consequently, researchers are actively pursuing innovative approaches to enhance enzymatic performance and process viability. Significant progress has been made in enzyme immobilization, which improves stability, reusability, and operational control, and has been shown to enable intensified continuous-flow processes [24].

Among these possibilities, the implementation of ATA-immobilized membrane reactors under continuous-flow conditions appears particularly relevant for chiral amine synthesis. Such systems can function simultaneously as catalysts and separation units, potentially improving purification efficiency and reducing energy consumption—both critical in the pharmaceutical sector—while also addressing thermodynamic limitations inherent to transaminase-catalyzed reactions [25]. ATA-immobilized membrane reactors have been well studied in batch configurations [26–30], demonstrating promising results. For example, membrane-immobilized ATAs on functionalized polymeric surfaces have shown, in addition to good stability, activity improvements of up to 340% compared to the free form [30]. However, few studies have successfully implemented these systems under continuous-flow conditions [26], and substantial improvements are still required to achieve industrially relevant processes.

In the present work, a comprehensive state-of-the-art review will be conducted to demonstrate how enzymatic processes can provide an effective and sustainable solution for chiral amine production, with a particular focus on transaminase-based membrane reactor implementation in continuous-flow systems. In the second part, an experimental study will employ a recently discovered transaminase to investigate how flow processing can enhance both biocatalytic membrane preparation and enzymatic performance—two essential factors for increasing the efficiency of chiral amine production.

I.2 Chiral amine compound : Definition, Applications and Production strategies

I.2.1 Definition

Chiral amine compounds are defined as molecules which contain a nitrogen atom bonded to a stereogenic carbon atom Fig.I.1. These compounds correspond to all molecules characterized by α-chiral amine function, which can present two main features [31]:

- A nitrogen which can be either primary, secondary, tertiary and same quaternary
- An adjacent carbon which can be either secondary or tertiary.

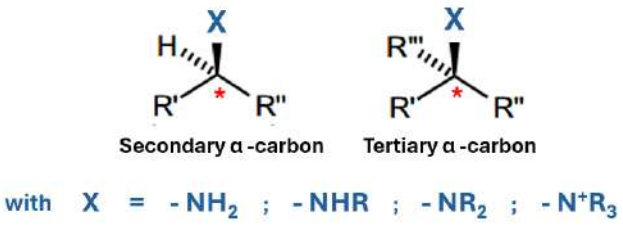

Fig.I.1 - General representation of different molecules corresponding to chiral amine compounds [31]

I.2.2 Applications

The chirality of amine compounds imparts unique and highly specific properties to molecules, enabling their application across several key sectors [31]. These sectors include the pharmaceutical industry, where amines serve as essential building blocks in drug synthesis, as well as the production of fine and agrochemicals, where amines act as intermediates in the manufacture of agents such as biocides [32,33]. Chiral amines are also valuable in designing chiral ligands and organo-catalysts, which play a crucial role in asymmetric catalysis for organic synthesis [34]. Given the pharmaceutical sector's prominent role in the application of chiral amines, this domain will be explored in greater depth in subsequent sections.

- **Pharmaceutical Industry**

Chiral compounds are of particular interest in the pharmaceutical industry as they are essential for synthesizing active pharmaceutical ingredients (APIs) [11,35]. Since humans and most living organisms are predominantly composed of chiral biomolecules (e.g. L-amino acids, excluding glycine, and D-carbohydrates), the stereochemistry of a drug is critical to its biological activity. Indeed, most therapeutically active compounds require a specific and well-defined stereochemistry in order to interact precisely with their biological targets, which are typically chiral proteins [36,37].

Currently, many marketed drugs are chiral, with a significant proportion (40–45%) containing a chiral amine moiety [10,11]. A significant number of pharmaceutical companies are actively pursuing the development and production of drugs containing chiral amines, owing to their crucial role in therapeutic applications. These compounds are employed both as preventive measures and as treatments for a wide range of medical conditions [31]. The chemical structures of some currently available compounds are illustrated in Fig.I.2. For instance, clopidogrel (Plavix®, Sanofi) is widely prescribed for the prevention of cardiovascular events, such as myocardial infarction. Furthermore, chiral amines are integral components of medications targeting various health issues, including nasal congestion (pseudoephedrine; Sinutab®, Johnson & Johnson), depression and mental disorders (sertraline; Zoloft®, Pfizer), type 2 diabetes (sitagliptin; Januvia®, Merck), and neurodegenerative diseases such as Alzheimer's and Parkinson's (rivastigmine; Exelon®, Novartis). The following examples represent a subset of the numerous therapeutic agents that are currently available on the market [24].

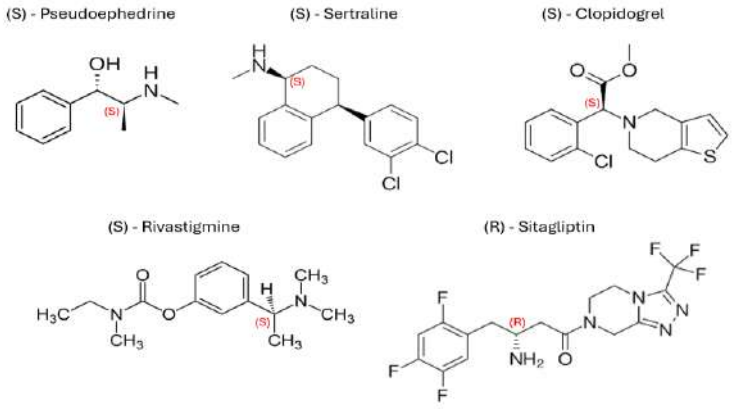

Fig.2 - Chemical structures of some currently available chiral amine compounds (from Wikipedia).

The significance of clearly defined drug stereochemistry, a factor which significantly influences pharmacokinetics and pharmacodynamics, has been demonstrated since the 1980s [38] and formally acknowledged by regulatory agencies such as the FDA and EMA [39]. In many cases, only one enantiomer (the eutomer) exhibits the desired pharmacological activity, while the other (the distomer) is less active or may even cause adverse effects [23]. Consequently, a substantial proportion of currently authorized pharmaceuticals are developed and marketed as single enantiomers [39].

Nevertheless, the synthesis and process design for enantiopure amines remains a major challenge. The synthesis of either the eutomer, necessitating enantioselective chemical methods, or a racemic mixture, necessitating resolution or deracemization, is required. These approaches are often costly and generate abundant waste [31]. Greener approaches are needed.

I.2.3 Production strategies

The enantiomeric purity of chiral amine compounds is critical for achieving the desired properties for specific applications. This represents a significant challenge in the development of production strategies, both for the synthesis process itself and for the isolation of the desired enantiomer from other compounds and unwanted by-products during the purification stages. In contemporary industrial practice, the predominant strategy for the large-scale production of chiral amine compounds involves the use of organometallic catalysts [31]. Nonetheless, there has been a growing interest in biocatalytic strategies that employ enzymes as catalysts over the past decade, with the aim of enhancing the sustainability of the process [18,40].

I.2.3.1 Conventional Chemical Routes

The conventional production strategy currently employed involves multistep processes featuring homogeneous organometallic catalysts. Two primary strategies can be identified: Asymmetric synthesis (AS) and Chiral resolution [24,31].

AS is the predominant method in the pharmaceutical sector. The hydrogenation of imines is typically achieved through the employment of enantioselective organometallic catalysts, which are based on transition metals such as ruthenium, rhodium, or iridium, in conjunction with chiral ligands [31,35]. In this approach, the amine compounds of interest are produced with a theoretical yield of 100% from either non-chiral or optically pure substrates. Indeed, several pharmaceutical compounds, such as S-Clopidogrel[41,42], R-Sitagliptin[43,44] and S-Rivastigmine [45,46], are synthesized using organometallic-catalyzed enantioselective hydrogenation. These processes have been shown to yield moderate to high (up to 95%) enantiomeric excesses (ee). Nevertheless, further downstream processes (e.g. preferential crystallizations, catalyst removal, chiral chromatography) are then required in order to obtain the isolated enantiopure product, which markedly increase the overall E-factor. In addition to using heavy metal-based catalysts, these routes often require pressurized hydrogen, chiral ligands, and, in certain instances, hazardous solvents [24].

In the context of chiral resolution, a racemic mixture of both enantiomers is initially produced. Through a series of purification steps, the undesired enantiomer is then eliminated, enabling a maximum theoretical yield of 50% [31,47]. A notable example is the synthesis of S-Sertraline, achieved by selective crystallization of a diastereomeric salt formed with a specific acid [48,49]. The second strategy, which is generally reserved for cases where no suitable enantioselective catalyst is available for direct asymmetric synthesis, is characterized by its limited theoretical yield and poor environmental performance associated with high solvent usage [24].

In conclusion, conventional chemo-catalytic processes are efficient ways to produce chiral amines compounds, but feature poor environmental performance (high E-factor)

owing to the large amounts of wastes (e.g. organic solvents, toxic organo-metallic catalysts, resolving agents) generated through such processes. Hence, the development of alternative greener routes to enantiopure amines is essential [24].

I.2.3.2 Alternative Biocatalytic Routes

Biocatalysis has emerged as a highly promising approach for the production of chiral amine compounds. Owing to the intrinsic chirality of biological systems, enzymes—nature's catalysts—demonstrate remarkable efficiency and selectivity in catalyzing these transformations. Specifically, they exhibit exceptional catalytic activity, with turnover rates ranging from 1 to 10,000 cycles per second [50], enabling the synthesis of chiral amines with outstanding enantioselectivity [51].

- **Types of enzymes and strategies**

A wide range of enzymes can be employed for the synthesis of chiral amine compounds, including transferases, oxidoreductases, hydrolases, lyases, and other classes [11,40,52,53] (Tab.I.S1 in Annex I.S). Depending on their biological origin and primary metabolic function, these enzymes require specific conditions and must be applied differently to achieve efficient chiral amine synthesis [31]. Indeed, not all promising enzymes for chiral amine production catalyze the same types of reactions (Tab.I.S1) and often exhibit restricted substrate affinity (towards highly specific substrates) [54]. Consequently, the implemented strategy can vary considerably depending on the type of enzyme used. It is generally accepted that three primary strategies may be employed in such cases: kinetic resolution (KR), asymmetric synthesis (AS), and deracemization [31]. A concise overview of each, along with their associated enzymes, can be found in Annex I.S1.

- **Form of biocatalyst used**

Regardless of the enzymes involved or the strategy employed, the biocatalysis approach can be implemented in three distinct ways: either with extracted enzymes directly exposed to the substrate in free or immobilized form, or as whole cells containing specific enzymes that function as catalysts [24]. In the case of whole cell use, the desired enzymes are naturally protected by the cytoplasmic membrane (and overexpressed in the cells). Nevertheless, it should be noted that there are certain limitations associated with the implementation of this strategy. The membrane has the capacity to restrict the transfer of substrate and product. Moreover, an additional requirement is necessary in order to maintain the viability of the cell, and the production of the desired product (i.e. the chiral compound) can be limited by competition with other metabolic pathways [55,56]. As cell-free enzymes are not constrained by these limitations (though other challenges may arise), they offer greater potential for enhancing the production of chiral amine compounds. The subsequent discussion will concentrate on cell-free extracts and their possibilities.

I.2.3.3 Advantages, Limitations and Perspectives of Different Strategies

It is evident that chemical and biocatalytic routes each exhibit distinct strengths and weaknesses. Tab.I.1 offers a visual representation of these disparities.

Tab.I.1 - Comparison of catalyst and process specificities of chemical and biocatalytic routes inspired from [24,31].

☐ *Strengths* ☐ *Weaknesses* ☐ *Neutral aspects*

	Aspect	Conventional Chemical Synthesis	Alternative Biocatalytic Synthesis
Catalyst specificities	**Catalyst type**	Homogeneous organometallic catalysts (heavy metals)	Enzymes
	Substrate scope	Broad (with optimized catalysts)	Often narrow (unless enzymes are) engineered
	Enantioselectivity	Variable, sometimes limited	Generally very high
	Stability and robustness	Good catalyst stability	Limited enzyme stability, sensitive to conditions
General process specificities	**Scalability and industrial use**	Well-established at industrial scale	Emerging, with promising advances flow processes, immobilization
	Reaction conditions	Harsh: organic solvents, high pressure, elevated temperatures	Mild: aqueous media, neutral pH, low temperatures
	Energy consumption	High due to purification and catalyst separation	Low simplified processes under mild conditions
	Process cost	High due to waste management, catalyst costs, purification	Potentially low though dependent on enzyme cost and stability
	Toxicity and environmental impact	High toxic metals and solvents, significant waste	Low biodegradable, non-toxic enzymes

The synthesis of chiral amines via conventional chemical methods, though well-established and robust, is not considered sustainable [24,54]. These processes often rely on toxic heavy-metal catalysts, hazardous solvents, and pressurized hydrogen, and may suffer from limited enantioselectivity, high waste generation, and energy-intensive purification steps [14,57]. Therefore, developing more sustainable approaches is crucial for greener chiral amine synthesis [16,58].

An implementation at industrial scale of the biocatalysis route might mitigate several of these issues and thus, improve the sustainability of the process [54]. In addition to their inherent enantioselectivity, enzymes offer several advantages over chemical routes relying on organometallic catalysts. Enzymatic processes typically require mild conditions: aqueous media, neutral pH, and low temperatures (in contrast to the elevated temperatures and organic solvents often required in conventional chemical strategies).

Furthermore, enzymes are biodegradable and significantly less toxic than organometallic catalysts [18,24]. Despite these sustainability advantages, it is imperative to acknowledge that biocatalytic synthesis of chiral amines faces several challenges [51,59]. Enzymes frequently exhibit low operational stability and a narrow substrate scope, particularly under industrial conditions. Industrially relevant biocatalytic reactions may also be thermodynamically limited, leading to low amine yields (unless specific equilibrium-shifting strategies are implemented). Additionally, substrate and product inhibition can further constrain reaction efficiency and process productivity, as they often require operating at lower substrate concentrations[10,59].

Nonetheless, innovative research has been undertaken to mitigate the weaknesses inherent in the biocatalytic approach, rendering this particular route of great interest. Advancements in the field of enzyme engineering [60,61], immobilization techniques [62,63], and the integration of continuous-flow processes [64,65] have had a significant impact on the performance of enzymes and have led to a considerable expansion in the range of applications of biocatalysis. Consequently, the advancement of this strategy appears to be particularly pertinent and promising for the future of chiral amine production.

I.3 Transaminase for Chiral Amine Production

Among the enzymes introduced in general biocatalysis, transaminases (TAs) are among the most promising catalysts for chiral amine synthesis. These enzymes use pyridoxal-5-phosphate (PLP) (derived from vitamin B6) (Fig.I.3 (b)) as a cofactor [66] and are able to catalyze the reversible transfer of an amino group from a donor to an acceptor molecule with high enantiospecificity, encompassing both (R)- and (S)-selective variants (RTAs and STAs) [21,31] (Fig.I.3 (a)).

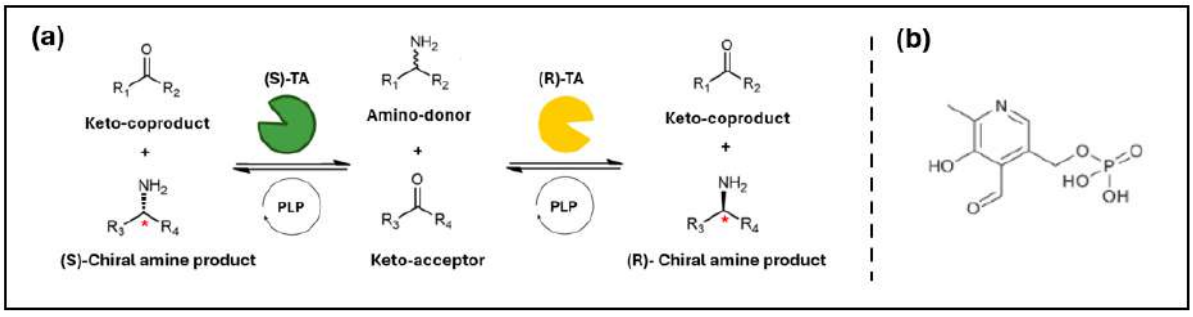

Fig.I.3 - (a) General representation of chiral amine synthesis via selective transaminase. (b) Pyridoxal 5'-phosphate (PLP), the cofactor of transaminase.

Primarily involved in amino compounds metabolism [21,67], TAs have been extensively studied, modified, and engineered over the past decade to improve their substrate tolerance and catalytic performance. Unlike many other biocatalytic reactions, the transamination cofactor PLP is continuously regenerated (and thus not consumed by the reaction), enhancing process sustainability and efficiency. Additionally, the absence of a need for protecting groups enables faster production and reduces chemical waste [68].

Owing to these advantages, TAs hold significant potential for the industrial production of chiral amines.

I.3.1 Description and Classification of Transaminases

These PLP-dependent enzymes can be classified into two main groups: α-transaminases (α-TAs) and ω-transaminases (ω-TAs). α-TAs catalyze the transfer of amino groups exclusively between α-amino and α-keto acids. In contrast, ω-TAs do not require the presence of an α-carbon, offering a broader scope of substrates for chiral amine synthesis. Among ω-TAs, amine transaminases (ATAs) are considered particularly relevant for industrial applications, as they can accept both ketones and aldehydes as substrates, thereby expanding their applicability beyond that of classical α- and ω-TAs [21,69].

Due to their promising industrial relevance, significant advances have been made in ATA research in recent years, including the discovery and characterization of enzymes and the development of transamination processes [68]. However, in accordance with the objectives of this thesis, the focus will be set on general reaction improvements and process implementation strategies rather than detailed enzymological aspects, which are discussed in Annex I.S2.

I.3.2 Reaction Strategies for Chiral Amine Synthesis

For chiral amine production using ω-TAs, three main reactional strategies with each its own strengths and weaknesses Tab.I.2 can be employed: Kinetic resolution (**KR**), Asymmetric synthesis (**AS**) and deracemization [69,70] (Fig.I.4).

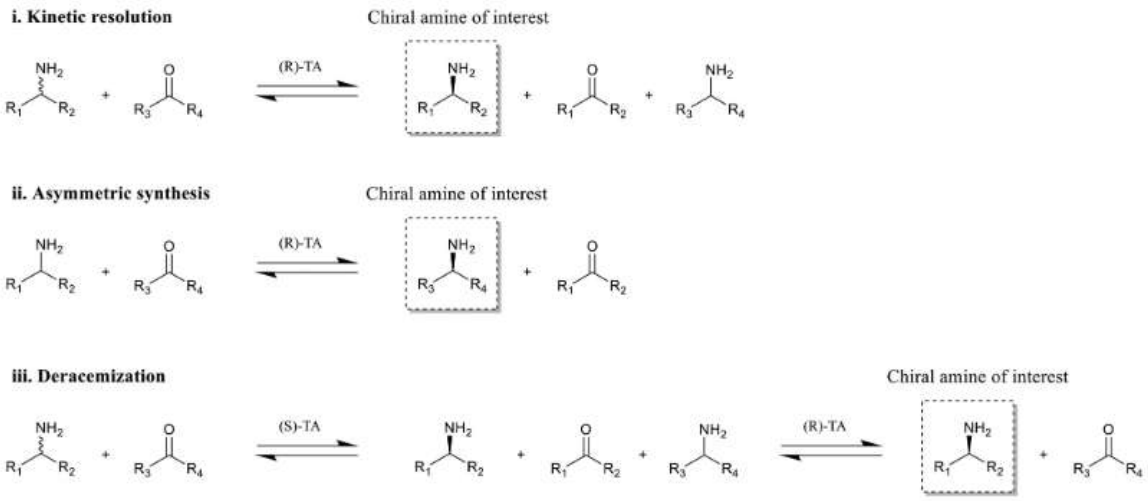

Fig.I.4 - Reactions catalyzed by transaminases for the production of chiral amines. (i), (ii) and (iii) respectively represent kinetic resolution, asymmetric synthesis and deracemization reactions. From Meersseman et al. [24].

In KR, a racemic amine mixture undergoes selective enzymatic transformation in which only one enantiomer is converted to the corresponding ketone, while the other remains unreacted. KR thus aims to remove the undesired enantiomer, enabling recovery of the unreacted chiral amine that retains the original structure of the racemic mixture (R1and R2 in Fig.I.4 (i). Despite its simplicity and the use of a single enzyme, this approach is limited to a maximum theoretical yield of 50% and is often hindered by ketone accumulation, which can inhibit enzymatic activity [68,69].

In contrast, AS converts a prochiral ketone into a single chiral amine using an amino donor, with a ketone by-product formed in the process. Unlike KR, the target chiral amine is the product of the reaction and features a new chemical structure derived from the ketone precursor (R3 and R4 in Fig.I.4 (ii)). This method can theoretically achieve yields of up to 100% if the enzyme exhibits high enantioselectivity and the thermodynamic equilibrium favors amine formation. However, challenges such as unfavorable thermodynamics and product inhibition by ketones often complicate the synthesis of non-natural amines[69,71].

It is possible to understand this thermodynamic challenge starting from the reaction naturally occurring in the living world (Fig.I.5). Natural transamination between α-amino acids and α-keto acids are typically thermodynamically balanced due to the similar free energies of the substrates and products (Fig.I.5 (a)). In contrast, simple amines are less stable than amino acids, while ketones are more stable than α-keto acids, resulting in an equilibrium shift toward ketone formation [68] (Fig.I.5 (b)). To favor chiral amine formation, α-amino acids can be replaced with less stable amino donors such as isopropylamine (ISO) (Fig.I.5 (c)). However, even in this case, the equilibrium remains significantly tilted toward the reactants, making the implementation of additional mitigation strategies necessary.

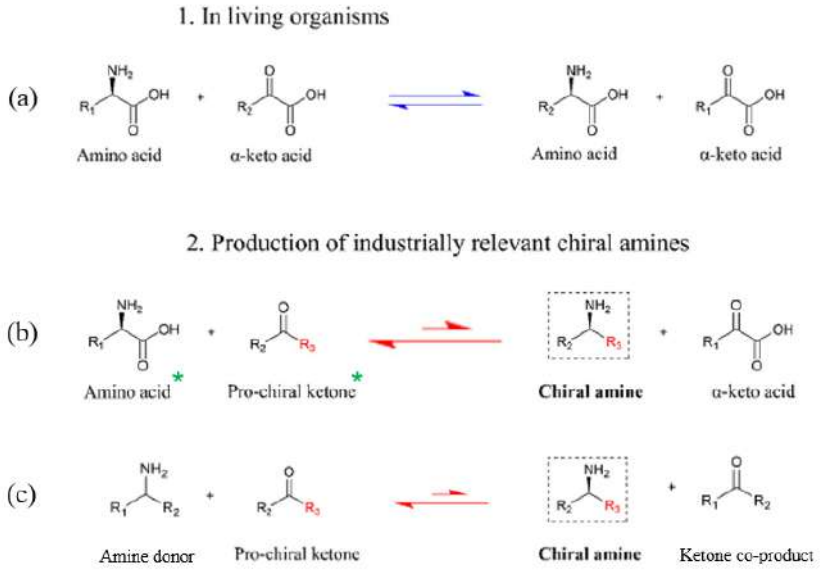

Fig.I.5 - Transaminase for the production of chiral amines. 1.(a) Transamination in living organism involving amino acid and α-keto acid is well-balanced. 2. Transamination used in chemical and pharmaceutical industry using a prochiral

*ketone as amino receptor. (b) Use of amino acid as amino donor is strongly unfavorable. * indicate most stable compounds. (c) Use of amine as amino donor is less unfavorable. Figure adapted from Meersseman et al. [24].*

Unlike the previous strategies, which rely on a single enzyme, deracemization employs two transaminases[1]. This approach integrates an initial KR step followed by an AS catalyzed by a second enzyme of opposite selectivity[2] (Fig.I.4). Theoretically, it allows full conversion (100%) to a single enantiomer without ketone accumulation. However, it remains subject to thermodynamic limitations in the second step [72,73].

Tab.I.2 - Main advantages and disadvantages of different reactional strategies involving transaminase for chiral amine production

Strategy	Advantages	Disadvantages
Kinetic Resolution	Simple to implement Requires only one enantioselective enzyme	Maximum yield limited to 50% Accumulation of inhibitory ketone by-products
Asymmetric Synthesis	Theoretically up to 100% yield Direct production of a single enantiomer	Ketone by-product inhibition Thermodynamically unfavorable for non-amino acid amines
Deracemization	Theoretically 100% yield No ketone accumulation if α-keto acid used	Requires two complementary transaminases Still suffers from unfavorable thermodynamics

While KR remains valuable for specific industrial cases where racemic substrates are readily available or when process constraints hinder AS, AS is generally the preferred strategy due to its potential for 100% theoretical yield and the avoidance of unreacted enantiomers, simplifying downstream processing and improving overall efficiency [31]. Nonetheless, AS remains constrained by thermodynamic limitations [68,69], and various strategies must be employed to overcome these barriers. These approaches will be discussed in detail in the following section.

I.4 Mitigation Strategies and Process Intensification for Chiral Amine Production via Transaminases

Despite the considerable potential of biocatalysis for the production of chiral amines, several challenges persist [74], primarily from the limited stability and robustness of enzymes, unfavorable thermodynamic equilibria, substrate and co-product inhibition, as well as difficulties associated with process scale-up. Consequently, a detailed investigation into the strategies aimed at overcoming these constraints is crucial, along

[1] Other deracemization strategies are possible, but in the context of this study, a focus will be placed on processes involving only TAs.
[2] Other types of deracemization strategies not necessarily involving enzymes with different selectivities are also possible, although less effective.

with the optimization of the overall biocatalytic process to meet the demands of industrial applications.

I.4.1 Industrial Relevance

Thanks to various mitigation strategies, the use of transaminases—particularly in asymmetric synthesis—has become a viable and promising approach for the production of chiral amine compounds. Several applications have already been implemented at scales ranging from a few grams to hundreds of kilograms for the synthesis of APIs or key intermediates, including sitagliptin (antidiabetic), suvorexant (sleep aid), and ivabradine (heart rate regulator) (Tab.I.S3). Because the types of transaminases, substrates, and targeted reactions vary significantly across applications, the associated processes differ significantly. A detailed description of each specific process (summarized in Tab.I.S3) is beyond the scope of this discussion. Instead, general trends across these applications are highlighted here.

Common operational features include the use of soluble engineered ω-TAs in batch mode to maintain simplicity and reduce production costs [75]. Reactions are typically carried out at moderate temperatures (30–60 °C), with co-solvents employed as needed to improve substrate solubility. To overcome unfavorable thermodynamic equilibria, large excesses of amino donors (typically, ISO) are frequently used, often in conjunction with in situ removal of inhibitory ketone by-products (e.g. acetone) through evaporation or biphasic extraction.

Although production volumes remain modest, the processes consistently exhibit excellent enantioselectivity, often exceeding 99% ee. Among these, several have reached pilot-scale implementation, most notably Merck's sitagliptin process, which achieved a concentration of 250 g/L [75,76].

I.4.2 General Strategies for Process Improvement

The following subsection briefly presents the general mitigation strategies that can be used to enhance catalytic performance and make biocatalytic processes viable at an industrial scale.

I.4.2.1 Enzyme-Related Improvements

The intrinsic properties of enzymes, specifically transaminase, can be enhanced through protein engineering [60,77]. Advances in directed evolution [78,79], site-specific mutagenesis [20,80], and the expression of enzymes from extremophilic organisms [81–84] have led to biocatalysts better suited for industrial applications. In addition to demonstrate an increased working, storage duration and demonstrating a broader substrate scope, these engineered enzymes can exhibit greater stability under non-physiological conditions,

including enhanced tolerance to organic solvents—used to process-related improvements—and to high concentrations of inhibitory substrates or products [68,77].

I.4.2.2 Process-Related Improvements

While protein engineering has been demonstrated to enhance the robustness of enzymes, the successful overcoming of thermodynamic barriers typically requires the implementation of additional physicochemical strategies. Typically, reaction equilibria are shifted by either using an excess of substrate or by selectively removing products through chemical, biocatalytic, or physical methods [24,85,86].

Although the selective removal of products is generally preferred [60,87] (owing to the enzyme's susceptibility to substrate inhibition), inhibition can also be mitigated through controlled substrate delivery methods, such as semi-flow operation (e.g., fed-batch), the use of organic co-solvents [88], or enzymatic substrate release [86]. Product removal strategies encompass a wide range of methodologies, including physical methods such as evaporation, liquid-liquid or liquid-solid extraction, etc. [89]; biochemical methods like selective crystallization [30,90] or multi-enzymatic cascades [86,87]; and spontaneous transformations such as auto-conversion, degradation, or intramolecular cyclization of co-products [91,92]. Some examples of cited strategies applied to transaminase are listed Tab.I.3.

Tab.I.3 - Non exhaustive list of different process-related mitigations strategies used to solve thermodynamic constraints. Adapted from Meersseman et al. [24].

Equilibrium Shifting Method	Transaminase Type	Substrates and Products	Comment	Efficiency / Improvement	Ref.
Substrate-related strategies					
Fed-batch feeding of amino donor (MBA or IPA)	ω-TA from Chromobacterium violaceum (whole cell)	GA or PA + HPA → ABT or APD (MBA or IPA; acetophenone or acetone)	Controlled substrate feeding to avoid inhibition and evaporation of coproduct to prevent toxicity and shift equilibrium	Up to 70% yield (IPA), 62% (MBA); up to 6× higher than two-step batch	93
Excess of amino donor (IPA)	ATA-103 (S) ATA-117 (R)	Acetophenone → (S)- or (R)-MBA (L-/D-alanine; pyruvate)	In addition of IPA excess, use of LDH/GDH cascade to remove pyruvate co-product for relieving inhibition and shifts equilibrium	95% conversion, >99% ee	94
(co-)Product-related strategies					
Spontaneous Evaporation of co-product (acetone)	ARmutTA (R-selective) or OATA (S-selective	2-oxobutyric acid → L-homoalanine (IPA; acetone)	Acetone (co-product) is removed by evaporation to drive the reaction forward	Effective product formation	95

L-L extraction of co-product (acetophenone)	ω-TA from *Vibrio fluvialis* (free or in whole cell)	Ketone 1 → (S)-1-(5-fluoropyrimidin-2-yl)ethylamine(MBA; acetophenone)	Use of toluene as organic co-solvent to extract acetophenone from aqueous phase for enhancing conversion	77% yield, 99.8% ee (free enzyme); 66% yield, 97.3% ee (whole cell)	96
Extraction of ketone co-product (L-alanine)	ω-TA from *Vibrio fluvialis* JS17 (whole-cell, immobilized)	(S)-α-MBA → Acetophenone (pyruvate; L-alanine)	Use of Isooctane membrane contactor to continuously remove inhibitory ketone for improving conversion	Enhanced rate and yield, High stability	97
Coupled α-/ω-TA with alanine/pyruvate shuttle (in whole cell)	α- and ω-TA (engineered co-expression)	3-methyl-2-oxobutyric acid + rac-MBA → (S)-valine + (R)-MBA(internal shuttle)	Alanine and pyruvate shuttling system drives ω-TA reaction by coupling with α-TA for simultaneous production	73–90% (S)-amino acid, 83–99% ee (R)-amine	98
In situ product crystallization with acetone evaporation	ω-ATA from *Silicibacter pomeroyi*	3MAP→ (S)-3MPEA (IPA-3DPPA; acetone)	Crystallization of salts (Continuous addition of ketone receptor and removal of amine product as a salt)combined with co-product (acetone) evaporation	High yield and purity Up to 1.27 M product salt (48 wt%); 85–96% yield; ee >99%	90,99
In situ product crystallization	*Thermomyces* stellatus (TsRTA)	FAP → (R)-FMBA (ISO; acetone)	Crystallization of FMBA product	Conversion improved from 44% to ~80%	30
Spontaneous transformation (tautomerization and polymerization of by-product)	ATA-113	Aryl- or cyclic ketones → Chiral amines (OXD; isoindole)	Polymerization of by-product (isoindole) drives equilibrium	>99% conversion for most ketones; 73% for 1-indanone; >99% ee in most cases	100
Use of LDH/GDH cascade to remove pyruvate	ATA-103 (S) / ATA-117 (R)	Acetophenone → (S)- or (R)-MBA (L-/D-alanine; pyruvate)	An excess of IPA is used in addition to pyruvate removal relieves inhibition and shifts equilibrium	95% conversion, >99% ee	94

ABT = 2-amino-1,3,4-butanetriol; APD = 2-aminopentane-1,3-diol; GDH = Glucose dehydrogenase; GA = Glycolaldehyde; HPA = Hydroxypyruvate; IPA = Isopropylamine; LDH = Lactate dehydrogenase
MBA = (S)-α-methylbenzylamine; OXD = Ortho-xylylenediamine; PA = Propionaldehyde; 3MAP = 3-methoxyacetophenone; 3MPEA = (S)-3-methoxyphenylethylamine; 3DPPA = 3,3-diphenylpropionic acid; ISO = Isopropylamine, FAP = 2'-fluoroacetophenone ; FMBA = (R)-2fluoro-α-methylbenzylamine

Despite these promising results, further advancements are required for asymmetric transamination to become a viable alternative to conventional chemical route. Notably, the lack of biocatalyst recyclability, along with limited enzyme robustness, hinders the industrial viability of such processes. Beyond enzyme engineering and thermodynamic optimization, heterogeneous biocatalysis offers promising avenues for addressing key limitations observed with free enzymes, particularly through the immobilization of transaminases on or within solid supports.

Compared to traditional homogeneous systems, enzyme immobilization introduces a wide range of possibilities that warrant deeper investigation. In particular, the integration of immobilized transaminases into continuous flow systems has attracted growing

interest for industrial applications. The following section will focus on the use of heterogeneous flow biocatalysis for the synthesis of chiral amine compounds.

I.5 Enzyme Immobilization for Flow Processes: Towards the Intensified Production of Chiral Amines

Homogeneous biocatalysis has been extensively studied for its efficiency under mild conditions and its high chemo-, regio-, and stereoselectivity. However, the direct use of free enzymes in solution presents significant limitations. Free enzymes are highly sensitive to non-physiological environments, often exhibiting rapid loss of activity in response to temperature or pH fluctuations, or the presence of organic solvents. Additionally, the recovery of enzymes and cofactors (which are often expensive) from the reaction medium remains difficult, hindering their reuse and ultimately increasing overall process costs and E-factor [101–104]. Furthermore, the use of free enzymes is predominantly constrained to batch processes, which impose significant limitations. Despite their operational simplicity, batch systems frequently exhibit limitations in scalability, exhibit limited mass transfer and control over critical parameters such as temperature and pH, which can result in variability in product quality. Moreover, safety concerns emerge from the handling of large amounts of reactive materials, and overall efficiency is reduced due to downtime between cycles for cleaning and setup [105,106].

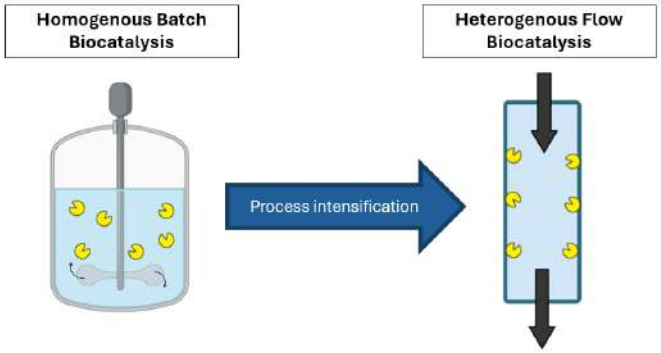

Fig.I.6 - Process intensification from heterogenous batch biocatalysis to heterogenous flow biocatalysis system

These limitations significantly restrict the industrial applicability of batch-based homogeneous biocatalysis, particularly where stability and cost-efficiency are crucial. In contrast, heterogeneous flow biocatalysis, combining enzyme immobilization with continuous processing, offers a robust and scalable alternative for process intensification (Fig.I.6) [106–108].

A focused evaluation of immobilization strategies and flow technologies is therefore essential to fully exploit biocatalysis for the selective and sustainable synthesis of chiral amines.

I.5.1 Enzymes Immobilization

I.5.1.1 Opportunities and Challenges of Enzyme Immobilization

Immobilized enzymes can present interesting opportunities compared to the free form. It has been often demonstrated that the immobilization of enzymes on solid supports has a significant impact on structural and functional stability [63,109]. Immobilization can increase the enzyme's resistance towards denaturation by restricting excessive conformational flexibility. In the case of multimeric enzymes, immobilization can prevent subunit dissociation. This structural stabilization results in a more resilient catalyst capable of operating under harsher process conditions – especially useful if organic co-solvents are employed [101,110]. Furthermore, it has been documented that certain immobilized enzymes can, under certain circumstances, demonstrate increased catalytic activity, along with enhanced specificity and selectivity, as a consequence of the establishment of a favorable microenvironment at the support interface [29,110]. Beyond potential intrinsic enzyme properties improvement, immobilization offers key advantages at the process engineering level. By confining enzymes to a fixed location, recovery and reuse become feasible—an important factor for high-cost biocatalysts [102,103,111]. Physical separation of the enzyme from the product stream simplifies purification, reduces contamination, and enhances process robustness and economic efficiency [106,107,112]. Additionally, strategies such as cofactor immobilization and co-immobilization with other catalysts are being explored to further intensify heterogeneous biocatalysis [113–116].

However, enzyme immobilization is not without challenges. The success of an immobilized biocatalyst is highly dependent on both the intrinsic properties of the enzyme and the selected immobilization strategy. The immobilization sometimes results in partial or complete loss of stability or catalytic activity, due to steric hindrance, conformational restriction, or improper orientation of the enzyme on the support surface [63]. Additionally, leaching of the enzyme from the support can compromise process performance and increase downstream purification burden [102]. Mass transfer limitations represent another frequent drawback, especially in systems employing porous carriers, where substrate diffusion to the enzyme's active site may be hindered [112,117]. Furthermore, the choice and preparation of solid supports introduce complexity in reactor design and scale-up, potentially increasing cost and reducing overall sustainability [106].

Although these challenges exist, the potential process enhancements make heterogeneous biocatalysis an increasingly attractive option for modern chemical manufacturing, especially in the pharmaceutical industry, where controlled, scalable, and efficient processes are critical [118–121]. So, a brief focus on different immobilization strategies which can be apply to transaminase.

I.5.1.2 Main Types of Enzyme Immobilization Techniques

Two main approaches exist for enzyme immobilization: whole-cell systems and isolated (purified) enzymes [107,109,122]. While whole-cell systems present limitations (Section I.2.3.2), purified enzymes offer higher specificity, faster kinetics, and simplified downstream processing [123]. Despite the cost of enzyme purification and potential stability issues outside the cell, their compatibility with immobilization and enhanced process control make them preferable for industrial applications [107,122]. This subsection focuses exclusively on the immobilization of purified enzymes and their use in flow processes.

In the context of immobilizing purified enzymes, three predominant strategies have been identified Fig.I.7: surface binding to a carrier, entrapment within a matrix or gel, and carrier-free cross-linking of enzymes (e.g., CLEAs or CLECs)[3] [63,101,111,124,125]. Each method exhibits distinct advantages and limitations (Annex I.S4), contingent on the support type, process conditions, and the targeted improvements (stability, activity, specificity or selectivity) [62,63].

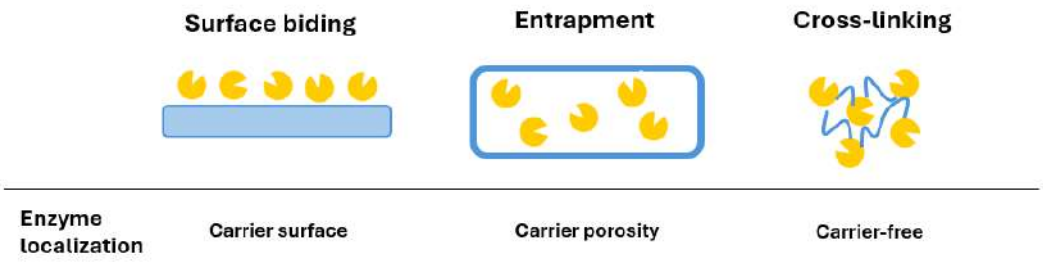

Fig.I.7 - General immobilization strategies

The binding of enzymes to surface carriers, which may be natural polymers, synthetic materials, or composites, represents the most well-established technique. The immobilization can involve different type interactions such as adsorption, affinity-based, or covalent interactions. The nature of biding exerts generally a significant influence on performance and must be meticulously adapted to suit the specific application [101,126]. For example, covalent grafting can be a relevant immobilization strategy as it enables strong interactions that limit enzyme leaching—which is especially advantageous when coupling immobilized enzymes with flow processes [107]. However, this strategy can also lead to over-rigidification, reducing the catalytic performance of the enzyme [127]. More detailed comments about the different binding strategies are given in Annex I.S4, and some relevant binding strategies, particularly when immobilized enzymes are used in continuous flow processes, are also presented in Section I.5.2.3.

[3] CLEAs = Cross-Linked Enzyme Aggregates and CLECs = Cross-Linked Enzyme Crystals. CLEAs are formed by precipitating enzyme molecules into physical aggregates followed by chemical cross-linking, while CLECs involve crystallizing the enzyme prior to cross-linking [111]

In contrast, entrapment involves the confinement of enzymes within porous structures. This strategy is generally easier to implement compared to surface biding immobilization and enables an stabilization of the enzyme thanks to protected microenvironment. However, diffusional limitations of substrate can occur, and enzyme leaching is frequently observed. Concerning cross-linking strategy, it involves direct covalent bonding between enzymes, thereby eliminating the need for external supports [63,101].

Although these strategies are presented separately, the implementation of different immobilization approaches can be used simultaneously to mitigate the adverse effects of individual factors, such as leaching or instability [63].

I.5.1.3 Practical Examples in the Specific Case of TA

Since each immobilization process depends on a specific combination of enzyme, support, and operational conditions, a wide range of strategies has been explored in the literature. A comprehensive review of all immobilization approaches involving TAs would be out of the scope. Therefore, Tab.I.4 presents a representative example for each of the main immobilization strategies previously described. All selected studies report at least one improvement in enzymatic performance, highlighting the broad potential of enzyme immobilization for enhancing catalytic efficiency and process robustness. Other relevant immobilization techniques, particularly those investigated in combination with flow processes, are presented in Section I.5.2.3.

Tab.I.4 -- Non-exhaustive immobilization strategies applied to transaminase with its benefits adapted from Meersseman et al. [24].

Immobilization Strategy	Support/Carrier	Enzyme and type of reaction catalysed	Benefits Observed on TAs	Ref.
Biding to carrier surface				
Covalent biding	Chitosan beads + glutaraldehyde	ω-TA s (kinetic resolution)	Enhanced thermal stability; improved activity after heat treatment	128–130
Adsorption (Hydrophobic intercations)	Hydrophobized silica (Sepabeads® octadecyl-grafted resin)	ATA-117-11Rd (asymmetric synthesis)	Retained activity in organic medium and at high temperature (60°C)	131
Affinity biding (His-tag)	Glass metal-derivatized carriers	ω-TA (kinetic resolution)	Retained activity in organic solvent and at 50 °C	132
Entrapment				
Entrapment	Sol–gel matrix with celite	ω-TA (kinetic resolution and deracemization)	Maintained activity at pH 11; stable over 5 cycles; >99% enantioselectivity	133,134
Cross-linking				
CLEAs	(No support) aggregation with glutaraldehyde	Glutamic transaminases	/	135

I.5.2 Flow Processes

I.5.2.1 Opportunities and Challenges of Flow Processes

The integration of enzymes into continuous flow systems also offers clear benefits over batch processes [65,107,136]. Flow reactors provide improved control over key parameters (e.g., temperature, pressure, residence time) due to their high surface-to-volume ratios [106], enhancing reaction efficiency, safety, and reproducibility [107,108,122,136]. Continuous substrate supply and immediate product physical removal (or direct consumption) can reduce equilibrium constraints and help overcoming product inhibition issues, thereby enhancing conversion and space-time yield. In addition to potential productivity enhancement, continuous operations also enable easier scale-up and simplified downstream processing, making large-scale production more economically viable [107,108,122].

However, the implementation of continuous flow systems also presents challenges. Enzymes may suffer from progressive deactivation due to shear forces, mechanical stress, or prolonged exposure to non-optimal temperatures during extended reaction times [123]. Flow processes can also limit substrate accessibility to the active site of the enzymes—mass transfer limitations [137]—and enhance enzyme leaching when enzymes are immobilized [122]. These factors, in the absence of stabilization strategies, can result in declining activity and, consequently, reduced productivity.

I.5.2.2 Main Types of Flow Reactors with Immobilized Enzymes

Flow biocatalysis is characterized by its exceptional flexibility, which arises from the wide range of possible reactor configurations and operational modes. This versatility enables its application across diverse synthetic challenges, from early-stage development to industrial-scale production of APIs and fine chemicals [107,121]. Various reactor types have been successfully implemented in continuous biocatalytic processes, each presenting distinct advantages depending on the scale of operation (microfluidic to production scale), the physical state of the biocatalyst (free or immobilized), and the physicochemical properties of the reaction system (Tab.I.S5).

At the laboratory scale, recent trends favor the use of microreactors and mesoreactors (Fig.I.8 (a)), which offer significant benefits such as precise control over residence time, temperature, and mass transfer due to their high surface-area-to-volume ratios. These reactors typically require minimal equipment and are particularly valuable for rapid reaction screening and early-phase optimization [106,123].

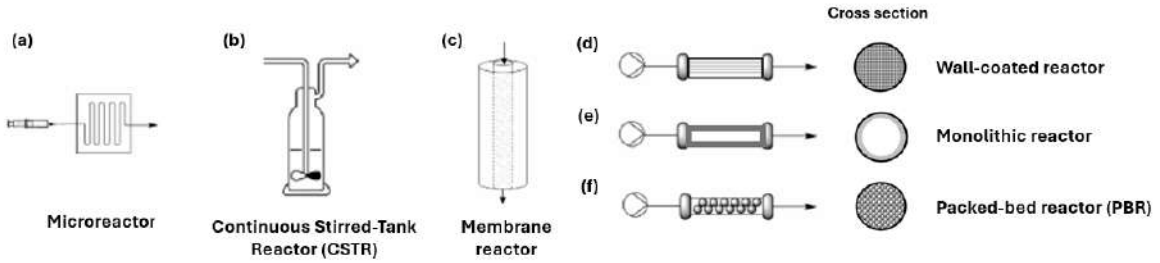

Fig.I.8 - Main types of flow reactors used in biocatalysis. (a) Microreactor (b) Continuous Stirred-Tank Reactor (CSTR) (c) Membrane reactor (d) Wall-coated reactor (e) Monolithic reactor (f) Packed-bed reactor (PBR). Adapted from [136]

For larger-scale applications (from bench to pilot or industrial scale), a broader array of reactor designs can be employed. Continuous Stirred-Tank Reactors (CSTRs) (Fig.I.8 (b)) provide homogeneous mixing and are adaptable to both free and whole-cell biocatalysis. This type of reactor is generally used as first preliminary reactor to test immobilized enzymes on specific support (beads, membranes,...). More sophisticated systems, such as Plug Flow Reactors (PFRs) adapted with specialized features—including membrane reactors (Fig.I.8 (c)) and tube-in-tube systems—enable enhanced process control, including gas-liquid handling and in situ separation [65,107]. Among reactors specifically suited for immobilized enzymes, Packed-Bed Reactors (PBRs) (Fig.I.8 (f)) are widely adopted due to their ability to support high catalyst loadings, offering excellent space-time yields and operational stability [108,121]. Wall-coated and monolithic reactors (Fig.I.8 (d) and (e)) can be employed to reduce mass transfer limitations by allowing intimate contact between substrate and the immobilized enzyme surface, while membrane reactors (Fig.I.8 (c)) facilitate simultaneous reaction and selective separation [65,123]. A detailed table with the main strengths and weaknesses of different reactors types are presented in Tab.I.S5.

Independent of reactor type, flow biocatalysis also benefits from multiphase system integration, wherein liquid–liquid or gas–liquid phases are introduced either in parallel or segmented (slug) flow configurations. These dynamic flow modes enable efficient mass transfer across phase boundaries, facilitate the use of immiscible substrates, and allow for in situ product removal, which in turn reduces enzyme inhibition and simplifies downstream processing [107,108].

I.5.2.3 Practical Examples in the Specific Case of TA

A mentioned in Section I.5.1.1 and I.5.2.1, enzyme immobilization and the implementation of continuous flow processes present each their respective challenges. To offer a synergistic solution to these individual limitations, heterogeneous flow biocatalysis—which combines enzyme immobilization with continuous flow processing—appears relevant. Indeed, the convergence of these two strategies can generate highly efficient and robust biocatalytic systems. In fact, the strategic coupling of these technologies is at the core of modern process intensification efforts in pharmaceutical production including chiral amine compounds [24,65,121]. While flow

processes can also be used with cell-free enzymes, the following section therefore focuses only on strategies and applications involving immobilized TAs in flow reactors.

Several immobilized TAs have been used in continuous flow systems to improve the production of chiral amines. Tab.I.S6 presents some of these applications. Since many different reaction processes (e.g., KR, AS, deracemization) and mitigation strategies (e.g., biphasic systems) have been investigated, a detailed description of all processes would be excessive and outside the scope of this paper. However, commenting briefly on the most current or promising strategies, with a particular emphasis on enzyme immobilization techniques and reactor configurations, seems relevant.

Among the variety of purified TAs immobilizations reported, affinity and covalent bindings on either porous glass-based materials or functionalized polymeric resins emerge as dominant strategies compared to adsorption strategies (electrostatic or hydrophobic interactions), which are more susceptible to leaching (Annex I.S4). Classical affinity-based immobilization uses His-tagged TAs on metal-chelated carriers (e.g., EziG™—a commercially available material based on controlled porosity). This technique is widely adopted because its dual role in purification and immobilization, offering control over the orientation and microenvironment of TAs [138–140] (Annex I.S4). Because they ensure strong binding, covalent grafting methods have also been widely investigated. Most of these methods use epoxy-activated resins (e.g., Sepabeads®—commercially available resins typically composed of methacrylate or polyacrylic matrices) [127,141,142] or other glutaraldehyde-functionalized resin [143–145]. Additional support functionalization is generally performed to direct TAs toward the carrier and/or enhance binding stability (e.g., metal derivatization to favor interactions with His-tagged TAs [146]; addition of polyelectrolytes such as polyethyleneimine (PEI) [147] or ethylenediamine (EDA) [148]; or use of crosslinking agents like glutaraldehyde (GLU) or bi-epoxides [143,149]. Generally, these covalent grafting strategies result in low enzyme leaching, an improvement to co-solvent tolerance and recyclability [56,149], although sometimes at the cost of enzymatic activity and selectivity due to structural constraints [127]. Some TA entrapment approaches, including sol–gel encapsulation or immobilization in polyvinyl alcohol hydrogels (e.g., Lentikats®), have also been used [150], particularly when mild immobilization conditions are required. The system employed have been shown to enhance the stability of different TAs. In some processes, TA and its PLP-cofactor are co-immobilized by non-covalent or covalent attachment, creating self-sufficient, durable biocatalytic systems [151–153]. Some other designs have investigated immobilized whole cells expressing TAs [154–157] and co-immobilization of TAs with other enzymes [158–160].

Among flow configurations, PBRs are the most commonly employed due to their simplicity, efficient catalyst retention, and compatibility with solid-phase biocatalysts [127,138,143,149] (Tab.I.S5). Alternative formats such as enzyme membrane reactors (EMRs) [161], microreactors [147,155,162], and monolithic supports [145,163] have been investigated, although these remain largely limited to exploratory or proof-of-concept applications. For a

majority of the investigated processes, it is also interesting to note the frequent integration of auxiliary modules (e.g., in situ product removal) has been implemented to address equilibrium constraints and improve process efficiency [146,157].

Together, these strategies demonstrate a convergence toward robust, reusable, and modular biocatalytic systems optimized for the continuous production of chiral amines under industrially relevant conditions. Among them, membrane reactors appear particularly promising due to their ability to integrate separation and catalytic functions in one unit. While industrial-scale implementation remains challenging, and only a few proof-of-concept studies have examined their application to transaminases for chiral amine production, closer examination of this reactor type is warranted.

I.6 Enzymatic Membrane Reactors to Improve Chiral Amine Compound Production

Among all the flow processes presented in the previous section, the synergistic use of transaminases and membrane flow processes appears particularly promising for intensifying chiral amine production. Firstly, membrane flow processes can mitigate thermodynamic limitations either by progressively adding substrates – limiting potential substrate inhibition- or by removing (co-)products, thereby enhancing conversion by shifting the equilibrium [164,165]. Secondly, membranes specifically employed for progressive product removal can simultaneously enable initial product purification, which is particularly relevant in the pharmaceutical sector, where purification steps often represent the primary cost driver [99,136,166]. Thirdly, an enhancement in product selectivity can be achieved by using multiple membranes in series with different molecular weight cut-offs (MWCO) [25,167].

In addition to mitigating thermodynamic constraints and offering purification advantages, membrane processes are energy-efficient compared to other unit operations [168–170], offer relatively simple reactor operation, and can be easily adapted to larger scale—providing thus a wide range of possibilities [171–173]. When coupled with continuous flow mode, they offer the potential to enhance both productivity and cost-effectiveness of the overall process. Therefore, a more detailed focus on this approach appears relevant.

I.6.1 Main Strategies and Applications

The synergic use of enzymes and membranes in reactors is generally referred to as an “enzymatic membrane reactor” (EMR), which can be employed in two different ways: either free enzymes and the membrane are used separately, or the enzymes are directly immobilized on the membrane (Fig.I.9). In this latter case, referred to as a biocatalytic membrane reactor (BMR), the membrane performs both the catalytic and separation functions in a single operation [25,171]. By integrating both functionalities, BMRs coupled

with flow processes enable process intensification and, therefore, offer improved cost-effectiveness compared to other flow configurations [167].

Because of these significant advantages and wide-ranging possibilities—particularly due to the broad spectrum of enzymatic activities—EMRs have already proven effective in various industrial sectors such as agro-food (e.g., pectin hydrolysis, lactose reduction in milk), biomedical/pharmaceutical (e.g., production of antibiotics, vitamins, amino acids, and APIs), energy (e.g., hydrolysis of fats and vegetable oils), and environmental applications (e.g., pollutant degradation in wastewater treatment plants, CO_2 capture) [167,174–178].

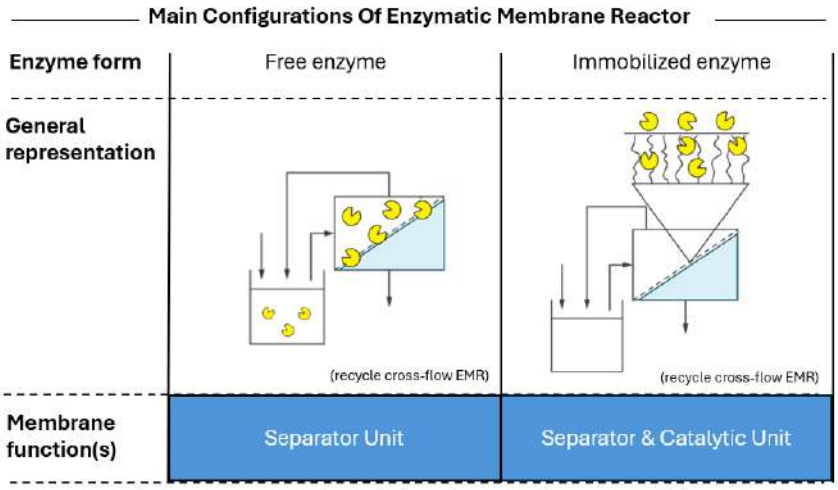

Fig.I.9 - Main configurations of enzymatic membrane reactors. In the first case, enzymes and the membrane are used separately—the membrane serves solely as a separation unit. In the second case, enzymes are immobilized on or within the membrane, forming a biocatalytic membrane that combines both catalytic and separation functions.

Before focusing in detail on BMRs—the most promising strategy—general considerations on the various EMR process configurations are briefly presented. A wide range of process strategies can be implemented within the EMR framework. Regardless of the enzymatic system used (free or immobilized), multiple membrane configurations and flow modes are available, each with specific advantages and limitations.

I.6.2 Enzymatic Membrane reactors (EMR)

Depending on the overall strategy and the intended application of the membrane reactor, different types of membranes, flow regimes, and reactor designs can be employed.

I.6.2.1 Types and Selection of Membranes

Membranes generally used in enzymatic membrane reactors are typically composed of either ceramic (inorganic) or polymeric (organic) materials [171,179]. While ceramic/inorganic membranes offer several advantages such as excellent thermal and chemical stability, resistance to harsh solvents, and high mechanical strength [176,180,181], they are generally expensive and offer limited tunability. On the other hand, polymeric membranes (e.g.,

cellulose derivatives, polyethylene (PE), polypropylene (PP)) represent a more flexible and cost-effective alternative. Their properties are more easily adjustable due to a broader range of manufacturing techniques [182,183]. However, certain drawbacks associated with polymeric membranes—depending on their composition—must be noted, such as potential mechanical fragility and a higher susceptibility to fouling. Fortunately, the development of more robust membranes, including uniform polymeric formulations or mixed polymeric–ceramic composites, along with pre-treatment modifications, can mitigate these issues, making polymeric membranes highly promising candidates for enzymatic membrane reactors [167,184]. Additionally, beyond membrane composition, membranes can present two morphologies: either symmetric (homogeneous porosity) or asymmetric (heterogeneous porosity) (Fig.I.10). Asymmetric membranes, characterized by a skin layer and a support layer, are generally preferred for enzyme immobilization due to their greater loading capacities [167,174,179].

Using membranes is of interest due to their ability to separate different components within a system. Various membrane properties contribute to physical separation, among which the molecular weight cut-off (MWCO, expressed in kDa) is particularly critical [177]. This parameter, governed by membrane porosity, determines the type of filtration (microfiltration (MF) (0.1–10 µm, ultrafiltration (UF) (10–100 nm), nanofiltration (NF) (1–10 nm), or reverse osmosis (RO) (<1 nm). When enzymes are used separately from the membrane, MWCO selection is especially crucial to ensure retention of the soluble free enzymes in the system without compromising the selective passage of target compounds (substrates or (co)-products) [167]. Since enzyme molecular weights typically range from 10 to 150 kDa, UF and NF are the most commonly employed filtration modes [25,167]. In addition, some membranes—exhibiting affinity or rejection toward specific compounds—can also display selective properties. Other key characteristics of the membrane's active layer and porous sublayer, such as hydrophobicity/hydrophilicity and surface charge, are therefore critical factors to consider when selecting this type of membrane [176].

These properties must be carefully selected based on the specific components to be retained or permeated through the membrane. Ideally, the membrane material should be chosen to exhibit sufficient stability under the operating conditions—such as temperature, pH, and presence of organic solvents—that are required to maintain optimal enzymatic activity [25], while also ensuring that its intrinsic properties—particularly hydrophobicity or hydrophilicity—are favorable to enzyme stability and activity. In this regard, hydrophilic membranes are generally preferred, as enzymes tend to perform more effectively in aqueous environments [177,185].

Depending on the desired application, different membrane configurations ("modules") – illustrated in Fig.I.10 - are possible [167,175,176,186]. Flat sheet modules are generally used during the preliminary development stages of membrane-based processes, but are typically limited by a relatively low surface-to-volume ratio. More advanced modules,

such as hollow fiber, tubular (capillary) membranes and spiral wound, not only provide an increased specific surface area but also exhibit better mass transfer efficiency [187,188]. Owing to their high performance, these configurations are commonly employed at pilot and industrial scales. While they are not detailed in this work, such modules - exhibiting various characteristics of interest for specific applications [186] - do exist, further demonstrating the high potential for customization of EMRs.

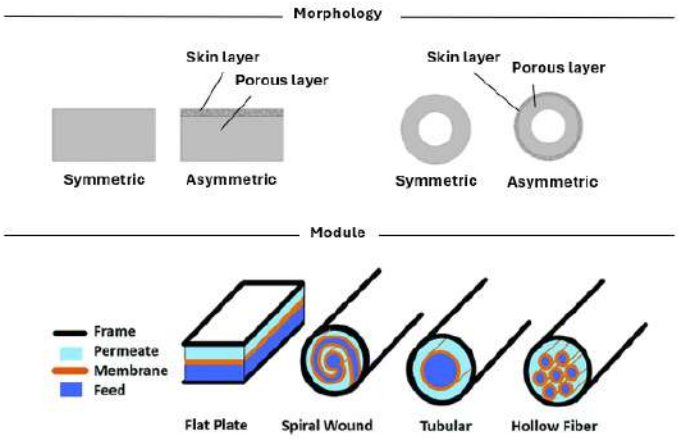

Fig.I.10 - Membrane morphologies and the modules that can be used in EMR. Adapted from [179,189].

I.6.2.2 Types of Reactors and Flow Modes

While batch reactors are used for preliminary tests, EMRs generally involve flow processes in order to exploit the functionality of the membrane in an optimal way. Membrane flow processes can be incorporated into different reactor types. The most commonly used are CSTRs or PFRs [176,190,191]. The reactor type has an influence on the enzymatic kinetics and must be carefully chosen depending on various characteristics of the system. While PFR is generally preferred for its volumetric efficiency, CSTR may prove to be advantageous in certain contexts, such as when the enzyme suffers from substrate inhibition [190].

Generally, when considering pressure-driven membrane processes, two main flow modes can be used independently of the reactor type: "cross-flow or tangential flow (TF) mode" and "dead-end flow (DF) mode".

In the case of “dead-end flow” mode, the solution is pushed perpendicularly through the membrane, and only one solution residue is harvested: the permeate. As the (biocatalytic or not) membrane is mainly used as a “classical filtration operator” to separate molecules of different sizes, this mode—generally used in single-pass systems—offers fewer application possibilities and is more prone to fouling issues [167,176]. In contrast, dead-end flow allows for better exploitation of membrane porosity, which can be particularly interesting when enzymes are immobilized within the membrane matrix [192]. This flow

mode, used with flat-sheet membranes, is the typical system employed at the bench scale due to its simplicity [167].

When the flow is tangential to the membrane surface, we refer to “cross-flow” mode[4]. Contrary to dead-end flow (where pressure is the main driving force of separation), diffusion due to the concentration gradient between both sides of the membrane is generally the primary driving force. In addition to being less sensitive to fouling issues [167], this flow mode generally allows for more application possibilities, making it particularly attractive for continuous processes. The retentate can be recirculated [167,176], enabling multiple exposures of the solution to the membrane, which can improve separation efficiency and substrate conversion, especially when enzymes are immobilized on the membrane. In addition, this type of flow mode is typically coupled with more advanced and efficient membrane modules such as tubular or hollow fiber membranes [167]. As the membrane can serve as an interface between two different environments, more complex processes—such as dialysis [193], pervaporation [165,169] , and others—can be implemented to add or isolate one or several specific compounds [167]. This is especially useful for addressing thermodynamic limitations encountered in the production of chiral amine compounds using biocatalytic strategies.

I.6.2.3 Application Configurations for Small Biomolecule Production

When we consider the membrane configuration, reactor type, and flow mode, many different combinations are possible—this is notably one of the reasons why EMRs are particularly interesting. Several reviews have proposed various classification strategies to distinguish these associations and their applications [25,167]. Fig.I.11 presents some enzymatic membrane reactors involving immobilized enzymes that are commonly investigated at the lab scale for the development of small biomolecule synthesis.

[4] Cross-flow mode corresponds to tangential flow in which at least one component of the system passes through the membrane and is collected in the permeate. In certain configurations, no permeate is collected; in such cases, the system is referred to simply as operating in tangential-flow mode.

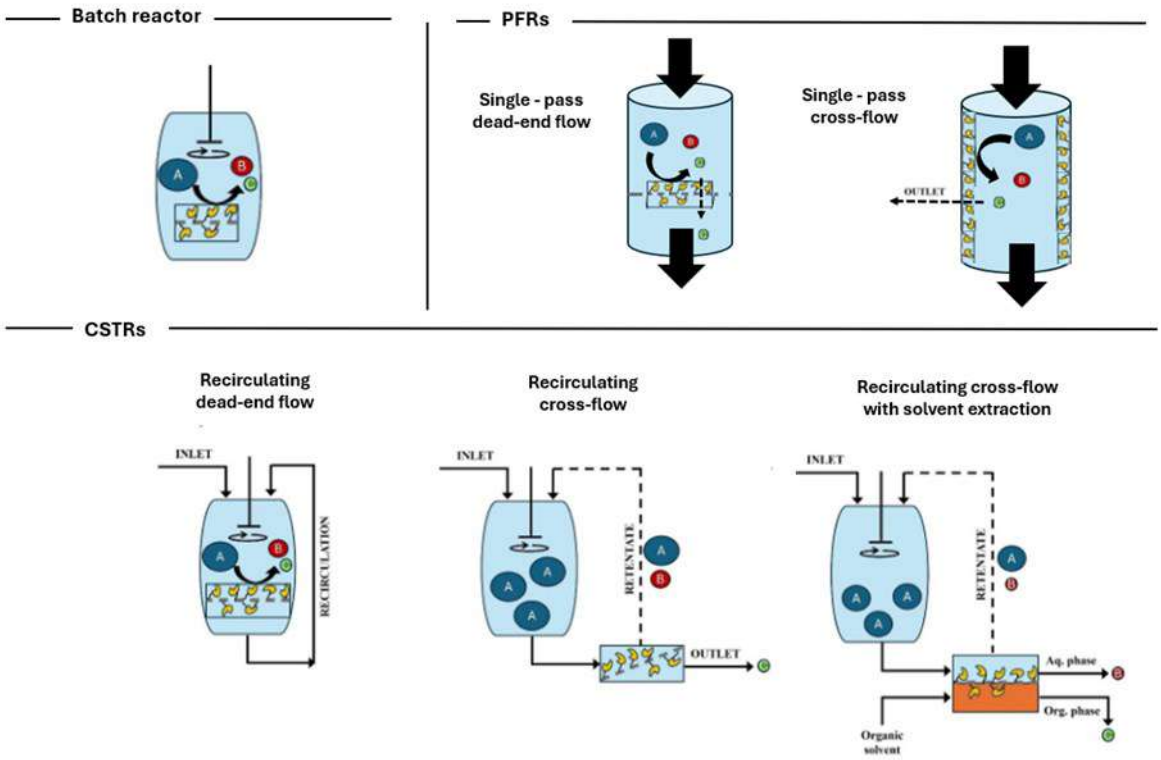

Fig.I.11 - Non-exhaustive representations of the some enzymatic membrane reactors using different flow modes and involving immobilized enzymes. Adapted from Meersseman et al.[25].

I.6.3 Biocatalytic Membrane Reactors (BMR)

The immobilization on membranes can offer several advantages, notably improved enzyme reuse and the one-pot use of the membrane as both a catalyst and a separation unit simultaneously. As this strategy appears particularly promising for process intensification, a brief focus on membrane-specific immobilization strategies will be presented.

I.6.3.1 Membrane Immobilization Strategies

In the case of immobilization on membrane, enzymes can be directly bound to the external surface, individually or in agglomerated form (enzymatic cross-linked structure), via different types of binding (adsorption, covalent, or affinity binding), or entrapped within the membrane porosity through physical means (physically blocked and/or adsorbed) or chemical interactions (covalent bonding and cross-linking).

- **Membrane Biding**

Similarly to the general immobilization strategies presented in Section I.5.1.2, different types of binding (adsorption, affinity, and covalent binding) can be used for effective enzyme immobilization [171,179,182,194,195]. In conventional approaches, immobilization generally starts with membrane modification steps prior to the addition of the enzyme for binding. A brief comment is provided below.

In conventional approaches, immobilization generally starts with membrane modification steps before the addition of the enzyme for binding. A brief comment is provided below.

Generally, the membrane (ceramic or polymeric) is not able to directly interact (either by adsorption, affinity, or covalent binding) with enzymes for effective immobilization and therefore requires specific modifications to enhance enzyme attachment and stability [171]. By modifying the membrane's surface chemistry, these initial "activation" or "functionalization" steps enable the introduction of functional groups (either attractive or reactive), depending on the type of binding targeted. While some sophisticated treatments such as UV or gamma irradiation or plasma treatments can be employed, the most common strategy remains wet chemical treatment, where the membrane is immersed in an organic solvent containing the desired functionalizing molecule [171,194]. For example, silanization of inorganic membrane surfaces using 3-aminopropyltriethoxysilane (APTES) [145,163] and the advanced coating of polydopamine (PDA) [29,30,196,197] on polymeric membranes to confer amino groups at the surface have been successfully demonstrated [171,174,184].

While immobilization is sometimes already possible after a first modification step, additional membrane modifications can be carried out to improve immobilization efficiency and enhance enzyme stability and activity. For instance, cross-linking agents such as GLU [29,163] or bi-epoxide compounds [29,30,149], could create junctions between the enzymes themselves and/or between the functionalized membrane and the enzyme. In this latter case, the cross-linking agent served as a linker arm to improve enzyme–substrate accessibility and to establish spatial arrangements conducive to optimal enzyme conformation, stability, and flexibility, thereby enhancing the conversion potential [171,174,194]. Another general approach involves creating a stabilizing fibrous environment for the immobilized enzymes via electrostatic interactions; polyelectrolytes such as PEI [29,30,198], polyallylamine hydrochloride (PAH) [199], chitosan [200] can be used for this purpose [201,202].

- **Membrane Localization**

Depending on the immobilization process, enzymes can be more or less localized in different areas of the membrane. Indeed, as membranes are porous materials, immobilization can occur in two main zones: on the external surface, which is directly exposed to the solution, and within the membrane porosity [167,171,192,195].

Surface binding is the most direct strategy, allowing enzymes to interact immediately with substrates as they pass over or through the membrane surface. While surface binding provides high substrate accessibility, it remains vulnerable to fouling and potential enzyme leaching during dynamic operation. On the other hand, entrapment within the porosity can provide a protective environment that enhances enzyme stability over extended periods, but it may also introduce mass transfer limitations, restricting substrate access and reducing catalytic efficiency (Annex I.S4).

While surface immobilization is easily achievable (e.g., via a simple batch immersion process), immobilization within the membrane porosity is generally more challenging. More sophisticated strategies can be implemented to promote enzyme incorporation into the pores. For instance, enzyme incorporation during membrane synthesis has been investigated [203,204], but this approach is often associated with activity loss due to the harsh conditions used during membrane fabrication [171]. Another promising strategy consists of using dead-end flow processes, either in normal or reverse mode, to force enzyme penetration into the porosity of an asymmetric membrane —compared to batch processes [171,192,205–207]. Such a strategy has demonstrated relatively good immobilization efficiency with strong conservation of enzymatic activity. By using such "membrane-fouling" immobilization strategies, Luo *et al.* [205] identified different types of immobilization techniques that influence enzyme localization [5] (Fig.I.12).

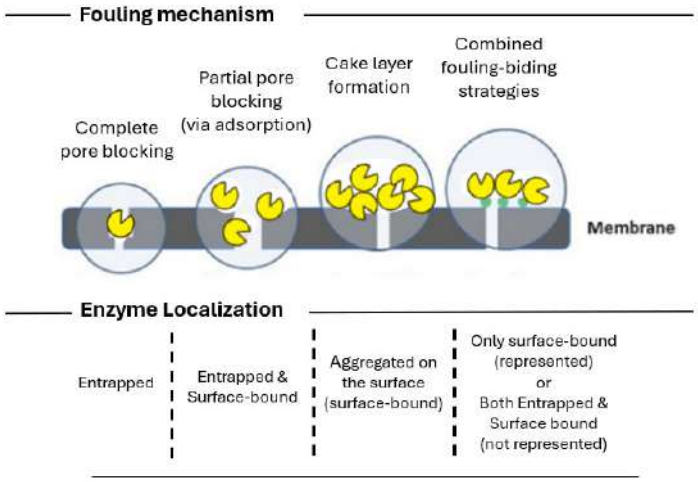

Fig.I.12 - Different membrane immobilizations using fouling mechanism. Adapted from Luo et al.[205]

Overall, the selection of enzyme immobilization techniques for biocatalytic membranes must balance stability, activity retention, and process efficiency. The optimal method depends on the intended application, membrane material, and operational conditions. Also, even if effective immobilization strategies can be implemented, the integration of the biocatalytic membrane into a flow process reactor may face certain challenges.

I.6.4 Challenges of EMR

When considering EMRs, both the effective functionality of the membrane—as a separation unit—and the enzymes—as biocatalysts (immobilized or not)—must be maintained and preserved to ensure an industrially viable and productive process. This dual requirement can present several challenges [167,171,179].

[5] The localization depends on the specific enzyme–membrane characteristics and properties, such as porosity, enzyme size, and surface charge.

I.6.4.1 Linked to the Membrane and the Process: Preservation of Separation Efficiency

About the membrane, two main issues that can affect its performance—namely permeability and selectivity—must be considered [171]. Firstly, the membrane can be negatively modified or damaged by process conditions (e.g., pH, temperature, exposure to harsh solvents, mechanical constraints, etc.). Secondly, membranes tend to lose separation efficiency due to the fouling of their surface and porosity by undesired compounds [167,171]. While the severity and rate of this phenomenon may vary depending on the process (e.g., flow mode) and application, fouling is influenced by the mixture composition, the intrinsic membrane properties, and hydrodynamic conditions, and is inherent to all membrane flow processes [208–210]. Although a detailed description of fouling mechanisms is beyond the scope of this work, it is still important to highlight that—regardless of the flow mode—the formation of a gel layer composed of macromolecules due to concentration polarization is generally one of the main causes of fouling [167].

In the context of BMRs, these issues must be given particular attention. The immobilization steps (functionalization and the immobilization process itself) can alter or damage the membrane surface properties (e.g., charge, polarity). In particular, fouling during the enzyme loading phase, especially when using flow-based immobilization processes, can drastically reduce membrane porosity and thus compromise permeability [174]. Therefore, a trade-off must be found between maximizing enzyme immobilization—which enhances overall catalytic activity—and preserving membrane integrity, which ensures effective separation.

Additional consequences of progressive fouling include increased pressure drop and greater mass transfer resistance, both of which can negatively impact system performance (affecting both separation efficiency and catalytic activity—see below) [171,174].

Fortunately, advances in the understanding of fouling mechanisms [209], the development of membranes with antifouling properties, and improved strategies for enzyme–membrane immobilization have made it possible to mitigate fouling issues effectively.

I.6.4.2 Linked to the Enzymes: Preservation of Biocatalyst Stability and Activity

Another important criterion to consider is the preservation of the catalytic activity of the enzyme. As already mentioned in Sections I.4.2.1 and I.5.1.1, one of the main challenge in biocatalysis lies in improving enzyme stability and maintaining its activity over time, which naturally decreases. However, enzymes are highly sensitive catalysts, and this natural loss of activity can be exacerbated under suboptimal conditions.

Flow processes (whether associated with membrane operations or not) can generate shear stress, which may negatively impact enzyme conformation, leading to a loss of activity [211–213]. In the case of BMRs, enzyme immobilization on the membrane could either mitigate or, conversely, contribute to this issue by rigidifying the enzyme's conformation [110]. Additionally, progressive fouling of the biocatalytic membrane and excessive enzyme loading on or within the membrane during immobilization can reduce the "free-movement" space required for optimal activity of the immobilized enzymes [171,174]. Beyond this potential loss of activity, other undesired effects such as enzyme leaching and limited substrate accessibility to immobilized enzymes (caused both by the immobilization itself and by progressive membrane fouling) can also impair the overall system efficiency [174]. This is why a proper and optimized immobilization strategy is essential, not only to enhance enzyme stability and preserve catalytic activity over time but also to avoid substrate diffusion limitations and enzyme leaching.

I.6.5 EMR applied to TAs

Coupling TA use with membrane (either separately or as a single biocatalytic membrane) can be highly relevant to solve thermodynamic issues (as explained in the introduction of this section). Indeed, by performing in situ (co)-product removal and/or controlled substrate addition, membrane technologies can be used to achieve high transamination yields by avoiding TA inhibition. To date, fewer than ten studies have investigated different strategies and EMR configurations. Some of them use free TA and membrane separately, while others employ TAs directly immobilized on the membrane (BMR). A brief description of these strategies, summarized in Tab.I.5 and Tab.I.6, is presented in the following section.

I.6.5.1 TAs and Membrane Used Separately : Free TA

Tab.I.5 - Examples of free TAs combination with membrane technologies for bioctatalytic processes intensification. Adapted from Meerssemen et al.[25]

Substrate	Product	Membrane	Operation	Mode	Ref.
Pro-sitagliptin ketone + isopropylamine	R-Sitagliptin + acetone	Polymeric (Psf, 10 kDa) + dense PDMS	UF (for enzyme retention) + solvent extraction	Recirculation	214
Benzyl acetone + isopropylamine	R-1-methyl-3-phenylpropylamine + acetone	Polymeric (PP, N.D.)	Solvent extraction	Recirculation	166
Acetophenone + isopropylamine	R-MBA + acetone	Dense PDMS	Pervaporation	Batch	165

N.D. – non-specified ; Psf – polysulphone ; PDMS – Polydimethylsiloxane, UF – ultrafiltration ; MBA methylbenzylamine ; PP – polypropylene

- **Equilibrium Shifting by Removing of Co-product**

The membrane technologies can be used to remove the co-product of the transamination reaction by pervaporation. Because it can be performed at relatively moderate temperatures, this type of separation is particularly interesting for thermo-sensitive enzymatic processes. Specifically, Satyawali *et al* [165] performed pervaporation for the removal of acetone by-product from the system using a PolyDimethylSiloxane (PDMS) membrane (acetone-selective). Such transamination coupling with pervaporation resulted in a 13% increase in product yield after 9 hours of reaction compared to the equivalent transamination process where no pervaporation was performed. While this result is already very promising, the process effectiveness shows a strong dependency on acetone concentration. The effect remains minimal at low acetone concentrations, highlighting the need to use a large excess of substrate and to couple this strategy with another product separation technique targeting the amine product.

- **Equilibrium Shifting by Removing of Product**

Some studies have also investigated the removal of product by using membrane contactors [166,214]. For example, Satyawali *et al* [166] conducted an AS with free TAs in organic solvent and employed a PP membrane contactor to remove the amine product *in situ*. In this case, organic solvent was used to optimize the keto-substrate ratio to push the reaction toward product formation as much as possible without inhibiting the TAs. This approach drastically increased the yield from 69% (without membrane extraction) to 99%. In another study, Yang *et al*. [214] successfully produced R-sitagliptin by AS in aqueous medium using PDMS as a membrane contactor.

I.6.5.2 Membrane-immobilized TA reactors

Tab.I.6 - Examples of membrane-immobilized TAs for biocatalytic processes intensification. Adapted from Meersseman et al.25

Reaction(s)	Substrate/ Product	Immobilization	Comments	Membrane	Mode	Ref.
Transamination	S-MBA + pyruvate → Acetophenone + L-alanine	Coordination (His-tag) (23%)	Retained productivity after 5 days of continuous operation was 81% (24 h operation)	Polymeric blend (Cu-functionalized PVDF)	Flow	[26]
Transamination	S-MBA + pyruvate → Acetophenone + L-alanine	Covalent grafting + His-tag driving (43.6%)	/	Polymeric blend (Co-derivatized PCADE/PVDF)	Batch	[27]
Cascade (transamination + (de)hydrogenation)	Cinnamaldehyde → Cinnamylamine	EPC entrapment	/	N.D. (12 kDa dialysis membrane)	Batch	[28]

Transamination (KR)	Rac-BMBA + pyruvate → S-BMBA + BAP + D-alanine	Covalent grafting (85%)	Unaltered initial sp. activity after 8 catalytic cycles (c.a. 16 h operation)	Polymeric (PDA + GDE + PEI-modified-PP)	Batch	[29]
Transamination (AS)	ISO + FAP → Acetone + FMBA	Covalent grafting	Sp. activity improvement compared to free form (340%)	Polymeric (PDA + GDE + PEI-modified-PP)	Batch	[30]

PVDF - polyvinylidene fluoride ; PCADE - polycarvone acrylate di-epoxide ; EPC – enzymes-polyelectrolytes complex ; N.D. – non-determined ; Rac-MBA – Racemic methylbenzylamine ; Rac-BMBA – Racemic bromo-α-methylbenzylamine ; BAP bromoacetophenone ; PDA – polydopamine ; PP – polypropylene ; PEI – polyethyleneimine, GDE - glycerol diglycidyl ether ; ISO – isopropylamine ; FAP - 2'-fluoroacetophenone ; FMBA - (R)-2fluoro-α-methylbenzylamine

As immobilization is already very challenging, coupling BMR with flow processes proves to be even more challenging. Actually, only one study have investigated immobilized-TA reactor under flow condition [26]. Sketa *et al.* demonstrate an immobilization of His-tagged ATA on nanofiber. The resulting biocatalytic membrane was then tested to synthetize L-alanine in a two-plate microreactor under various continuous flow conditions, where different flow rates and temperatures were evaluated. The process demonstrated highly promising results, including a high space-time yield and turnover number. After five days of continuous operation, 81% of the initial activity was retained, demonstrating the excellent stability and reusability of the system.

Other interesting immobilization strategies on polymeric supports have been investigated, but only in batch reactors, which do not allow optimal use of all potential membrane properties (being used solely as a passive support). Montanari *et al.*[27] immobilized ATA via covalent binding on a polymeric blend (co-derivatized polycarvone acrylate di-epoxide (PCADE) / polyvinylidene fluoride (PVDF)) using a His-tag strategy as the driving force, achieving an immobilization yield of 43.6%. L-alanine production was then evaluated. In another study [28], TAs were immobilized together with other enzymes in the presence of a polyelectrolyte (forming enzyme–polyelectrolyte complexes (EPC)) by entrapment on/in a dialysis membrane in order to perform a transamination/(de)hydrogenation cascade. Meersseman Arango *et al.* [29] investigated different immobilization strategies, either via adsorption or covalent grafting. Among these, a particularly effective immobilization on a functionalized PP membrane (via covalent grafting) was demonstrated, achieving an immobilization yield of 81%. Catalytic tests showed successful retention of the initial specific activity after eight catalytic cycles during the kinetic resolution of racemic bromo-α-methylbenzylamine (Rac-BMBA) . In another study [30], the same team, using the same immobilization strategy, investigated a different reaction (AS) and successfully implemented an appealing crystallization strategy to improve the overall conversion. As this last model case appears relevant and promising, it is discussed in detail in the final section.

I.7 Relevant BMR Case: Immobilization of TsRTA on PP membrane for Chiral Amine Production

Meersseman Arango et al [29,30] demonstrated an efficient immobilization of TsRTA, an R-selective TA from *Thermomyces stellatus,* on a commercially available flat-sheet porous PP membrane. The performance of the biocatalytic membrane was further evaluated by performing AS through various catalytic tests in batch mode, and additional strategies to overcome thermodynamic limitations were successfully implemented.

I.7.1 Selection of Transaminase : TsRTA, a Thermophilic Enzyme

To optimize chiral amine production, TsRTA a transaminase sourced from a thermoresistant fungus (Annex I. S7), was selected to perform a targeted AS. Due to its thermophilic origin, this enzyme exhibits enhanced resistance to elevated temperatures and co-solvent exposure compared to homologous transaminases, offering significant potential for industrial applications [215].

I.7.2 Immobilization: Strong Covalent Grafting to Avoid Leaching

As leaching is not desired flow processes, covalent grafting was chosen for its superior resistance to leaching. In Meersseman Arango *et al* work [29,30], effective multi-point covalent grafting—either of TsRTA alone or of both TsRTA and the PLP cofactor—onto pre-functionalized PP membranes was demonstrated and optimized under batch conditions.

First, a PDA coating is applied to introduce reactive functional groups (catechol and quinone) on the membrane surface, enabling facile reaction with various chemical functions. This not yet fully understood mechanism involves the self-polymerization of dopamine monomers, inspired by mussel surface chemistry [196,197,216]. A bifunctional epoxide linker, glycidyl diether (GDE), is then added to provide greater conformational flexibility to the subsequently immobilized enzymes. Its epoxide groups can selectively form covalent bonds with nucleophilic groups (e.g., amino, thiol, phenolic, and imidazole) of amino acid residues such as lysine or cysteine found on the enzyme surface [149,217,218]. Although the resulting covalent bonds are highly stable, epoxide groups exhibit low intermolecular reactivity [218]. To enhance the immobilization reaction and stabilize the enzyme–membrane complex, PEI (polyelectrolyte)—is added [152,153,198]. After the functionalization steps, TsRTA is introduced and, under the influence of PEI, spontaneously reacts with the epoxide groups of GDE to form covalent bonds.

Such a strategy demonstrates good immobilization yield and robustness—no leaching and good recyclability (Section I.6.5.2) [29].

I.7.3 Catalytic Test: Optimization of Asymmetric Synthesis via Product Crystallization

In a previous work [30], Meersseman Arango *et al.* investigated an AS using the following model reaction to evaluate the catalytic performance of the enzyme: the transamination of 2'-fluoroacetophenone (FAP) with isopropylamine (ISO) to produce (R)-2-fluoro-α-methylbenzylamine (FMBA) and acetone (Fig.I.13).

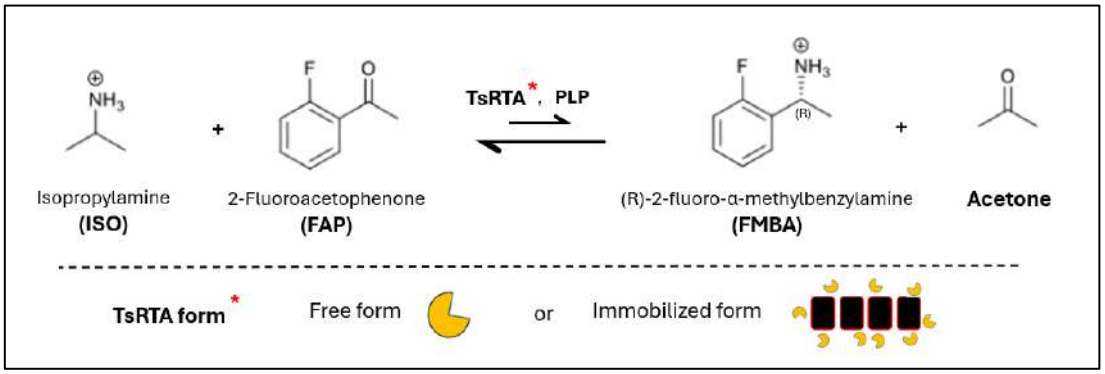

Fig.I.13 - Model reaction used to evaluate the catalytic performance of TsRTA investigated by Meersseman Arango et al. 30. Asymmetric synthesis is carried out via the transamination of 2'-fluoroacetophenone (FAP) to form (R)-2-fluoro-α-methylbenzylamine (FMBA), using isopropylamine (IPA) as the amino donor, with acetone as the co-product. The reaction can be catalyzed by either free or immobilized TsRTA.

An improvement in the catalytic activity of covalently grafted immobilized *Ts*RTA compared to the free enzyme was demonstrated (the specific activity of the biocatalytic membrane was 2 to 3 times higher than that of free *Ts*RTA)[6].

While immobilization provided advantages over the free *Ts*RTA, the overall process remained limited by thermodynamic constraints: an unfavorable equilibrium (theoretical $K = 4.7 \times 10^{-2}$) and substrate/(co-)product inhibition, particularly due to the relatively low tolerance to the ketone substrate concentration (inhibition observed at [FAP] > 25–30 mM, with severe inhibition above 50 mM). To address these limitations, various mitigation strategies were successfully implemented in batch reactors to enhance chiral amine production. A particularly relevant strategy involved the use of an appropriate excess of reagents (ISO/FAP) to reduce inhibition, combined with the addition of a crystallizing agent, diphenylpropionic acid (DPPA), which forms poorly soluble crystalline salts with the amine compounds (FAP (substrate) and FMBA (chiral amine product)) (Fig.I.S4). This approach enabled a significant shift in equilibrium without inhibiting the immobilized enzyme, increasing FAP conversion from ~44% to over 80% [30].

[6] This observation is presumed to result from the favorable microenvironment created by the hydrophilic compounds—PEI (and PDA)—used to functionalize the polypropylene membrane, which enhance enzyme stabilization.

I.7.4 Limitation of Batch Reactor

While effective, the overall performance of these investigated systems remained limited by the use of batch reactors, preventing them from becoming viable solutions for chiral amine production at industrial scale. By enabling the continuous addition of substrates (FAP/ISO) and removal of (co-)products (FMBA/acetone), the implementation of a biocatalytic membrane in a continuous flow process could intensify the reaction and improve the productivity. In addition, flow reactor integration would allow the use of the biocatalytic membrane as a separation unit to shift the unfavorable equilibrium, notably through in situ removal of (co-)products. For example, the integration of an acetone-selective PDMS membrane in a pervaporation system [169,219], as demonstrated by Satyawali *et al*. [165], could be a promising strategy to enhance process efficiency—particularly if combined with crystallization strategies optimized in Meersseman Arango *et al*. work [30].

II. Objectives

The main objective of this project is to develop an efficient biocatalytic approach for the production of chiral amine compounds, involving membrane-immobilized transaminases.

To achieve this goal, TsRTA[7] was selected to optimized a targeted AS, with a potential yield of up to 100%. However, cell-free *Ts*RTAs are generally difficult to recover and reuse and, like all transaminases, suffer from significant thermodynamic limitations (unfavorable equilibrium) and kinetic limitations (substrate inhibition) during asymmetric synthesis. These issues represent major obstacles to achieving efficient and viable processes. To address these limitations, the implementation of *Ts*RTA in an enzyme membrane reactor (EMR) appears to be a relevant strategy. Indeed, immobilizing the enzyme directly in or on a selective membrane would help tackling two different limitations simultaneously: (i) improve the reusability of the enzyme (and potentially its stability) and (ii) the membrane could act as a separation unit to remove one of the products from the reaction medium (e.g., via pervaporation or dialysis), thereby shifting the equilibrium towards the product side, and hosting intensified reaction-separation processes. Previous studies have already demonstrated good immobilization of TsRTA on membrane and interesting strategy to enhance catalytic reaction [29,30]. However, all experiments were conducted in batch mode, limiting immobilization efficiency and preventing optimal use of the membrane (e.g., as a separation unit, operating in flow conditions).

Therefore, the specific objective of this master thesis work is to investigate the transition of these previous studies from batch to flow processes. This work aims to demonstrate how the implementation of efficient continuous systems can enhance both enzyme immobilization (by reducing immobilization time and increasing enzyme loading) and catalytic performance (by improving process productivity). Demonstrating an effective transition thus represents a further step toward process intensification.

[7] R-ATA coming from *Thermomyces stellatus*, a promising thermoresistant fungus.

III. Strategy

III.1 TsRTA Immobilization: From Batch to Flow – Optimizing Biocatalytic Membrane Preparation

While the batch immobilization (Fig.III.1(a)) demonstrated by Meersseman Arango *et al.*[29,30] appear reproducible, this robust covalent-biding immobilization strategy exhibited limited enzyme loading, likely due to suboptimal exploitation of membrane porosity.

By using a similar approach, this work aims to demonstrate a new efficient flow process that improves immobilization by reducing immobilization time and increasing enzyme loading, notably through better exploitation of membrane porosity – as demonstrated by Luo et al [192,205–207]. To achieve this, progressive immobilization of the pre-functionalized membrane (in batch conditions) is performed under dead-end flow mode (Fig.III.1 (b)), using a syringe pump system. To determine optimal immobilization parameters, various flow rates will be tested and compared with conventional batch immobilization based on fixed incubation time. Subsequent catalytic tests are then conducted to assess the influence of enzyme loading on catalytic activity.

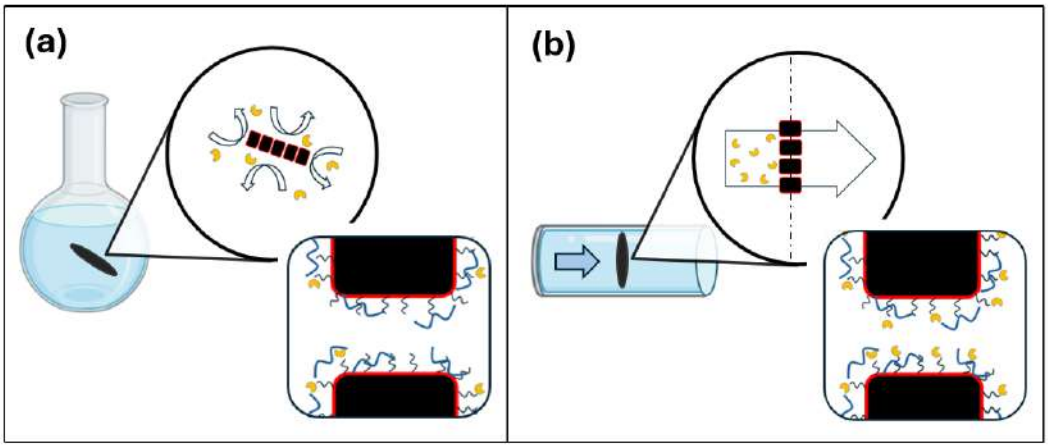

Fig.III.1 - Schematic representation of the different process types investigated in this study for the preparation of the biocatalytic membrane. (a) In the batch process, enzymes are randomly exposed to the functionalized membrane surface, with distribution influenced by stirring. The extent to which membrane porosity is exploited remains uncertain. (b) In the dead-end flow process, enzymes are directed perpendicularly toward the functionalized membrane and are forced through the porous structure, promoting enhanced interaction with internal surfaces.

III.2 Catalytic Evaluation: From Batch to Flow – Demonstrating Intensification Potential

As the integration of biocatalytic membranes into continuous flow systems appears essential to increasing productivity—through process intensification and advanced separation strategies—a transition from batch to flow setups is thus necessary. Beyond

demonstrating potential productivity gains, this setup transition also serves to assess the feasibility of future pervaporation system implementation [169].

To this end, different flow process strategies (involving *Ts*RTA immobilized on membrane) are explored as proof-of-concept and compared with "classical" batch processes involving either free or immobilized *Ts*RTA (Fig.III.2 (a) and (b), respectively). Specifically, several catalytic tests are conducted under varying flow rates in both single-pass dead-end (Fig.III.2 (c)) and recirculating tangential flow modes[8] (Fig.III.2 (d)). In both configurations, the robustness and operational lifespan of the biocatalytic membrane–flow systems are evaluated through leaching assessments and prolonged catalytic testing.

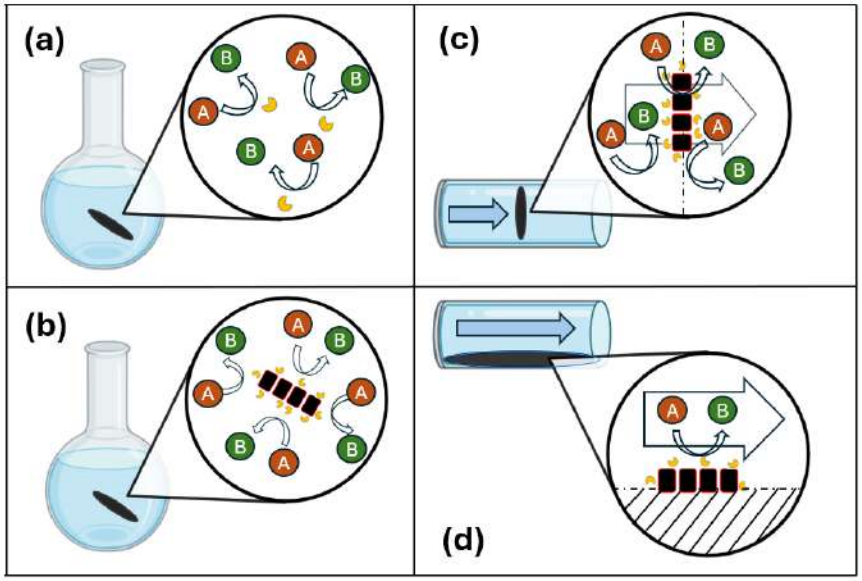

Fig.III.2 - Schematic representation of the different types of processes investigated in this study for catalytic testing.(A) and (B) represent, respectively, the substrates—isopropylamine (ISO) and 2-fluoroacetophenone (FAP)—and the (co-)products—(R)-2-fluoro-α-methylbenzylamine (FMBA) and acetone. (a) Batch process using free TsRTA. (b) Batch process using TsRTA immobilized on a polypropylene (PP) membrane. (c) Dead-end flow process using TsRTA immobilized on a PP membrane. (d) Tangential-flow process using TsRTA immobilized on a PP membrane (Note: recirculation is not depicted in this scheme).

[8] As no components are expected to pass through the membrane, the term tangential flow is more appropriate than cross-flow.

IV. Experimental

IV.1 Materials

Hydrochloric acid (HCl; 37 wt%, aqueous solution), pyridoxal 5'-phosphate hydrate (PLP; ≥98%), glycerol diglycidyl ether (GDE; technical grade), carbonate-bicarbonate buffer capsules, and Bradford reagent were obtained from Sigma-Aldrich. Sodium hydroxide (NaOH; ≥99%), N-(2-hydroxyethyl)piperazine-N'-(2-ethanesulfonic acid) (HEPES; ≥99.5%), and HEPES sodium salt (≥99%) were purchased from Carl Roth. Branched polyethyleneimine (PEI; 50 wt%, aqueous solution, M_n 60,000) and isopropylamine (ISO; 99%) were obtained from Acros Organics. Dichloromethane (DCM; HPLC grade) and ethanol (EtOH; absolute) were sourced from VWR Chemicals. Tris(hydroxymethyl)aminomethane (Tris; >99%), dopamine hydrochloride (3-hydroxytyramine hydrochloride; 98%), and 2'-fluoroacetophenone (FAP; 97%) were purchased from Tokyo Chemical Industry. Racemic 2-fluoro-α-methylbenzylamine (rac-FMBA; 97%) was obtained from BLD Pharm.

Commercial polypropylene flat-sheet membranes (PP) were acquired from 3M (USA). Single-use 5 mL polypropylene syringes with Luer-lock fittings (Omnifix) and 5 mL glass syringes were obtained from Carl Roth. Whatman reusable stainless steel syringe filters (13 mm) were purchased from Fisher Scientific. A single-channel syringe pump (model PSNE1000) was obtained from ProSense. Two magnetically driven gear pumps (ref. DGS.5P7PP72N00E00SM425) and their corresponding variable frequency drives (VFDs; ref. ODE-3-140022-3F12, model IP20 3x400 V, 2.2 A, 3PH) were sourced from Flowtec BVBA. Additional components, including PTFE tubing and a tangential flow membrane holder composed of metal and plastic plates secured with nuts, were also employed; their suppliers are unknown.

IV.2 Methods

IV.2.1 TA Production

In this work, R-ATA from *Thermomyces stellatus*, shortly called TsRTA, was produced following the procedure described by Paradisi *et al.* [215,220], with the lyophilization step replaced by flash-freezing. The enzyme was used as a cell-free extract for the asymmetric synthesis of chiral amines. A more detailed protocol for *Ts*RTA expression is provided in Annex IV.S1.

IV.2.2 TA Immobilization onto Polypropylene (PP) Membrane

In this work, TsRTA was immobilized onto functionalized solid polypropylene (PP) flat-sheet membranes (exhibiting pore sizes ranging from 200 to 400 nm) for subsequent heterogeneous transamination reactions. Circular membranes with diameters of 12 mm and 44 mm (referred to as 12M and 44M, respectively) were selected for the various experiments. The desired dimensions were obtained using a cookie cutter. Structural properties of the membranes are detailed in Annex IV.S2.

IV.2.2.1 Functionalization of PP membrane

To enable effective covalent grafting of TsRTA onto the membrane, a three-step membrane functionalization was first performed, following the procedure described by by Meersseman Arango *et al* [29] (Fig.IV.1).

First, membranes were coated with polydopamine (PDA) to introduce reactive amine groups that serve as anchoring sites for subsequent modifications (Fig.IV.S1). A dopamine hydrochloride (3-hydroxytyramine) solution was prepared in 10 mM Tris buffer (pH 8.5) at a concentration of 2 mg/mL and stirred. After approximately 15 minutes, PP membranes—previously soaked in ultrapure ethanol to ensure surface and pore wetting—were added to the solution and incubated for 20 hours at room temperature under gentle stirring. The resulting membranes (PP_PDA), which exhibited a dark brown coloration, were removed and rinsed with distilled water for 1 hour, repeated three times.

Second, the PP_PDA membranes were modified with a bifunctional epoxy coupling agent, glycerol diglycidyl ether (GDE), to introduce linker arms for enzyme immobilization. The PP_PDA membranes, pre-wetted with ethanol, were immersed in an ethanol solution of GDE (100 mg/mL) and stirred for 18 hours at room temperature. The modified membranes (PP_PDA_GDE) were then rinsed once with ultrapure ethanol and three times for 1 hour with distilled water.

Finally, the PP_PDA_GDE membranes were partially functionalized with branched polyethyleneimine (PEI) to promote the covalent grafting of the enzyme onto the epoxy linkers. The membranes were immersed in a 0.1 M carbonate-bicarbonate buffer (pH 9.5) containing 5 mg/mL PEI and stirred for 90 minutes at room temperature, unless stated otherwise. After incubation, the resulting PP_PDA_GDE_PEI membranes were rinsed three times with distilled water, each for 1 hour.

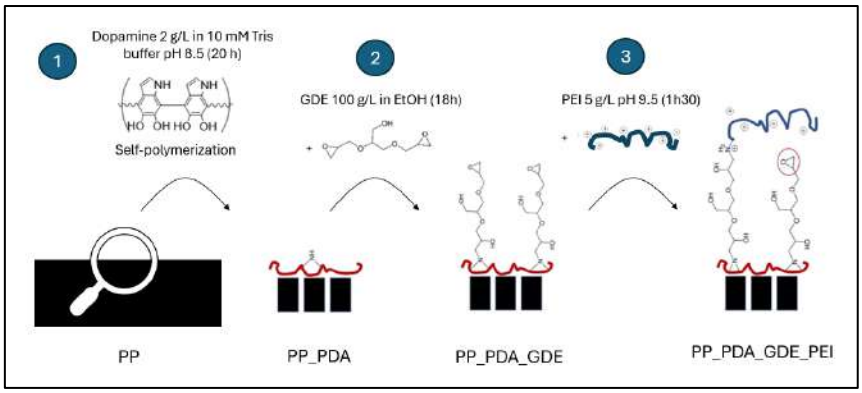

Fig.IV.1 - Schematic representation of polypropylene (PP) membrane functionalization before TsRTA immobilization (1) Polydopamine (PDA) coating (2) Glycerol diglycidyl ether (GDE) addition (3) Polyethyleneimine (PEI) addition. Adapted from [29]

Depending on membrane size (12M or 44M), different volumes were used to ensure complete immersion during each functionalization step. Typically, volumes of 50 mL and 150 mL were employed for the preparation of each solution for 12M and 44M membranes, respectively.

IV.2.2.2 Immobilization of TA on PP Membrane

The functionalized membrane (PP_PDA_GDE_PEI) was exposed to a solution containing a defined concentration of TsRTA (the preparation of immobilization solutions is described in Annex IV.S4 and Annex IV.S5). The enzyme, guided by the presence of PEI, spontaneously reacts with the epoxide groups of GDE to form covalent bonds. The resulting biocatalytic membrane is referred to as PP_TA. Depending on the reactor configuration and the process employed, specific considerations must be taken into account.

- **Batch immobilization strategy**

Similarly to Meersseman Arango *et al* procedure [29], the functionalized PP membranes (PP_PDA_GDE_PEI) were immersed in immobilization solutions (C_0 = 0.2, 0.25, or 0.5 mg/mL; Annex IV.S5) and incubated for 18 hours at 35 °C in round-bottom glass flasks under gentle stirring. Following immobilization, the resulting membrane-bound transaminases were rinsed with buffer solution (HEPES 0.1 M buffer, PLP 1 mM) for 30 minutes, repeated three times, to remove loosely adsorbed enzymes. The immobilization solution and the three rinsing fractions were collected for protein loading analysis.

The volumes of immobilization and rinsing solutions were adjusted according to the membrane area. Typically, 12M and 44M membranes were immersed in 4 mL and 20 mL of solution, respectively. The resulting membranes are referred to as 12M-PP_TA-B and 44M-PP_TA-B, where the suffix “B” denotes immobilization carried out in batch mode.

- **Dead-end flow immobilization strategy**

Dead-end flow immobilization using 12M membranes was performed with either glass or plastic syringes mounted on a syringe pump. The functionalized 12M PP membrane (PP_PDA_GDE_PEI) was placed inside a Whatman stainless steel filter holder and manually pre-wetted using a syringe containing 1 mL of buffered solution (HEPES 0.1 M buffer, PLP 1 mM).

Following pre-wetting, a new syringe filled with the immobilization solution (typically 3.5-4 mL) at the desired enzyme concentration (0.25 or 0.50 mg/mL) was connected to the Whatman cell and mounted on the syringe pump. A specific flow rate (0.5, 1.0, or 1.5 mL/h) was applied to progressively push the solution through the membrane (at room temperature). The effluent, corresponding to the permeate, was collected at regular time intervals in 1.5 mL tubes at the outlet of the system (Fig.IV.2 (a)).

Once the entire immobilization solution was passed through the membrane, a rinsing step was carried out by pushing buffer solution (loaded into a new syringe) through the membrane in the same manner as during the immobilization (Fig.IV.2 (b)).

The resulting membrane is referred to as 12M-PP_TA-F, where “F” indicates that immobilization was carried out in a flow-through reactor configuration.

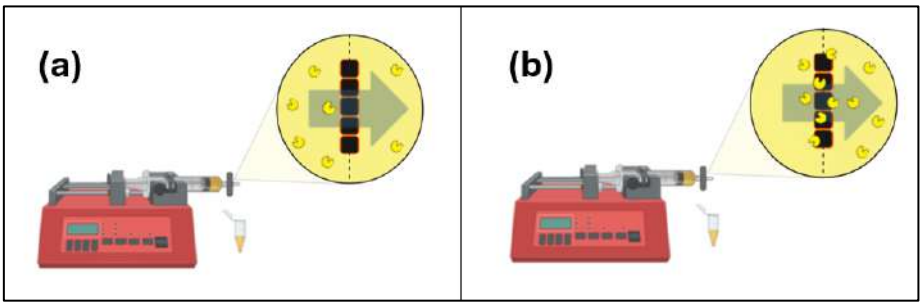

Fig.IV.2 - General representation of the immobilization strategy investigated in the dead-end flow configuration.(a) In the first step, the immobilization solution (TsRTA at 0.25 or 0.5 mg/mL in HEPES buffer, 0.1 M, pH 8, containing 1 mM PLP) is perpendicularly pushed through the pre-functionalized membrane at a selected flow rate (0.5, 1.0, or 1.5 mL/h) using a syringe pump. (b) In the second step, buffer solution (HEPES 0.1 M, 1 mM PLP) is flushed through the membrane under identical conditions to remove non-covalently bound enzyme. Both effluents (from the immobilization and rinsing steps) are collected at the outlet for protein quantification by Bradford assay.

IV.2.2.3 Immobilized Enzyme Loading Evaluation

The collected solution (post-immobilization and rinsing solutions) during the immobilization steps are analyzed to determine protein loading.

The immobilized enzyme loading (L), defined as the mass of enzyme bound to the support, was determined by mass balance using the Bradford assay (Annex IV.S6). Although the overall strategy was similar for both immobilization methods (Eq.IV.1), specific distinctions are required for clarity. In batch mode, immobilization was evaluated as a function of incubation time, whereas in flow mode, it was assessed based on the applied flow rate. In both cases, C0, C1(i), and C2j represent the concentrations (mg/mL)

of the initial immobilization solution, the residual solution after immobilization, and the rinsing solutions, respectively.

In batch immobilization, only one residual solution is collected after the immobilization period, with a volume (V_1) corresponding to the initial solution volume (V_0). The rinsing step is then performed three times using buffer volumes identical to the initial immobilization solution volume ($V_0 = V_{2j}$).

$$(a)\ L = V_0 \times \left(C_0 - C_1 - \sum_{j=1}^{m=3} C_{2j}\right)[mg] \qquad \text{(b) } L = V_0\, C_0 - \sum_{i=1}^{n} V_{1i} C_{1i} - \sum_{j=1}^{m} V_{2j} C_{2j}\ [mg]$$

Eq.IV.1 - (a) General equation for calculating enzyme loading in the batch immobilization process with three rinsing steps. The same volume is used for the initial immobilization solution, the residual solution, and each rinsing solution (V0=V1=V2j). (b) General equation for calculating enzyme loading in the flow-based immobilization process. The volumes of the collected residual and rinsing solutions may vary depending on sampling intervals and are measured using a micropipette. In this case, the initial volume V0 corresponds to the sum of the collected residual volumes (V0=∑V1i).

In flow immobilization, multiple residual solution volumes (V_{1i}) are progressively collected at regular time intervals. The total volume of residual solution thus corresponds to the initial immobilization solution volume ($V_0 = \sum V_{1i}$). A defined volume of rinsing solution ($\sum V_{2j}$) is then pushed through the membrane and also collected progressively as individual fractions (V_{2j}). Specifically, progressive loading (PL) can be monitored as the residual immobilization solution is collected over time (Eq.IV.2).

$$PL = V_{1i} \times (C_0 - C_{1i})\ [mg]$$

Eq.IV.2 - Equation for calculating progressive enzyme loading in the flow immobilization process

In both cases, the immobilization yield (%) is calculated as the ratio of the immobilized TA mass (L) to the total mass of TA initially introduced during immobilization ($V_0 \times C_0$) (Eq.IV.3).

$$Immobilization\ yield = \frac{L}{V_0 \times C_0} \times 100\ [\%]$$

Eq.IV.3 - Equation for calculating immobilization yield in batch and flow immobilization process

IV.2.3 Catalytic Test : AS of R-2-Fluoro-α-methylbenzylamine ((R)-FMBA).

The asymmetric synthesis (AS) of (R)-2-fluoro-α-methylbenzylamine ((R)-FMBA) was carried out using either free or immobilized *Ts*RTA. Typically, a reaction mixture (RM) containing 2'-fluoroacetophenone (FAP) as the amino acceptor and isopropylamine (ISO) as the amino donor was prepared using optimized concentrations to favor equilibrium shifting while avoiding enzyme inhibition.

The reaction was carried out using an excess of ISO. Typically, ISO (250 mM) was added to solution buffer (HEPES 0.1 M buffer, PLP 1 mM), and the pH was adjusted to 8 using concentrated HCl (37%). Subsequently, FAP (25 mM) was added to the solution, which was then exposed to *Ts*RTA, either in its free or immobilized form, to initiate the

biocatalytic reaction. While this preparation protocol was consistent, specific considerations must be addressed depending on the type of reactor used for the catalytic assay.

IV.2.3.1 Catalytic Test : Set-ups

- **In Batch Reactor**

Similarly to Meersseman Arango *et al* procedure [29], the ISO solution was first transferred into a round-bottom glass flask, followed by the addition of the catalyst, and finally FAP.

Depending on the catalyst form (free or immobilized) and the membrane size (12M-PP_TA-B or 44M–PP_TA-B), different reaction volumes were used. Free enzymes and 12M membranes were typically tested in 5 mL of reaction mixture in small round-bottom flasks, whereas catalytic assays involving 44M membranes were performed in 50 mL of reaction mixture. In all cases, reactions were carried out at 35 °C (the optimal temperature for *Ts*RTA activity) under moderate magnetic stirring, for variable incubation times.

- **In Dead-end Flow Reactor**

Dead-end flow catalytic testing was performed using the 12M membrane. The membrane, previously exposed to the immobilization solution under dead-end flow conditions (resulting in 12M-PP_TA-F), was directly exposed to the (RM) after completion of the rinsing steps—without being removed from the Whatman cell between immobilization and catalytic testing. A new syringe, prefilled with 5 mL of RM, was connected to the Whatman device containing the freshly prepared 12M-PP_TA-F and mounted on a syringe pump. A defined flow rate was applied to drive the RM through the membrane, and the permeate was collected at the outlet in 1.5 mL microtubes for subsequent GC analysis (Fig.IV.3). In contrast to batch-mode assays, the flow-based catalytic tests were conducted at room temperature.

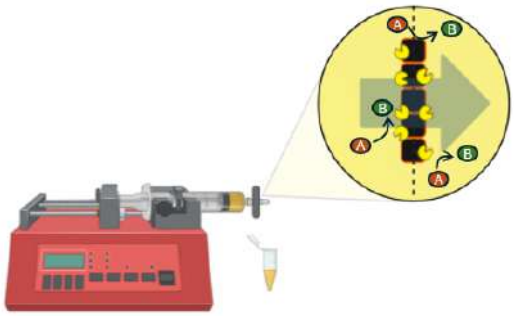

Fig.IV.3 - Illustration of flow dynamics during catalytic operation in the single-path dead-end flow setup. The reaction mixture (RM), driven at a defined flow rate set on the syringe pump, is perpendicularly directed through the biocatalytic membrane. In this configuration, all components—substrates and (co)products—pass through the membrane pores. Labels (A) and (B) correspond to the substrates (FAP/ISO) and the (co)products (FMBA/acetone), respectively.

- **In Reciruclating Tangential Flow Reactor**

Recirculating tangential flow catalytic testing was performed using 44M membranes previously functionalized by batch-mode immobilization (44M-PP_TA-B).

The general set-up employed is represented in Figs.IV.4 (left). The catalytic assay was conducted in a tangential flow setup composed of a pump connected to a membrane holder and a reaction vessel via PTFE tubing. Pressure and flow rate were monitored using pressure gauges positioned on both sides of the membrane holder and a flow monitor, respectively. Flow rate was controlled via a frequency drive connected to the pump.

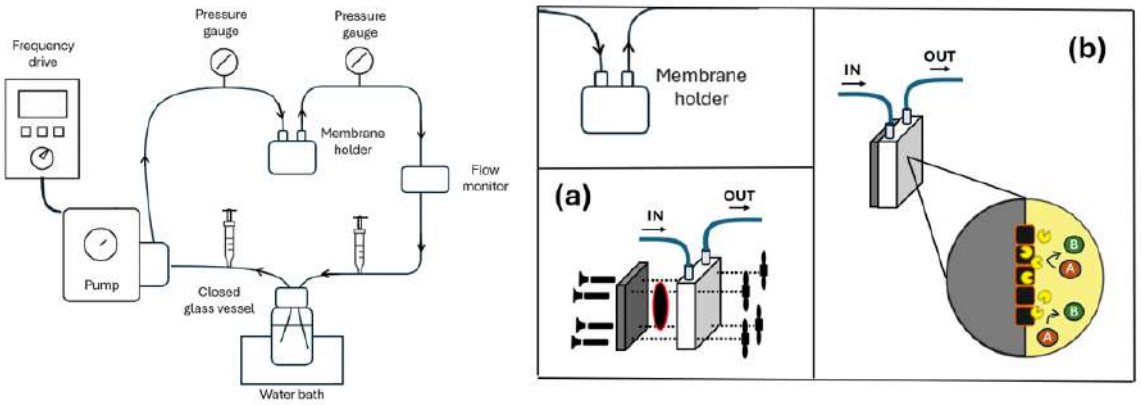

Figs.IV.4 – (Left) Typical setup used in the recirculating tangential flow system for catalytic testing (closed system). The reaction mixture (RM), contained in a sealed glass vessel, is maintained at 34 °C using a temperature-controlled water bath and recirculated through the system via PTFE tubing using a pump controlled by a frequency drive. The RM is tangentially exposed to the biocatalytic membrane within the membrane holder. To monitor the system, two pressure gauges (positioned at the inlet and outlet of the membrane holder) and a flow monitor are employed. Additionally, two syringes are installed at the inlet and outlet lines of the membrane holder to collect samples for analysis. (Right) membrane holder used in the recirculating tangential flow system for catalytic testing. (a) Schematic showing the positioning of the membrane within the setup. The membrane is clamped between a metallic plate and a perforated plastic distribution plate using tightly sealed nuts. In this configuration, only one side of the membrane is exposed to the reaction mixture (RM). (b) Illustration of flow dynamics during catalytic operation. Substrates are tangentially delivered to the membrane surface on the side of the plastic plate. The RM is continuously introduced and withdrawn through inlet and outlet PTFE tubing, respectively. Labels (A) and (B) correspond to the substrates (FAP/ISO) and the (co)products (FMBA/acetone), respectively.

The membrane was mounted between a metallic base plate and a perforated plastic distribution plate, both sealed with nuts to form the membrane holder assembly (Figs.IV.4 (right) (a)). In this configuration, only one face of the membrane was exposed to the RM, which was tangentially introduced and removed through inlet and outlet ports connected to the tubing system (Figs.IV.4 (right) (b)). The RM, maintained under constant magnetic stirring, was contained in a closed glass vessel (100 or 200 mL) and held at 34 °C using a thermostatic water bath. The inlet and outlet PTFE tubes entered the RM vessel through a tightly sealed cap. Sampling ports were integrated by attaching syringes to both the inlet and outlet lines via metal needles, allowing periodic collection of RM for GC analysis (Figs.IV.4 (left)).

Two tangential flow configurations, each using a different pump with distinct flow rate capacities, were investigated (Annex IV.S7). Setup 1, equipped with pump A, included all the components described above, with a total tubing length of 535–545 cm. It operated

with 100 mL of RM (in a 200 mL glass vessel) recirculated at flow rates of 50, 150, and 300 mL/min. Setup 2, equipped with pump B, was simplified (no flow monitor, shorter tubing length = 310-320 cm) and used for catalytic testing with 50 mL of RM recirculated at 150 mL/min.

IV.2.3.2 Sample Analysis

To determine the concentrations of the various components, collected samples from the catalytic tests were prepared for GC analysis (Annex IV.S8).

Typically, 100 µL of the reaction mixture was transferred into a 1.5 mL microtube, followed by the addition of 25 µL of 2 M sodium hydroxide (NaOH) to quench the reaction and deprotonate amines, thereby facilitating extraction into the organic phase. After vortexing for a few seconds, 400 µL of dichloromethane (DCM) was added, vortexed again briefly, and allowed to stand for 5 minutes to enable the extraction of reactants (ISO, FAP) and products (FMBA, acetone) into the organic phase. The upper aqueous phase was then transferred to a new microtube for a second DCM extraction. This extraction step was repeated a third time. The three organic phases were pooled into a single GC vial for analysis (Annex IV.S8). The resulting peak areas were converted to concentrations using previously established calibration curves (Annex IV.S9).

IV.2.3.3 Catalytic Activity Assessment

To evaluate the catalytic performance of the enzyme, several indicators were used, including conversion, yield, and specific activity. At a given time (t), conversion corresponds to the amount of FAP converted, while yield refers to the amount of FMBA formed, both expressed relative to the initial amount of FAP (FAP_0) (Annex IV.S10).

To enable an effective comparison of the results obtained across different setups and time scales, productivity—expressed in µmol FMBA produced per hour—was calculated by dividing the total amount of FMBA produced (measured concentration multiplied by the sample volume, in µmol) by the reaction time (h). When dead-end flow catalytic tests are performed, the space–time yield (STY), a typical indicator for evaluating flow process efficiency, can also be determined (Eq.IV.S3).

Specific activity is particularly useful for comparing data across different experiments, as it provides a normalized indicator that accounts for both reaction time and the amount of enzyme involved. It is defined as the number of micromoles of (R)-2-fluoro-α-methylbenzylamine (FMBA) produced per minute per milligram of enzyme. The method of calculation varies depending on the type of catalytic test employed (Eq.IV.4).

$$(A)\ Specific\ activity\ (t) = \frac{[FMBA]_t \times V_t}{t \times L}[\mu mol_{FMBA}.min^{-1}.mg_{TA}^{-1}]$$

$$(B)\ Specific\ activity\ (t) = \frac{[FMBA]_t \times F}{L}[\mu mol_{FMBA}.min^{-1}.mg_{TA}^{-1}]$$

Eq.IV.4 - (A) Equation used to determine the specific activity in batch and recirculating tangential flow systems. [FMBA]t is the concentration of FMBA at a given time (in µmol/mL), t is the reaction time (in minutes), V_t is the volume of the reaction mixture at time t (in mL), and L is the immobilized enzyme loading (in mg), determined by mass balance using the Bradford assay. (B) Equation used to determine the specific activity in the dead-end flow system. [FMBA]t is the concentration of FMBA at a given time (in µmol/mL), F is the flow rate set on the syringe pump (in mL/min), and L is the immobilized enzyme loading (in mg), determined by mass balance using the Bradford assay.

V. Results and Discussion

In the following section, only a limited quantity of enzyme was used for both the immobilization and catalytic testing experiments due to restricted enzyme availability. Consequently, the catalytic performance results obtained are expected to be significantly lower than those typically reported in the literature.

V.1 Batch immobilization and Reaction : Scale-up and Reproducibility

Although batch reactors are not the primary focus of this study, it is relevant to briefly assess their efficiency with membranes of different sizes. Previous studies have examined membranes with surface areas of 5 and 7 cm^2 [29,30], whereas the present work employed membranes of 1.13 and 15.21 cm^2 (for 12M and 44M membrane, respectively) for dead-end and tangential-flow catalytic investigations, respectively. Batch-mode immobilization and catalytic tests were therefore conducted to confirm reproducibility with previous results [30] and to ensure that subsequent flow-experiment outcomes are not influenced by scale-dependent factors such as volume or concentration.

V.1.1 Immobilization and Catalytic Test

Tab.V.1 presents key metrics for all membranes whose immobilization was performed in batch. These results serve as a reference for the following section. Both 12M and 44M were investigated in batch (B) for immobilization and catalytic testing. In addition, part of the 44M membranes immobilized in batch were also used for tangential flow experiments (further comments are provided in Section V.3). To identify the membranes, an identification number—based on the preparation timeline—was placed after the final hyphen.

Tab.V.1 - Main metrics used to evaluate immobilization efficiency (loading per surface area and immobilization yield) and biocatalytic performance (specific activity) of membranes used in batch mode. Membranes with diameters of 12 and 44 mm—referred to as 12M-B and 44M-B, respectively—were employed. The final number in the membrane name corresponds to an identification number based on the preparation timeline. For immobilization, different volumes, concentrations, and process times were employed. More detailed conditions are provided in Tab.V.S1. For catalytic tests, membranes were immersed in RM containing 250 mM ISO and 25 mM FAP in 0.1 M HEPES with 1 mM PLP, maintained at 35 °C for 20 h.

Membrane from batch immobilization (loading)	Loading per surface area [mg_{TsRTA}/ cm^2]	Immobilization yield [%]	Type of reactor used for catalytic test	Sp. Activity after 20 h [$\mu mol.mg^{-1}.min^{-1}$]
12M Membrane (Diameter 12mm – Surface area : 1.13 cm^2)				
12M-B-1 (0.071 mg)	0.063	8	Batch	0.032
12M-B-2 (0.147 mg)	0.130	15	Batch	N.A.
12M-B-3 (0.044 mg)	0.038	2	Batch	0.046
12M-B-4 (0.113 mg)	0.1	6	Batch	0.020

12M-B-5 (0.166 mg)	0.147	9	Batch	0.009
44M Membrane (Diameter 44mm – Surface area : 15.21 cm^2)				
44M-B-1 (2.853 mg)	0.188	24	Batch	0.006
44M-B-2 (1.340 mg)	0.088	35	Tangential flow	See section V.3
44M-B-3 (1.249 mg)	0.082	31	Tangential flow	See section V.3
44M-B-4 (1.394 mg)	0.092	39	Tangential flow	See section V.3
44M-B-5 (4.040 mg)	0.266	37	Batch	0.010
44M-B-6 (3.417.mg)	0.225	33	Tangential flow	See section V.3

In addition to the typical 20 h catalytic tests, batch catalytic tests involving 44M-B-5 membranes and free TsRTA were also performed over a longer time scale in an attempt to reach equilibrium conversion. The conversion over time are shown in Fig.V.1.

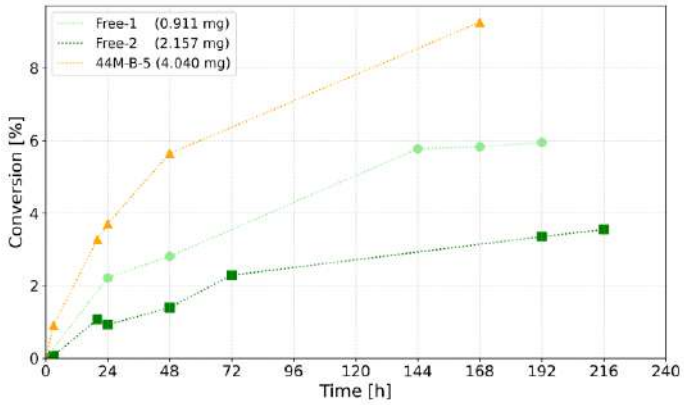

Fig.V.1 - Conversion over time for free and immobilized (44M-B-5) enzyme activity. Batch catalytic tests were performed with a typical RM (250 mM ISO, 25 mM FAP in 0.1 M HEPES with 1 mM PLP) maintained at 35 °C. Volumes of 50 mL and 4 mL were used for the 44M-B-5 and free TA tests, respectively.

V.1.2 Discussion

Some evaluation of biocatalytic preparation and catalytic performance was performed to improve the comprehension of the process and facilitate the comparison with flow processes. Here a brief comment.

Comparing the results obtained for 12M and 44M in Tab.V.1, the 44M membrane logically immobilized more enzymes than 12M due to its higher availability of binding sites, and consequently demonstrated higher productivity. However, such results do not truly allow an evaluation of the scalability of the process, which requires more randomized indicators.

Deeper investigations, presented in Annex V.S1 and Annex V.S2, demonstrated that batch immobilization and catalytic tests are relatively scalable. While the immobilization yield appeared relatively stable, enzyme loading increased proportionally with the concentration of the immobilization solution, independently of the membrane area (Annex V.S1 and Figs.V.S1). This suggests that the number of fixation sites was not a limiting factor for enzyme immobilization under the conditions tested (at least within the concentration range investigated). For similar incubation times, a comparable increase in

loading per surface area is therefore expected for membranes of different sizes when using the same enzyme concentration (Annex V.S1). Regarding the catalytic performance of 12M membranes, the amount of immobilized enzyme appeared to influence enzymatic activity, which tended to decrease proportionally with increasing loading (Annex V.S2 and Fig.V.S3). The similar range of specific activities obtained for 12M and 44M membranes with the closest loading per surface area (12M-B-5 and 44M-B-1) confirms that batch catalytic tests are relatively scalable (Figs.V.S2 and Fig.V.S3). However, an optimal comparison is not feasible, as the enzyme loadings per surface area were not identical. In addition, the tendency for specific activity to decrease, observed for 12M membranes, was no longer evident for 44M membranes. Characterized by higher loadings per surface area, the 44M membranes instead exhibited relatively stable specific activity across the tested loading range, as illustrated in Fig.V.S3.

As demonstrated in the work of Meersseman *et al.* [30], the immobilized enzyme (44M-B-5) exhibited higher productivity than the free form (Fig.V.1 and Tab.V.2). As noted by Meersseman *et al.*, this improvement in productivity may result from a more favorable microenvironment provided to the enzymes by hydrophilic compounds such as PDA and PEI, originating from the membrane functionalization [201,221]. Regarding the conversion trend observed in Fig.V.1, it appears unexpectedly less efficient than that obtained in the work of Meersseman et al., as only ~8% conversion was achieved after about 150 h of catalytic testing, whereas at the same time FAP conversion in the Meersseman study tended to stabilize around 35–40%. This difference could be partially explained by differences in the reaction mixture, since 10% v/v methanol was used as a co-solvent in their case. Nevertheless, equilibrium conversion could not be reached in this study, where the catalytic test was performed over nine days, while at least two weeks was required to reach equilibrium Annex V.S3 [30].

When comparing more precisely the results obtained for catalytic tests with those of the previous study over a shorter time (Tab.V.2), one can assume that the process is relatively reproducible, as similar results were obtained.

Tab.V.2 - Specific activity of different biocatalytic systems obtained after 20 h of batch catalytic testing. All catalytic tests were performed in batch with the same reaction mixture (25 mM FAP, 250 mM ISO in 0.1 M HEPES with 1 mM PLP). Note: Different volumes were used depending on the catalyst type and membrane area.

Type of Catalyst	Surface area [cm2]	Loading per Surface Area [mg_{TsRTA}/ cm^2]	Specific activity [$\mu mol.mg^{-1}.min^{-1}$]	Source
12M-B-5 (0.166 mg)	1.13	0.147	0.0090	This study
44M-B-1 (2.853 mg)	15.21	0.188	0.0063	This study
30M-B (~1.650 mg)	7	0.236	0.0051	Meersseman et al. [30]
44M-B-5 (0.266 mg)	15.21	0.266	0.0095	This study
Free 1 (0.911 mg)	x	x	0.0017	This study
Free (~1.500 mg)	x	x	0.0017	Meersseman et al. [30]

Comparing the results previously obtained by Meersseman *et al*. [30], the biocatalytic results obtained in this study suggest an equivalent, or even better, enzymatic activity than those reported earlier. When comparing biocatalytic membranes with the closest loading per surface area, 44M-B-1 and the previously investigated 30M-B appear to exhibit a similar activity range, with the slightly lower values being consistent with previous considerations (Annex V.S2). The identical specific activity obtained in batch catalytic tests with the free enzymes[9] suggests that the activity of TsRTA—originating from different batches and slightly different final production steps—remains comparable. These results therefore demonstrate that the enzymes produced through slightly different processes, as well as the biocatalytic membranes prepared in this study, exhibit performances similar to those reported in earlier work.

Altogether, these results suggest that batch processes are scalable and reproducible—at least over the first 20 hours of catalytic testing—providing an optimal reference for further comparison with flow results.

V.2 Dead-end Flow processes Investigation

To perform immobilization and catalytic test in dead-end flow mode (flow-through), 12M membranes (1.13 cm^2) were used, and different types of syringes—glass and plastic—were evaluated. The reader should be aware that several technical challenges arose while implementing this operation mode (syringe deformation, leaks, etc.); their description and resolution are described in Annex V.S4.

V.2.1 Immobilization

In the following section, different membranes are referred to in a manner similar to that presented in Section V.1. As three different flow rates were investigated (0.5, 1, and 1.5 mL/h) for immobilization, the 12M membranes were defined by the DF label, standing for "Dead-end Flow," followed by the corresponding flow rate (12M-DF0.5, 12M-DF1, and 12M-DF1.5). Additionally, an identification number based on the preparation timeline was added at the end of the membrane name when the same strategy was employed multiple times. The different experimental conditions of the resulting membranes are provided in Annex V.S5.

V.2.1.1 Experimental Loading and Loading Profile

The loading, corresponding to the total amount of enzyme immobilized at the end of the immobilization process (including rinsing steps), obtained for each flow rate is presented in Fig.V.2.

[9] In the case of free enzymes , performance should not be influenced by the amount of enzyme involved, unlike in biocatalytic membranes.

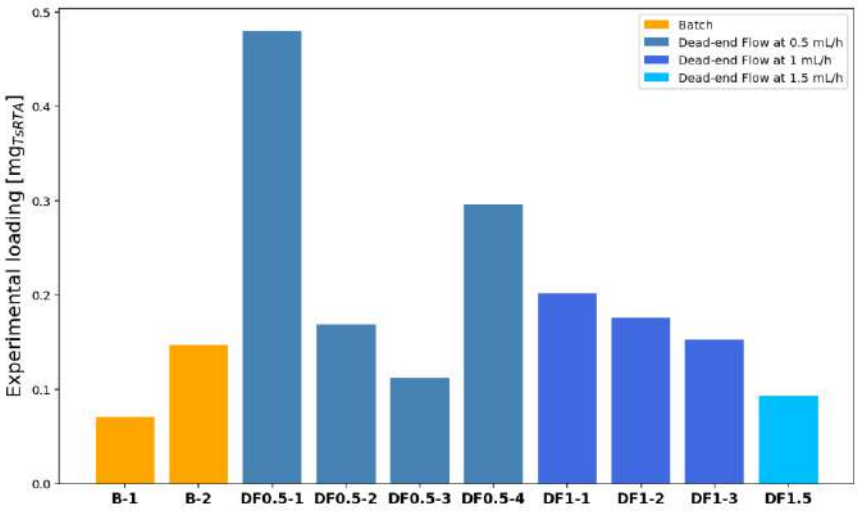

Fig.V.2 - Experimental loading obtained using Batch (B) and Dead-end Flow (DF) strategies. All immobilizations were performed on 12 mm diameter membranes (pre-functionalized), using a TsRTA solution (3.5-4mL) prepared in HEPES buffer (0.1 M, PLP 1 mM, pH 8) at a fixed concentration of 0.25 mg/mL. For flow-based immobilization, the solution volume ranged from 3.5 to 4 mL and was contained in Luer-lock plastic syringes. Three flow rates were investigated: 0.5 mL/h (DF0.5 - 4 replicates), 1 mL/h (DF1 - 3 replicates), and 1.5 mL/h (DF1.5 - 1 replicate), referred to as 12M-DF0.5, 12M-DF1, and 12M-DF1.5. Note: The number indicated after the hyphen serves to identify membranes when identical processes were employed. This number was assigned according to the chronological order of the experiments.

A maximum loading of 0.48 mg of TsRTA was achieved with sample 12M-DF0.5-1 at a flow rate of 0.5 mL/h, while only 0.071 mg was immobilized in the least efficient case (12M-B-1) under batch conditions. This initial observations suggest that batch immobilization generally results in lower immobilization efficiency compared to flow-based processes. Furthermore, immobilization efficiency appears to be influenced by the flow rate, with a decreasing trend observed as the flow rate increases.

The loading dynamics, which depend on the dead-end flow rate, can be analyzed from the cumulative loading profiles shown in Fig.V.3, presenting data for samples 12M-DF0.5-4, 12M-DF1-1, and 12M-DF1.5.

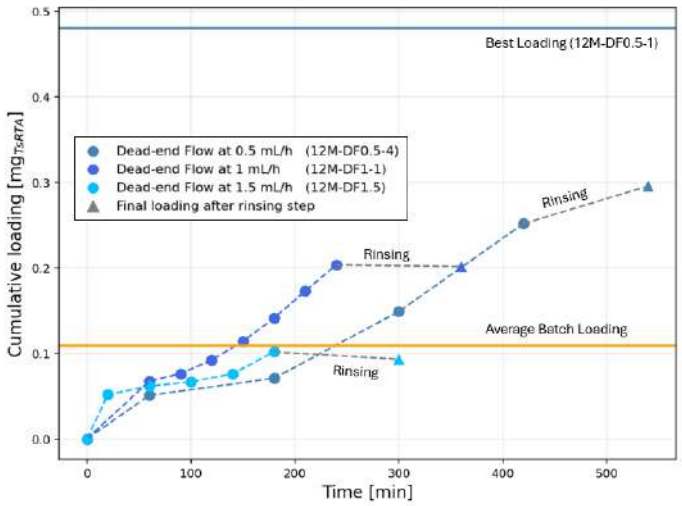

Fig.V.3 - Cumulative TsRTA loading (mg) over time for three membranes subjected to different radial flow rates (12M-DF0.5-4, 12M-DF1-1, and 12M-DF1.5-1). Each data point represents an experimental measurement. The final point

corresponds to the actual amount of immobilized TsRTA measured after the rinsing step. For all three radial flow experiments, a rinsing duration of 2 hours was considered; this value is arbitrary and was used solely to enhance graphical representation. The loading value shown for the batch process corresponds to the average of two batch immobilization experiments (12M-B-1 and 12M-B-2). Note: While immobilization was completed at the end of the immobilization step for 12M-DF1-1 and 12M-DF1.5, continued immobilization was observed during the rinsing step for 12M-DF0.5-4 (final loading resulting from rinsing step, represented by triangle, is higher than the last experimental point of cumulative loading).

For three flow rates investigated, a higher amount of enzyme is logically immobilized at the beginning of the process, when a greater number of available binding sites (epoxide functions from the GDE) are present on the membrane surface—resulting in a steeper initial slope. After the first few minutes, the immobilization rate appears to stabilize, depending on the selected flow rate. Across the three profiles considered, maximum immobilization does not appear to be reached, as loading continues to increase gradually while the solution passes through the membrane[10]. This observation suggests that free binding sites remain available for further TsRTA immobilization. This interpretation is consistent with the fact that up to 0.48 mg of TsRTA was successfully immobilized in the most efficient experiment (12M-DF0.5-1), indicating that the immobilization capacity of a 12M membrane can reach at least this value under certain conditions.

V.2.1.2 Impact of Fow Rate on Enzyme Immobilization Efficiency

To ensure meaningful comparison between the different immobilization strategies, the immobilization yield was calculated (Annex V.S5). As the experimental conditions (concentration and volume of the immobilization solution) are similar, the overall trend observed for immobilization yield is consistent with that of the experimental loading (Fig.V.2). To effectively compare batch and flow immobilization, and to evaluate the effect of flow rate, the average immobilization yield for each strategy (Batch, DF0.5, DF1, and DF1.5) and their associated theoretical loading was presented in Fig.V.4.

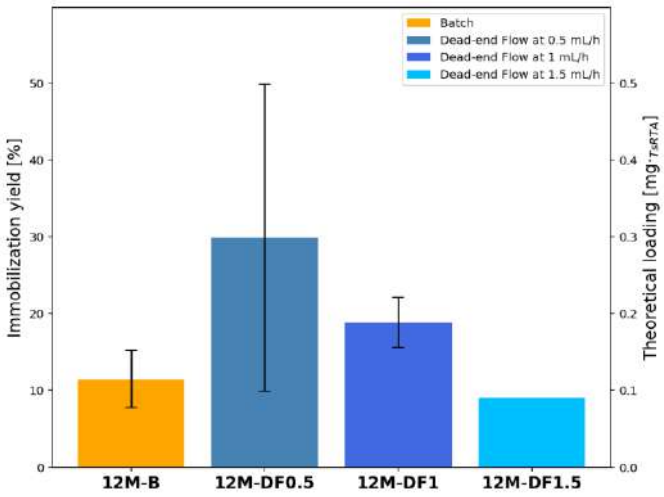

Fig.V.4 - Immobilization yields—and the resulting theoretical loading—obtained using obtained using Batch (B) and Dead-end Flow (DF) strategies. All immobilizations were performed on 12 mm diameter pre-functionalized membranes,

[10] The final, flatter portion of the curve should not be considered, as it corresponds to the passage of the rinsing solution through the membrane.

using a TsRTA solution prepared in HEPES buffer (0.1 M, PLP 1 mM, pH 8) at a fixed concentration of 0.25 mg/mL. For flow-based immobilization, the solution volume ranged from 3.5 to 4 mL and was contained in Luer-lock plastic syringes . Three flow rates were investigated: 0.5 mL/h (4 replicates), 1 mL/h (3 replicates), and 1.5 mL/h (1 replicate), referred to as 12M-DF0.5, 12M-DF1, and 12M-DF1.5, respectively. Theoretical loading was calculated based on the immobilization yield, assuming that 0.4 mL of the 0.25 mg/mL immobilization solution was used for both batch and dead-end flow immobilization. Error bars represent standard deviations, where applicable.

For a similar immobilization solution volume, a greater quantity of enzyme appears to be immobilized when lower immobilization flow rates are used, as illustrated in Fig.V.4 and Fig.V.5.

At a flow rate of 0.5 mL/h (DF0.5), approximately 30% of the enzyme initially present in the solution was immobilized (representing theoretical loading of 0.300 mg). This condition resulted in immobilization that was approximately 2.5 times more effective than in batch mode, and 1.5 and 3 times more effective than immobilizations performed at 1 mL/h (DF1) and 1.5 mL/h (DF1.5), respectively (Fig.V.4 and Annex V.S5). Although promising, this apparent improvement in immobilization at low flow rates should be interpreted with caution, as high variability was observed for the DF0.5 condition (CV = 66.98%). While the best-performing membrane (12M-DF0.5-1) showed excellent results, with a TsRTA loading of 0.480 mg (Figure 3) and an immobilization yield of 58%, 12M-DF0.5-2 and12M-DF0.5 -3 were less effective (19% and 12%, respectively), showing yields lower than those obtained at DF1 (~20%) and, in some cases, comparable to those from batch mode. The results obtained for DF1 appear more reliable in supporting the advantages of flow-based systems in improving immobilization efficiency. Indeed, the three replicates demonstrated better reproducibility and stability (CV = 17.31%) while yielding an immobilization efficiency of approximately 20% (representing a theoretical loading of 0.200 mg)—around 1.6 times higher than that achieved in batch mode(Fig.V.4 and Annex V.S5). Finally, the single experiment conducted at DF1.5 resulted in an immobilization yield similar to, or slightly lower than, that of the batch system (Fig.V.4 and Annex V.S5). However, this result should be interpreted with caution due to the absence of experimental replication.

While immobilization yield is an excellent indicator, it only evaluates the proportion of enzyme effectively immobilized relative to the amount initially exposed to the membrane, without considering immobilization time. However, flow-based immobilization also significantly reduces the immobilization time—a key factor in overall process efficiency. For a typical flow immobilization using 4 mL of solution, complete immobilization is achieved after 8 h, 4 h, and 2 h 40 min for DF0.5, DF1, and DF1.5, respectively—substantially faster than the standard 18 h incubation used in batch processes (excluding the rinsing step). This improvement in processing time is illustrated in Fig.V.3. An enzyme loading approximately equivalent to that obtained in batch mode is reached after just over 2 h and 4 h for DF1 and DF0.5, respectively. Even DF1.5, despite showing low immobilization efficiency (at identical immobilization volume), appears relevant, as nearly the same quantity of enzyme is immobilized but in a significantly shorter time.

Therefore, both enzyme loading and process time must be considered simultaneously when evaluating immobilization performance.

To evaluate both parameters and identify general patterns, the experimental loadings obtained from different experiments were normalized based on volume and time (Tab.V.S3). Assuming that the immobilization solution concentration is identical across all experiments, the averages for the different immobilization strategies are presented in Fig.V.5 to facilitate comparison. As expected (given the comparable volumes used), the loading per unit volume profile is similar to that observed for immobilization yield (Fig.V.4). However, the loading per unit time reveals a different dynamic.

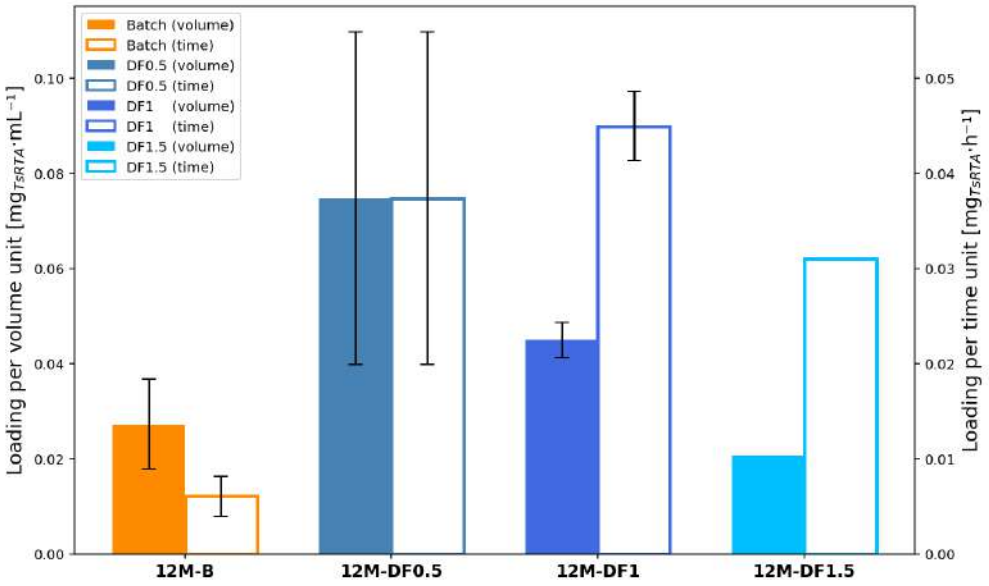

Fig.V.5 - Average loading per unit volume and per unit time obtained using Batch (B) and Dead-end Flow (DF) immobilization strategies. All immobilizations were performed on 12 mm diameter pre-functionalized membranes, using a TsRTA solution prepared in HEPES buffer (0.1 M, PLP 1 mM, pH 8) at a fixed concentration of 0.25 mg/mL. For flow-based immobilization, the solution volume ranged from 3.5 to 4 mL and was contained in Luer-lock plastic syringes .Three flow rates were investigated: 0.5 mL/h (4 replicates), 1 mL/h (3 replicates), and 1.5 mL/h (1 replicate), referred to as 12M-DF0.5, 12M-DF1, and 12M-DF1.5, respectively. Error bars represent standard deviations, where applicable.

In the case of flow processes operated in single-pass mode, the volume pushed through the membrane and the process duration are inherently determined by the selected flow rate, whereas in batch mode, volume and incubation time are independent variables. For a given batch volume, an improvement in immobilization could thus potentially be observed with increased incubation time. While both indicators are relevant for comparing flow processes among themselves, loading per unit time appears to be the most appropriate comparison metric for evaluating batch versus flow processes—especially when equivalent volumes are used.

In correlation with the immobilization yield results, the loading per unit volume (filled bars, Fig.V.5) obtained in batch mode appears generally lower than that of the flow processes. Among the flow conditions, the average loading per unit volume tends to decrease with increasing flow rate. Regarding process time efficiency (empty bars, Fig.V.5), all flow experiments are markedly superior to batch immobilization. Compared

to volumetric loading, the ranking of flow processes appears less clear when considering time-based efficiency, and DF0.5 does not necessarily emerge as the most effective immobilization strategy. While less relevant when focusing solely on volume, DF1 emerges as a time-efficient condition that is equally, if not potentially more, effective than DF0.5— considering the high variability observed in DF0.5 immobilization, largely due to sample 12M-DF0.5-1. If this observation is to be confirmed, a balance must be found between resource consumption and process duration. Since fewer enzymes are immobilized per unit volume of solution at higher flow rates, achieving equivalent total loading would require larger volumes of immobilization solution. Therefore, the choice of optimal flow rate should consider not only loading efficiency and time savings but also reagent -enzymes- usage.

However, these results must be interpreted with caution (as in the case of immobilization yield results) due to the high variability observed in some results (particularly for batch and DF0.5 processes), the lack of replicates (for DF1.5), and the potential influence of concentration variations. Additional experimental repetitions appear thus necessary to confirm these observations. In addition, careful consideration should also be given to the reliability of the system and the chosen strategy. Indeed, volume losses may occur during the transition between the immobilization and rinsing solutions—particularly problematic during the first rinse, which may still contain a portion of the immobilization solution due to dead volume. Ideally, another system without solution exchange between the immobilization and rinsing steps should be thus, considered.

V.2.1.3 Discussion

Impact of Reactor Type on Immobilization

Despite the necessary caution in interpreting the reported values, flow processes clearly demonstrated improved immobilization with a significant reduction in time compared to batch processes. This observation appears both consistent and reasonable. As flow processes force the immobilization solution through the membrane (i.e., pressure-driven processes), one can assume a facilitated exposure of enzymes to the binding sites (epoxide functions of the GDE)—some of which may be less accessible in batch mode (membrane porosity) —compared to batch processes, where enzyme–binding site contact relies primarily on heterogeneous agitation and diffusion phenomena.

In this context, a question also arises regarding the localization and distribution of enzymes immobilized via flow processes. Indeed, it can be hypothesized that these enzymes are immobilized in a manner different from that observed in batch mode, likely involving greater exploitation of the internal surface area within the membrane porosity. For an equivalent overall enzyme loading, a different spatial distribution of immobilized enzymes could be expected: dead-end flow immobilization may promote a more uniform distribution across both the external and internal surfaces of the membrane, whereas

batch immobilization likely results in enzyme deposition primarily on the external surface. Among possible mechanisms for such flow-through enzyme immobilization [205], complete entrapment and cake layer formation appear unlikely, as the enzyme size (a few nanometers) is significantly smaller than the average membrane pore size (200–400 nm). As membrane was functionalized with reactive functions, it can be assumed that immobilization is primarily due to covalent grafting (GDE-TsRTA biding) enhanced by pressure-driven forces, although minor contributions from cross-linking (due to GDE) and adsorption phenomena (enhanced by PEI) are also likely. Supposing that these molecules was located in membrane porosity after batch functionalization as suggested in Meersseman et al. work [29], an enzyme distribution through the membrane porosity is thus expected. However, other tests aimed at evaluating potential variations in permeate flux could help determine the dominant flow-through immobilization mechanism—and thus the enzyme distribution—similarly to the approach described in Luo et al. works [192,206]. Additional characterization techniques, such as SEM and AFM, also appear relevant to further evaluate membrane properties. While SEM imaging was performed in [29] to assess membrane integrity after functionalization, new analyses before and after the immobilization step could provide insight into whether or not a cake layer forms during immobilization.

Impact of the Flow Rate on Immobilization

Concerning the influence of flow rate, the observed decrease in immobilization yield (loading efficiency) with increasing flow rate can logically be attributed to the reduced residence time of enzymes within the membrane, leaving less time for reaction with the epoxide groups of GDE. Increased turbulence and shear forces generated at higher flow rates could also—at least partially—explain a less efficient loading, although this effect is likely negligible given the relatively low flow rates investigated. Immobilization, being still observed at all tested flow rates, suggests that the forces acting on the enzyme–binding site–PEI complex are stronger than those generated by the syringe pump pressure. However, it can be hypothesized that beyond a certain critical flow rate, immobilization would no longer occur. While the observed tendency of decreased performance with increasing flow rate appears reasonable, it must be interpreted with caution due to the high variability of the results—particularly for 12M-DF0.5—which suggests that flow immobilization is not well controlled. One or more unidentified variables, beyond the flow rate, may be influencing immobilization efficiency. Potential contributing factors include the functionalization steps, the time elapsed between the end of functionalization and the start of immobilization, and temperature (which was not controlled during the dead-end flow immobilization experiments), all of which could significantly affect the outcome.

Improvement of the Process

Thanks to its higher immobilization efficiency and reduced enzyme waste, dead-end flow immobilization appears more economically favorable than batch processing, particularly

given the high cost of enzymes. However, the flow process remains largely characterized by substantial resource losses—the lowest enzyme waste being 42% in the case of the most efficient immobilization (12M-DF0.5-1)—primarily due to the system design. This highlights that the single-pass system used in this study may quickly become economically limiting, particularly given the high cost of enzymes. Alternative membrane flow systems -as well described in Meersseman *et al.* [25]- could therefore be envisioned, such as a recirculating dead-end flow system or configurations allowing simultaneous exposure of multiple membranes, to optimize the use of the immobilization solution.

V.2.2 Catalytic Test - Evaluation of Biocatalytic Performance

V.2.2.1 Reagents and Product Control

Once dead-end flow immobilization was completed, the biocatalytic membrane was exposed to the RM, as described in the Section IV.2.3.1, to perform catalytic tests under selected flow rates. Initial results revealed a clear discrepancy between the conversion of FAP (the limiting reagent) and the yield of FMBA (the targeted chiral product), indicating an unbalanced mass profile—while ISO appeared to remain stable[11] (Figs.V.6(left)). A disproportionately large decrease in FAP concentration was observed relative to the initial concentration in the RM—and compared with FMBA production (Figs.V.6(right))—suggesting FAP loss during the catalytic test. Additionally, residual FAP concentrations appear to be influenced by the selected flow rates, whereas ISO concentrations remain stable. Lower FAP concentrations were measured at lower flow rates (Fig.V.7). These issues complicate accurate estimation of enzymatic activity.[12].

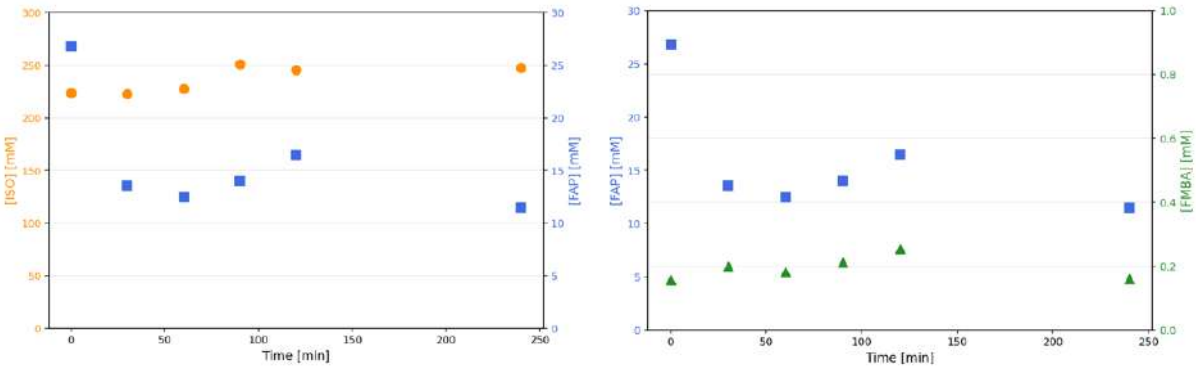

Figs.V.6 – (Left) ISO and FAP concentrations during a catalytic test performed under dead-end flow at 0.5 mL/h, using an initial reaction mixture containing 250 mM ISO and 25 mM FAP in HEPES buffer (0.1 M, PLP 1 mM, pH 8), with membrane 12M-DF0.5-3. (Right) FAP and FMBA concentrations during a catalytic test performed under dead-end flow

[11] Since ISO is present in large excess, a slight variation would not significantly impact the evaluation of the catalytic performance of the immobilized enzymes.

[12] The FAP concentration in the RM (25 mM) was selected to ensure optimal enzyme activity.

at 0.5 mL/h, using an initial reaction mixture containing 250 mM ISO and 25 mM FAP in HEPES buffer (0.1 M, PLP 1 mM, pH 8), on membrane 12M-DF0.5-3.

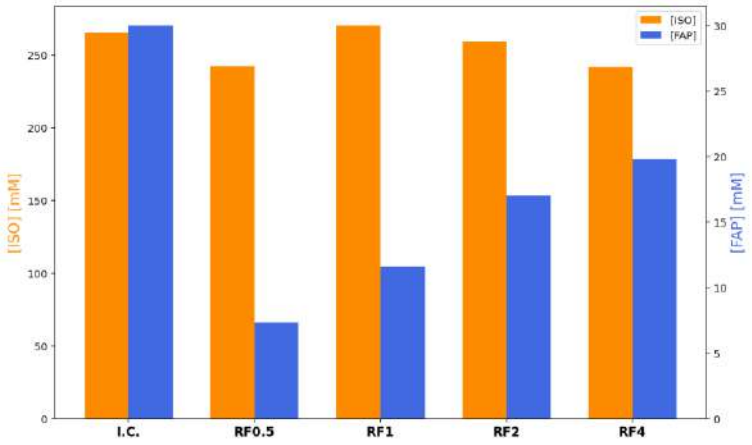

Fig.V.7 - ISO and FAP concentrations as a function of flow rate during catalytic tests, using an initial reaction mixture containing 250 mM ISO and 25 mM FAP in HEPES buffer (0.1 M, PLP 1 mM, pH 8), on membrane 12M-DF1-3. Four flow rates were tested: 0.5, 1, 2, and 4 mL/h. I.C. refers to the initial concentration measured before the start of the flow test.

To explain this apparent loss of reagent, two hypotheses were considered: (i) adsorption of FAP onto the internal surface of plastic syringes during and tubing the catalytic test, and (ii) evaporation of FAP due to the experimental setup. To evaluate both possibilities, experimental tests were conducted on the FAP reagent. While FMBA concentration does not appear to be affected, these experimental tests were also conducted on the FMBA product to confirm that no product was lost during the catalytic test and that the measured concentrations accurately reflected the total product formed by enzymatic activity. The strategies employed and the corresponding results are presented in Annex V.S6.

While no FMBA loss is observed (Fig.V.S6 and Fig.V.S8 (right)), results showed that the disappearance of FAP could be attributed to both evaporation and adsorption phenomena, with adsorption contributing only marginally. Pre-saturating the syringe with pure FAP solution and allowing it to sit overnight before the catalytic test effectively prevented FAP loss due to adsorption (Fig.V.S7). Regarding evaporation—which appeared to be the main cause of FAP disappearance—tests indicated that the open nature of the system (exposed to ambient air) promoted the loss of residual FAP-containing solution (after it passed through the membrane) during droplet formation. This stage is particularly susceptible to evaporation due to the high liquid–air surface area before the droplet is collected in the tube. This hypothesis was confirmed by isolating the residual solution from ambient air during collection, which completely prevented FAP loss (Fig.V.S8 (left)).

As the current experimental setup cannot operate in a fully closed configuration, subsequent catalytic tests will be conducted in an open system using pre-saturated syringes to minimize adsorption. FAP disappearance is assumed to occur only after membrane exposure. Therefore, the concentration available to the enzymes is expected to remain well above the threshold at which enzymatic performance would decline (~10

mM [30]), ensuring maximal activity. Catalytic performance indicators will be calculated from measured FMBA concentrations rather than FAP, as FMBA levels were stable and reliable.

V.2.2.2 Catalytic performance Evaluation

As only very small amounts of enzyme are used in the catalytic tests - due to the limited and costly enzyme stock - low conversion rates and FMBA production are expected in the following results.

Among all the membranes successfully immobilized in dead-end flow mode, various biocatalytic tests were conducted: membranes 12M-DF0.5-1, 12M-DF0.5-2, 12M-DF0.5-3, and 12M-DF1-2 were used to perform biocatalytic tests under a fixed flow rate, while membranes 12M-DF0.5-4 and 12M-DF1-3 were employed to screen different flow rates[13].

Evaluation at Constant Flow Rate

Production Profile

The progressive FMBA production of the three membranes investigated under constant 0.5 mL/h flow rate[14] - exhibiting different loading - over a time scale ranging from 4 to 5 hours (across two days) is presented in Figs.V.8 (left).

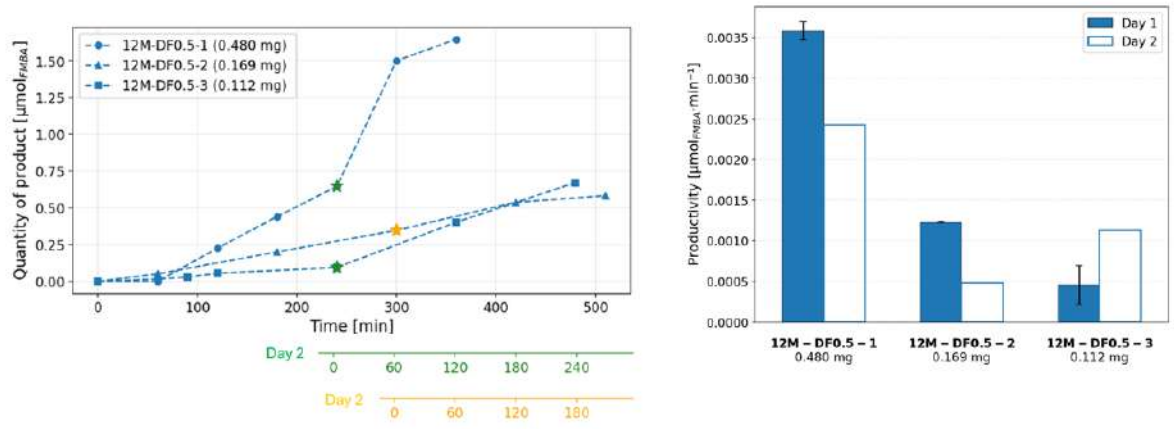

Figs.V.8 – (Left) Quantity of FMBA (expressed in µmol) produced over time for membranes 12M-DF0.5-1, 12M-DF0.5-2, and 12M-DF0.5-3. All biocatalytic tests were performed at a flow rate of 0.5 mL/h using the standard reaction mixture (250 mM ISO and 25 mM FAP in HEPES buffer with PLP, pH 8). The biocatalytic tests using membranes 12M-DF0.5-1 and12M-DF0.5 -3 were conducted for 240 minutes on Day 1, paused overnight, and resumed for 120 minutes and 240 minutes on Day 2, respectively. Membrane 12M-DF0.5-2 was tested for 300 minutes on Day 1 and 210 minutes on Day 2, after an overnight pause. (Right) Productivity (or production rate), expressed in µmol/min, for three biocatalytic membranes tested under a constant 0.5 mL/h flow rate (12M-DF0.5-1, 12M-DF0.5-2, and 12M-DF0.5-3) over two days. The values for the first day represent the average of several measurements, while the second-day values correspond to a single measurement. A red asterisk on the second-day value for 12M-DF0.5-3 indicates that the reaction mixture (RM) was replaced between the two days, whereas no change was made for 12M-DF0.5-1 and -2.

[13] Other biocatalytic tests involving membranes 12M-DF1-1 and 12M-DF1.5-1 failed.
[14] A low flow rate (0.5 mL/h) was selected for this analysis to avoid excessive pressure drop issues, which had been encountered during the flow immobilization step.

The amount of FMBA produced clearly increases in correlation with the quantity of immobilized enzyme. Indeed, at a given time point, membrane 12M-DF0.5-1 (0.480 mg), which exhibits the highest enzyme loading, produces more FMBA than 12M-DF0.5-2 (0.169 mg), which in turn produces more than 12M-DF0.5-3 (0.112 mg) during the 4–5 hours of catalytic testing on the first day. In addition, the production rate or productivity—corresponding to the slope of the dashed line connecting the experimental points—appears relatively stable for each membrane on a given experimental day, excluding the first measurement on the second day. The first experimental measurement on the second day (marked with a asterisk) shows a higher product quantity than expected based on the dynamic observed on the first day (indicated by a steeper slope of the dashed line). This enhanced production at the first sampling on Day 2 is primarily attributed to residual enzyme activity during the overnight pause, as a portion of the reaction mixture remained in the dead volume of the Whatman cell, in contact with the biocatalytic membrane. Therefore, to accurately assess FMBA production exclusively attributable to the flow catalytic test performed on the second day, one should consider the second data point of that day's experiment (i.e., the final point shown in Figs.V.8 (left)).

Comparing productivity[15] over two experimental days (Figs.V.8 (Right)) , 12M-DF0.5-1 and 12M-DF0.5-2 exhibit a reduced production rate compared to the first day (as indicated by a less steep dashed line in Figs.V.8), whereas 12M-DF0.5-3 shows improved productivity (as indicated by steeper dashed line in Figs.V.8). This difference may be explained by an experimental variation between the two cases. For membranes 12M-DF0.5-1 and 12M-DF0.5-2, the second-day catalytic test was carried out using the residual RM left in the plastic syringe (which had not been pre-saturated with FAP) during the overnight pause. A significant portion of FAP from the RM was therefore likely adsorbed onto the internal surface of the plastic syringe during the break (as demonstrated in Fig.V.S6). In contrast, the second-day test for 12M-DF0.5-3 used fresh RM contained in a new pre-saturated plastic syringe, likely avoiding this issue (see Fig.V.S7). Therefore, the lower productivity observed for 12M-DF0.5-1 and 12M-DF0.5-2 is not necessarily due to enzyme deactivation but rather may result from the enzymes being exposed to a FAP concentration lower than that required for optimal activity.

Comparison of Batch and Single Pass Radial Flow reactions

While Figs.V.8 (left) provides a clear visualization of the three experimental catalytic tests, it does not allow for an easy comparison with batch catalytic tests, as the reaction times differ substantially. To evaluate the effect of enzyme loading on biocatalytic performance and enable easier comparison with batch processes, the average productivity and

[15] Productivity corresponds to the slope of the dashed line shown in Fig.V8 (left).

specific activity obtained for 12M-DF0.5-1, 12M-DF0.5-2, and 12M-DF0.5-3 during the first day [16]of catalytic testing are presented in Fig.V.9[17].

It is important to note that the productivity and specific activity determined for batch and flow catalytic tests were not assessed over comparable time scales. For an optimal comparison with batch results, values corresponding to similar substrate conversions are required to avoid potential discrepancies arising from differences in enzymatic kinetics. In the flow experiments, the residence time was very short, suggesting operation within the linear range of substrate conversion, where maximal enzymatic activity is expected. In the batch experiments, all measurements were performed after 20 h of reaction to ensure sufficient FMBA production. Although sampling at earlier time points would have been preferable, it can reasonably be assumed that even after 20 h of catalysis the system remained within the linear range of substrate conversion and that enzymatic activity was still at its maximum, as it was still relatively far from equilibrium conversion (Section V.1.2 and Annex V.S3).

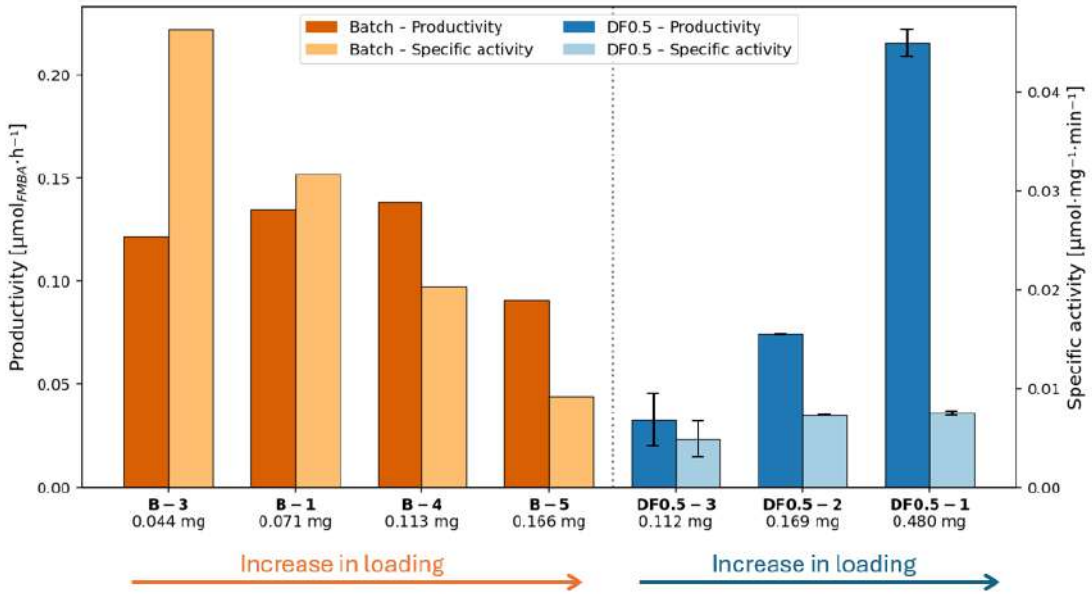

Fig.V.9 - Productivity and specific activity of biocatalytic membranes (12M-B-1, 12M-B-3, 12M-B-4, and 12M-B-5 from 18 h batch immobilization, and 12M-DF0.5-1, 12M-DF0.5-2, and 12M-DF0.5-3 from DF0.5 flow immobilization) exhibiting different loadings, obtained from batch and dead-end flow catalytic tests. Catalytic tests were performed using a standard reaction mixture (250 mM ISO / 25 mM FAP in 0.1 M HEPES / 1 mM PLP, pH 8), over 20 h in batch mode and 3–4 h at a constant flow rate of 0.5 mL/h in flow mode (only first day experiment). While batch values are based on a single measurement, flow values represent the average of multiple measurements from different samples collected during the catalytic test. Error bars represent standard deviations where multiple measurements were performed (flow mode only).

Contrary to batch catalytic tests (Annex V.S2), where a decrease in productivity is observed at some point as loading increases (performance of 12M-B-5 was lower than that of 12M-B-4), higher loading appears to improve the productivity of biocatalytic

[16]To avoid the influence of uncontrolled parameters from the second day of experimentation (e.g., incubation time during the interrupted flow process between experimental days).
[17] As the values appear relatively similar, considering an average value seems appropriate.

membranes investigated under flow conditions. Productivity increase is explained by the relatively stable specific activity (at least within the studied experimental range) which seems poorly affected by enzyme loading when dead-end flow catalytic tests are performed, compared to batch catalytic tests (Fig.V.S3). Specific activity even appears to exhibit a slight inverse trend[18] over the considered range as 12M-DF0.5-1, which had the highest enzyme loading (0.480 mg), exhibited a slightly higher specific activity than 12M-DF0.5-3 (0.112 mg), despite having more than four times the amount of immobilized enzyme.

Comparing batch and flow productivity, batch appear to be more productive than the dead-end flow processes investigated at comparable enzyme loadings. 12M-B-4 (0.113 mg) and 12M-B-5 (0.166 mg) exhibit a productivity 423 % and 23% higher than 12M-DF0.5-3 (0.112 mg) and 12M-DF0.5-2 (0.169 mg), respectively. This difference in productivity can be attributed to the lower specific activity of the enzymes immobilized under flow conditions compared to their batch counterparts. Among the three membranes tested under flow conditions, only membrane 12M-DF0.5-1 (0.480 mg), which exhibited a loading approximately three times higher than the best-performing batch membrane (12M-B-5; 0.169 mg), demonstrated better performance than batch processes. Compared to the most productive batch membrane, 12M-B-4, the productivity of 12M-DF0.5-1 is 56% higher.

In this context and based on the above results, assuming that the specific activity remains relatively constant in flow catalytic tests, it is possible to determine the theoretical minimum amount of enzyme required to obtain a catalyst whose performance under flow conditions would surpass that of the batch process (considering the best-performing membrane in batch mode, 12M-B-4). To this end, two strategies, detailed in Annex V.S7 were employed. A average loading of 0.340 mg appear required to obtained a more efficient processes employing flow.

Evaluation at Variable Flow Rate

The flow rates applied during dead-end flow catalytic tests may also influence the productivity and specific activity of the immobilized enzymes. To assess the effect of flow rate independently of enzyme loading (i.e., the quantity of immobilized enzymes), catalytic tests were performed at various flow rates (0.5, 1, 2, and 4 mL/h) using the same membrane in dead-end flow mode. Two membranes were examined in this context: 12M-DF0.5-4 (0.296 mg) and 12M-DF1-1 (0.153 mg). The resulting productivity and specific activity data are presented in Fig.V.10 and Fig.V.S10, respectively.

[18] A clear decrease of specific activity is observed proportionally with the loading increased.

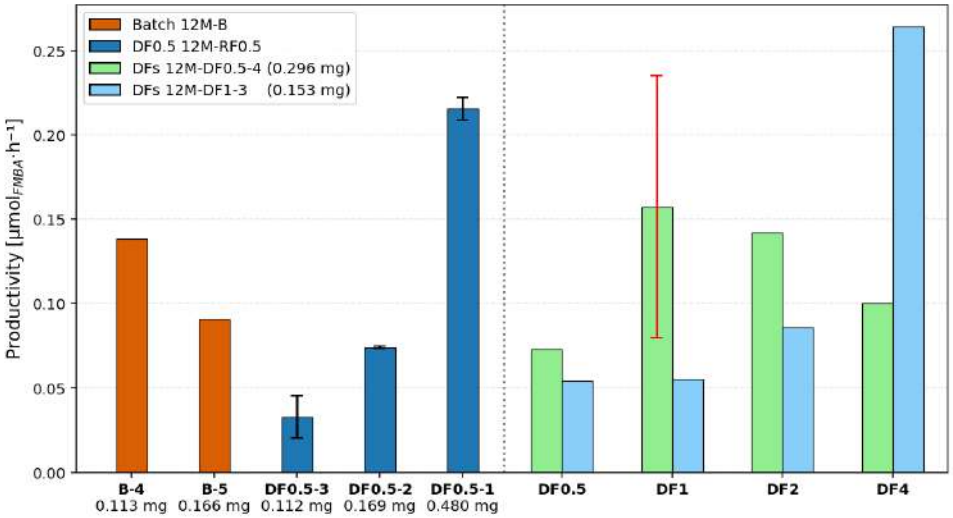

Fig.V.10 - Productivity obtained for 12M-DF0.5-4 and 12M-DF1-3 membranes investigated under different flow rates (0.5, 1, 2, and 4 mL/h) during catalytic tests. These values are compared to membranes used in batch mode that exhibited the highest and lowest productivity (12M-B-4 and 12M-B-5, respectively), as well as membranes tested under a 0.5 mL/h flow rate (12M-DF0.5-1, 12M-DF0.5-2, 12M-DF0.5-3). Dark error bars represent the standard deviation from multiple samples collected at the same flow rate. Red error bars indicate the variability from triplicate extractions of a single sample, reflecting experimental error associated with the extraction process.

The trends observed for both investigated membranes are notably different. While 12M-DF1-3 (light blue) appears to exhibit an increase in productivity Fig.V.10 and specific activity with increasing flow rates, the trend for the 12M-DF0.5-4 membrane (green) is less clear and seems to decrease beyond a certain flow rate threshold (somewhere between 1 and 2 mL/h). Indeed, 12M-DF1-3 shows its highest productivity at 4 mL/h , whereas the best productivity for 12M-DF0.5-4 is reached at 1 mL/h.

Since each membrane was tested at various flow rates with a fixed enzyme loading, the observed differences in productivity suggest that flow rate may influence enzyme activity, as indicated by the tendency toward increased productivity with higher flow rates observed for 12M-DF1-3. However, the absence of a clear trend for 12M-DF0.5-4 prevents drawing a definitive conclusion. In addition to the trend inconsistency, the results appear analytically unreliable, further complicating any interpretation. They are based on a single measurement rather than the mean of multiple replicates, as was done for the DF0.5 investigations at constant flow rate. Moreover, significant variability may arise from the extraction and GC analysis process (Annex VI.S1), as illustrated by the error bar for DF1 in 12M-DF0.5-4 in Fig.V.10, which represents the standard deviation of three extractions from the same sample—corresponding to approximately 50% variation.

V.2.2.3 Evaluation of Leaching and Enzyme Activity Longevity

To determine the robustness of the biocatalytic membrane with respect to flow processes, leaching tests were performed. Two experimental strategies were employed: an adapted hot filtration test and a Bradford assay analysis.

In the first strategy, all solutions collected during the first day of the radial flow biocatalytic test involving membrane 12M-DF0.5-3 were pooled in a round-bottom flask maintained at 35 °C. One sample of the mixed solution was taken immediately after mixing, and another was collected after 18 h of incubation at 35 °C. The results, presented in Figs.V.11 (left), demonstrate that no leaching of active enzyme occurred, as no increase in FMBA concentration was observed[19]. In another strategy, Bradford assay analysis was performed on 0.25 mL of residual solution (collected after passing through the membrane) from membranes 12M-DF0.5-2 and 12M-DF1-2 for protein quantification, using the RM mixture as a blank. Different samples from both the first and second days of catalytic testing were analyzed. The results obtained were below the quantification limit (0.001 mg $_{TsRTA}$/mL), suggesting that no leaching occurred. These two tests indicate that no leaching occurred at flow rates of 0.5 and 1 mL/h. However, it is important to note that these tests were performed only a few times, at the lowest flow rates, and during the initial hours of the catalytic test. Therefore, no conclusion can be drawn regarding potential leaching at higher flow rates (e.g., 2 mL/h or 4 mL/h) or over longer time scales.

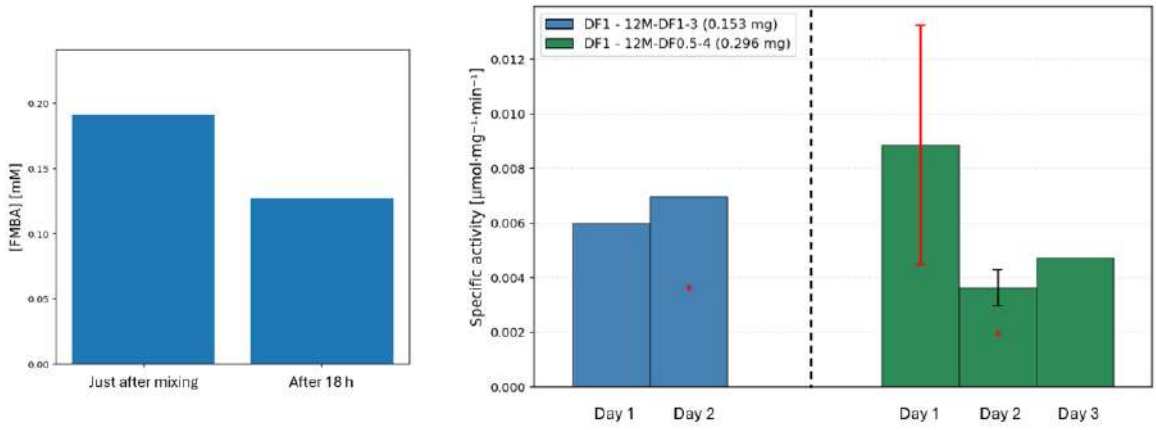

Figs.V.11 – (Left) Leaching test inspired by the "hot filtration test," applied to the residual solution from the dead-end flow catalytic test performed on membrane 12M-dF0.5-3 (at 0.5 mL/h). Residual solutions collected on Day 1 were pooled and maintained at 35 °C under gentle stirring. One sample was analyzed immediately after mixing, and another after 18 h of incubation. (Right) specific activity over time for membranes 12M-DF0.5-4 (3 days) and 12M-DF1-3 (2 days) investigated in dead-end flow catalytic tests at 1 mL/h. The value considered for Day 2 (or 3) excludes the first specific activity measurement of the day to avoid potential bias from residual dead volume. Dark error bars represent the standard deviation from multiple samples collected under the same flow rate (mean values are shown). Red error bars indicate the standard deviation from three extractions of the same sample, reflecting variability in the extraction process (mean values are shown). Red asterisks denote the use of fresh RM in a newly pre-saturated plastic syringe.

Catalytic tests were also performed over 2 and 3 days to evaluate potential enzyme deactivation over time. Unlike batch catalytic tests, continuous evaluation was not possible with the experimental flow system, as it was stopped between experimental days. To ensure that the measured activity was solely attributable to the flow catalytic test, specific precautions were taken. The membrane was rinsed with buffer between experimental days to prevent FMBA formation from residual RM—contained in the dead

[19] If enzymes had leached from the membrane due to flow-induced shear stress, an increase in FMBA concentration would have been expected due to the catalytic activity of free enzymes in solution.

volume of the Whatman cell—remaining in contact with the enzyme overnight. In addition, a new syringe, pre-saturated with pure FAP and containing fresh RM, was used each day to avoid potential FAP adsorption (Section V.2.2.1). Although 2–3 day tests were performed for several membranes, these two key precautions were applied only to 12M-DF0.5-4 and 12M-DF1-3, whose results are shown in Figs.V.11 (right).

The specific activity of 12M-DF1-3 appears relatively consistent over both days, with a slight increase on Day 2—likely attributable to variability in the extraction process, as no replicate measurements were performed. For 12M-DF0.5-4, the specific activity seems to have decreased. However, given the high variability and the fact that the values for Day 2 and Day 3 are relatively similar, it can reasonably be considered stable. While the results suggest preserved enzyme activity over -at least- two first days of catalytic test under these conditions, more robust experiments are required. It would be valuable to perform catalytic tests over longer time scales. Ideally, several measurements of successive samples should be collected each day under the same flow rate to account for variability and ensure more reliable assessment of enzyme recyclability.

V.2.2.4 Discussion

Considering the results presented in Fig.V.9, the use of flow does not appear to improve biocatalytic performance at least for similar enzyme loadings when a flow rate of 0.5 mL/h is employed. In fact, lower activity is even observed. Several hypotheses could explain the reduced performance/specific activity exhibited by immobilized enzymes in flow systems, which cannot be attributed to enzyme leaching (as demonstrated in Figs.V.11 (left)).

Firstly, temperature differences between the two processes must be considered. While both immobilization and catalytic tests are conducted at 35 °C in batch mode (the optimal temperature for TsRTA stability [215], dead-end flow immobilization and catalytic tests are carried out at ambient temperature (20–22 °C), since temperature regulation is more challenging in the flow setup. While full activity retention can be expected in batch, given the relatively short time between enzyme thawing and measurement (as demonstrated by Heckmann *et al.* [215]), the suboptimal temperature under flow conditions may negatively affect the stability and specific activity of the enzymes. It would have been interesting to perform a catalytic test in batch at ambient temperature in order to evaluate a potential influence of temperature. As this was not carried out in this work, an approximate evaluation based on deactivation profiles reported in the literature appears informative. No evaluation of the retained activity profile of TsRTA at room temperature could be found[20]. However, a study focusing on Cv-ATA[21], also a thermostable ATA, demonstrated complete deactivation at room temperature in HEPES buffer after approximately five days

[20] Since TsRTA is of interest for its thermostability, tests were only performed at temperatures above 35 °C, its temperature of optimal stability [215]

[21] Amine transaminase from *Chromobacterium violaceum*

(Fig.V.S11) [222]. Assuming linear deactivation and considering 25–30 hours between enzyme thawing and the first measurements, an approximate deactivation of 20–25% could be expected under flow conditions. Although these values must be interpreted with great caution, the recalculated specific activity for flow processes based on this deactivation suggests that specific activity for both processes would be similar if performed at the same temperature (Tab.V.3). However, experimental tests comparing both processes at identical temperatures are required to confirm this hypothesis.

Tab.V.3 – Comparison of batch and dead-end flow results considering time-dependent deactivation influenced by temperature based on Heckmann et al. [215] and Chen et al. [222] works.

	Types of reactor used for catalytic test (Temperature)	Sp. Activity [$\mu mol.mg^{-1}.min^{-1}$] (Time of measurement after enzyme thawing)	Recalculated Sp. Activity [$\mu mol.mg^{-1}.min^{-1}$] based on deactivation
12M-B-5 (0.166 mg)	Batch (35°C)	0.009 (40-45h)	Supposed similar
12M-DF0.5-2 (0.169mg)	Dead-flow (Room temperature)	0.007 (25-30 h)	~ 0.009 (if 25% of deactivation is considered)

By reducing the substrate residence time, immobilized enzymes could have insufficient time to effectively catalyze the reaction. Although the flow rates employed are relatively low, the residence times investigated in this study—only a few seconds (Tab.V.4)—are particularly short compared to other flow experiments involving immobilized TA that demonstrate performance improvements (ranging from minutes to several hours)[24].

Tab.V.4 – Residence time investigated for dead-end flow catalytic test according the selected flow rate.

Flow rate [mL/h]	Residence time [s]
0.5	86
1	43
2	22
4	11

In addition, flow could introduce shear stress—intensifying with increasing flow rate—which may potentially affect the conformational stability of the enzyme, thereby reducing its activity [211–213], although such effects should be minimal at the low flow rates tested. These hypotheses are supported by the results obtained for 12M-DF1-2 (0.176 mg), where a catalytic test performed at 1 mL/h showed significantly lower performance than 12M-DF0.5-2 (0.169 mg), tested at 0.5 mL/h with a similar enzyme loading, as shown in Tab.V.5. The specific activity obtained at 1 mL/h for 12M-DF1.0-2 appears to fall within the same range as that of the free enzyme, effectively "canceling" the activity gain resulting from enzyme immobilization.

Tab.V.5 - Specific activity of biocatalytic membranes with similar loadings, investigated under dead-end flow catalytic tests. Catalytic tests for 12M-DF0.5-2 and 12M-DF1-2 were performed at 0.5 mL/h and 1 mL/h, respectively. Specific activity obtained for free enzymes investigated under batch catalytic test (20h) was also represented.

	Catalytic test flow rate [mL/h]	Specific activity [µmol.mg^{-1}.min^{-1}]
12M-DF0.5-2 (0.169mg)	0.5	0.0073
12M-DF1.0-2 (0.176mg)	1	0.0013
Free 1 (0.911 mg)	X	0.0017

However, these hypotheses contradict the trend observed for 12M-DF1-3 in Fig.V.10, which suggests that increasing flow rates could enhance enzymatic performance. In this case, flow processes may allow better substrate access to the enzyme through enhanced mass transfer resulting from increased turbulence [106,107,122]. The contradiction between these results indicates that further experiments are needed to draw a definitive conclusion regarding the influence of flow on biocatalytic performance. In particular, experiments conducted at variable flow rates—similar to those performed for 12M-DF1-3 and 12M-DF0.5-5—but including a greater number of replicate measurements for each flow rate, would be relevant to minimize the impact of variability observed in Fig.V.10.

Finally, the lower specific activity may also result from a different spatial distribution of immobilized enzymes within the membrane (Section V.2.1.3). Since enzymes in the flow catalytic tests were immobilized under dead-end flow conditions, it is plausible that their spatial arrangement is less favorable—potentially limiting enzyme flexibility and/or substrate accessibility [63,112,117]—compared to batch-immobilized counterparts. To evaluate the potential effect of spatial distribution resulting from different immobilization strategies, cross-experiments in which immobilization is performed in one reactor type followed by catalytic testing in the other could be informative.

Even if the impact of flow could not be clearly defined, the results shown in Fig.V.9 demonstrate that flow-based processes appear more effective than batch at a fixed flow rate, once a certain threshold of immobilized enzyme is reached (theoretical required quantity: 0.340 mg for 12M). While specific activity decreases with increasing enzyme loading in batch systems, it remains relatively stable under flow conditions. Hence, a lower—but stable—specific activity can be compensated by increasing the amount of immobilized enzyme, as demonstrated by the 12M-DF0.5-1 results in Fig.V.9. One can also assume that further increasing the loading could enhance the performance of membranes investigated under flow conditions. In this context, the flow process—combining both immobilization and subsequent catalytic testing—appears superior to batch systems, which cannot immobilize as much enzyme and whose performance becomes limited above a certain loading. It would therefore be relevant to perform catalytic tests using membranes with higher loadings than those experimentally obtained at the same flow rate, in order to evaluate the potential productivity improvement and

monitor the evolution of specific activity. Optimizing the immobilization step thus becomes essential to maximize enzyme loading on the membrane. While the high loading obtained for 12M-DF0.5-1 (0.480 mg) could not be reproduced, some parameters appear worth investigating. The time between the end of membrane functionalization and the immobilization step may be critical, as an exceptional delay of two weeks was used in that case, while typically only 2 to 3 days were allowed. Additional experiments are therefore highly relevant, as well as the investigation of alternative strategies to potentially improve immobilization.

V.3 Recirculating Tangential Flow Reactor Investigation

Unlike in the previous section, the results and discussion are presented together here. This structure was chosen because the new setup was investigated through a progressive and iterative approach, making a combined presentation more coherent and constructive.

V.3.1 Immobilization

In the following investigation, all membranes used for tangential-flow and batch catalytic tests had a diameter of 44 mm (44M). Immobilization was carried out with a defined concentration of enzyme solution in HEPES buffer at 35 °C for 18 h in batch mode, as described in Section IV.2.2.2. Further comments are provided in Section V.1.1 (Part immobilization).

V.3.2 Catalytic Test - Evaluation of Biocatalytic Performance

V.3.2.1 Reagents and Product Control

A recirculating cross-flow experiment was performed under the same conditions as the catalytic test. First, the test was carried out without any biocatalytic membrane (44M-PP_TA-B), in order to verify the stability of reagent concentrations (as non-catalyzed spontaneous AS transamination reactions are known to be very slow). In this setup, a non-functionalized/non-immobilized 44M membrane was fixed in the system, and the RM (250 mM ISO and 25 mM FAP in 0.1 M HEPES/1 mM PLP) was recirculated at selected flow rates for a duration corresponding to a typical catalytic test. Samples were regularly collected for time profiling. Additionally, a similar test was performed with a fixed concentration (25 mM) of the chiral product FMBA (in 0.1 M HEPES, 1 mM PLP) to ensure that no product loss occurs within the system and that the FMBA concentration measured during the catalytic test accurately reflects enzymatic activity. Results of both tests are presented in Fig.V.12.

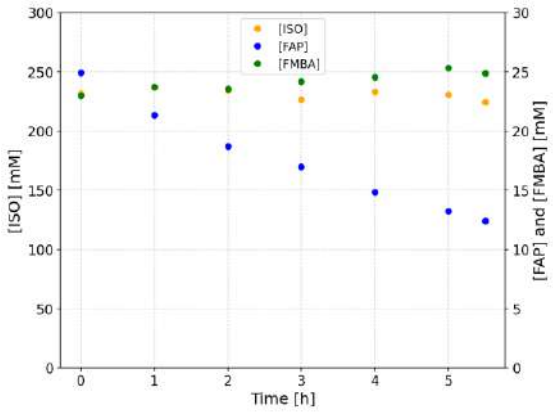

Fig.V.12 - ISO, FAP, and FMBA concentrations over time during a control experiment conducted under the same conditions as the catalytic test (5 h 30 min) but without a biocatalytic membrane (Set-up 1: 100 mL RM recirculated at

150 mL/min). Initial target concentrations were 250 mM for ISO and 25 mM for both FAP and FMBA. The initial experimental concentration, shown at time 0, corresponds to the compound concentrations before RM recirculation begins.

While ISO and FMBA concentrations appear stable, these tests demonstrated a decrease in FAP concentration within the system. Similarly to the dead-end flow catalytic tests, this decrease may be attributed to adsorption within the PTFE tubing and/or evaporation of a portion of FAP—initially present in the aqueous phase—into the gaseous phase within the dead-air volume of the RM-containing bottle (Annex V.S10). While limiting evaporation appears challenging, pre-saturating the system by recirculating RM containing a higher concentration of FAP for several hours prior to the catalytic test proved relatively effective in maintaining FAP at a sufficient concentration for optimal enzymatic activity—by minimizing adsorption phenomena (Annex V.S10). Therefore, this strategy was implemented and applied in all subsequent catalytic tests.

Accordingly, in the following experiments, it will be assumed that the FAP concentration remains above the minimum threshold required for optimal enzymatic activity (i.e. ~ 10 mM [30]) throughout the catalytic test. Moreover, only performance indicators based on the measured FMBA concentration will be considered, as FMBA, appearing relatively inert with respect to the system, provides a more robust metric for evaluating enzymatic activity.

V.3.2.2 Catalytic Performance Evaluation

Impact of Tangential Flow Rates

In a first tangential flow investigation, Set-up 1 employing Pump A (Section IV.2.3.1) was used to investigate different tangential flow rates. Tangential flow catalytic test (TFC.T.) was performed using a 44M biocatalytic membrane. The latter was obtained by applying an immobilization concentration of approximately 0.200 mg/mL[22] (20 mL in batch reactor). 100 mL of RM (agitated and maintained at 35 °C) was recirculated at 50, 150, and 300 mL/min[23] (TF50, TF150, and TF300) for 3 hours[24]. FMBA concentration obtained for three biocatalytic membrane investigated during the first hours of catalytic test was presented in Fig.V.13.

[22] A compromise between a reasonable immobilization level and sufficient enzymatic activity had to be found. This concentration was chosen to rationalize the limited enzyme stock while still aiming to observe measurable enzyme activity.
[23] The flow rates were randomly selected to cover a broad range of the pump's operational capacity.
[24] : While 20 hours is generally considered appropriate for evaluating enzymatic performance in preliminary tests, this shorter duration was selected due to logistical time constraints.

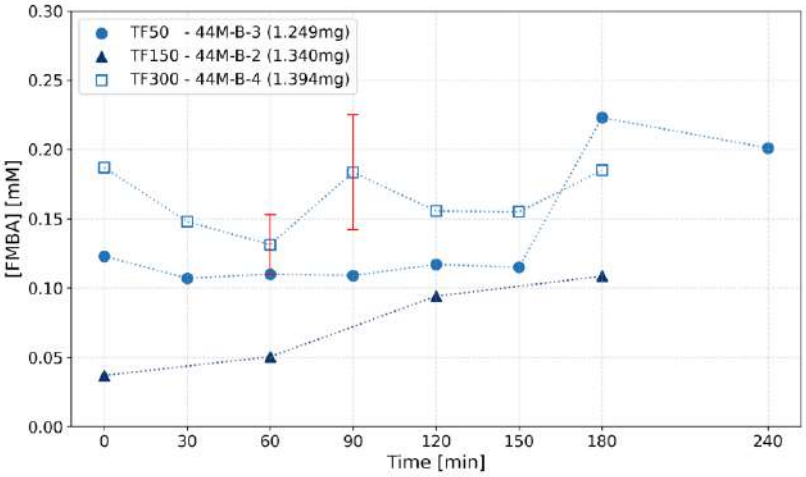

Fig.V.13 - FMBA concentration directly calculated from GC measurements obtained (not corrected values) when different flow rates was investigated during the first hours of catalytic tests. 100 mL of RM (maintained at 35 °C) was recirculated at various flow rates: 50 mL/min (44M-B-3, circle), 150 mL/min (44M-B-2, triangle), and 300 mL/min (44M-B-4, square). Red error bars correspond to the standard deviation from multiple extractions of the same sample. Note: Triplicate GC analyses of the same sample were also performed to assess GC variability; in this case, the average value was reported.

Based on the results presented in Fig.V.13, only the membranes tested at 50 mL/min (44M-B-3, circle) and 150 mL/min (44M-B-2, triangle) allow the conclusion that the measured FMBA concentration results from enzymatic activity, as an increase in FMBA concentration is observed compared to the initial value (t = 0 min)[25]. While FMBA concentration remains relatively stable at 300 mL/min (44M-B-4, square), it remains difficult to definitively conclude that no FMBA is produced, as a curiously high initial FMBA concentration was recorded. It could be assumed that a lower conversion occurs, but the resulting increase is masked by analytical variability as illustrated by the error bars (Annex VI.S1).

Regarding the observed dynamics, only the results obtained at 150 mL/min (44M-B-2, triangle) appear consistent, showing a progressive and linear increase in FMBA concentration. This behavior is expected, as the RM is continuously recirculated, producing a concentration profile similar to typical batch experiments. Given the short duration of the test (~3-4h) and the transamination reaction being far from thermodynamic equilibrium, a linear trend is anticipated (Section V.1.2 and Annex V.S3). Based on the equilibrium conversion value of approximately 44% reported by Meersseman *et al.* [30], the expected FMBA concentration would be close to 11 mM—substantially higher than the 0.20–0.30 mM observed in Fig.V.13. The plateau observed over 150 first min. of catalytic test and decrease on the last hour of experiment for 50 mL/min experiment (44M-B-3, circle) may be attributed to experimental variability (not shown), potentially concealing a small increase in FMBA concentration.

[25] FMBA concentration measured before the RM was recirculated in the setup—and thus brought into contact with the membrane.

Given these results, the interpretation of specific activity, briefly discussed Annex V.S11, or other performance indicators appears of limited relevance. To draw meaningful conclusions about the impact of flow rate on biocatalytic performance, catalytic tests over a longer timescale are thus needed to enable higher FMBA concentrations for analysis (Annex VI.S2).

Comparison with Batch Processes

Considering the cautionary remarks above, it is complicated to draw strong conclusions from this experiment. In an first attempt to position flow vs. batch, data points exhibiting most logical FMBA production can be nevertheless envisaged. Values obtained at 50 and 150 mL/min after 180 min of catalytic test (for 44M-B-3 and 44M-B-2, respectively[26]) were considered and compared with other batch experiments involving free and immobilized enzymes (44M-B-5). The specific activity and productivity values based on directly measured and corrected concentrations are presented in Fig.V.14. The corrected values were determined from the FMBA concentration measured at a given time, minus the initial FMBA concentration measured in the RM before the catalytic test. This approach ensures that only the production directly attributable to enzymatic activity is considered. These values will therefore be preferentially considered in the following discussion (Annex VI.S2).

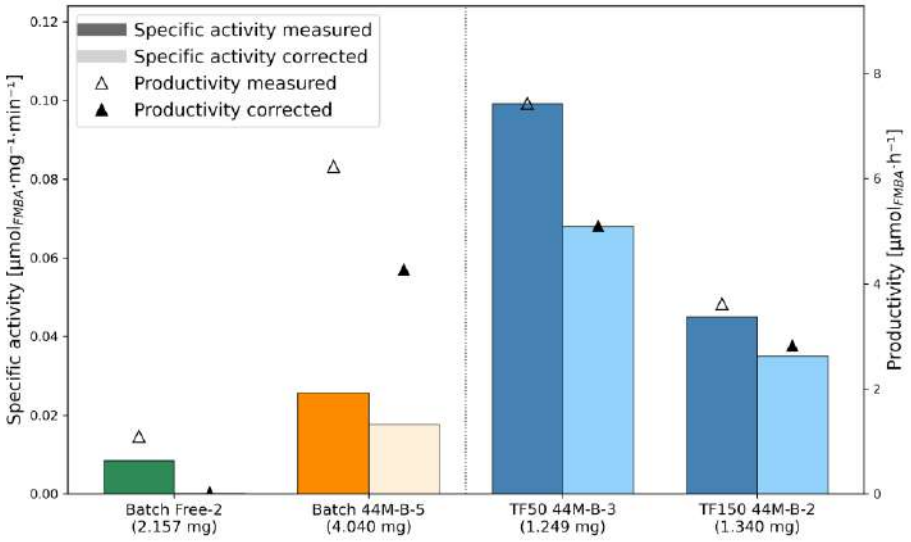

Fig.V.14 - Specific activity and productivity obtained after 3 h of catalytic tests in batch—free (green) and immobilized (orange) TsRTA—and tangential flow (blue) modes. Batch catalytic tests were performed using 4 mL and 50 mL of reaction mixture (RM), maintained at 35 °C, for free and immobilized TsRTA, respectively. Values are based on a single sample. For tangential flow catalytic tests, 100 mL of RM (maintained at 35 °C) was recirculated at 50 mL/min (44M-B-3) and 150 mL/min (44M-B-2). Dark colors represent values directly calculated from GC measurements, while lighter shades indicate corrected values, obtained by subtracting the concentration measured under initial conditions.

Comparing only the flow experiments, immobilized enzymes tested at lower flow rates appeared more active, with 44M-B-3 (50 mL/min) exhibiting a specific activity twice that

[26] Results for 44M-B-4 (TF300) were excluded, as no activity could be demonstrated and the data appeared unreliable, with no corrected value determinable.

of 44M-B-2 (150 mL/min), based on corrected values. Comparing processes, catalytic tests performed under flow conditions appear to exhibit higher activity and productivity than both the free enzyme (Free 2) and the immobilized enzyme (44M-B-5) tested under standard batch conditions. The enhanced FMBA production in the flow system—particularly for 44M-B-3 (TF50)—compared to 44M-B-5 operated in batch mode is all the more remarkable given that the membrane used in the flow setup contains approximately three times less enzyme. This improved biocatalytic performance compared to the free form is consistent with the previously demonstrated enhancement upon immobilization (Section IV.1). However, when considering only immobilized enzymes, a such better specific activity is somewhat unexpected, as fewer enzymes are typically involved in tangential flow configurations—only one side of the membrane being exposed to the RM (Section IV.2.3.1)—and thus a lower specific activity would generally be anticipated.

While this unexpected result is noteworthy, it should be interpreted with caution, as several critical parameters differ between the two experimental setups. Batch experiments were conducted in 50 mL of reaction mixture, whereas flow experiments were performed in 100 mL, making direct comparison challenging. As noted above, specific activity calculations for tangential flow do not account for the fact that only one side of the membrane is exposed to the reaction medium, whereas in batch mode, the entire membrane is fully immersed. Furthermore, the amount of enzyme immobilized on the membrane in batch experiments is approximately three times higher than in the flow setup. Since specific activity is known to decrease with increasing enzyme loading (Annex V.S2), this difference may significantly influence the results. Under identical batch conditions, the membranes used in the flow experiments (44M-B-2 and 44M-B-3), which have a smaller enzyme loading, would be expected to exhibit higher specific activity. It is also important to note that specific activity values are based on measurements taken during the first three hours of catalytic testing—a relatively short timescale during which the total amount of product formed remains low and is difficult to interpret due to analytical variability (Annex VI.S1). This limitation is particularly pronounced in larger volumes, such as the 100 mL used in flow processes, where FMBA is more diluted, further reducing analytical reliability. To draw meaningful conclusions regarding the effect of flow processes on biocatalytic performance, these parameters must be therefore considered when designing a new experiment that enables a more reliable and meaningful comparison between the two setups.

In order to compare more effectively catalytic tests performed either in batch or in tangential flow mode, a new setup approach was employed. An identical immobilization solution concentration (0.500 mg/mL[27]) was used during the batch immobilization step to immobilize approximately the same quantity of enzyme on the membranes. To ensure reduced and comparable RM volumes, Setup 2—characterized by a smaller recirculating

[27] A higher concentration (>0.200 mg/mL) was selected in the hope of improving conversion and obtaining higher FMBA concentrations for analysis.

volume—and a round-bottom glass flask were used to perform the tangential-flow (at 150 mL/min[28]) and batch catalytic tests, respectively, each with 50 mL of RM. With these adjustments, the only significant variable remaining between the two experiments—aside from the reactor type—was the side of the membrane not exposed to the RM. The quantity of produced FMBA; specific activity and productivity, obtained by performing catalytic tests (with RM maintained at 35 °C under stirring) over 48 hours for the different investigated systems, are presented in Figs.V.15 (left) and Fig.V.16, respectively.

While both measured and corrected values are presented, preference is always given to values corrected for the initial concentration (Annex VI.S2).To minimize the potential influence of the initial values used to calculate the corrected data, the analysis focuses primarily on the indicators determined after 20 h, 24 h, and 48 h (Annex VI.S2).

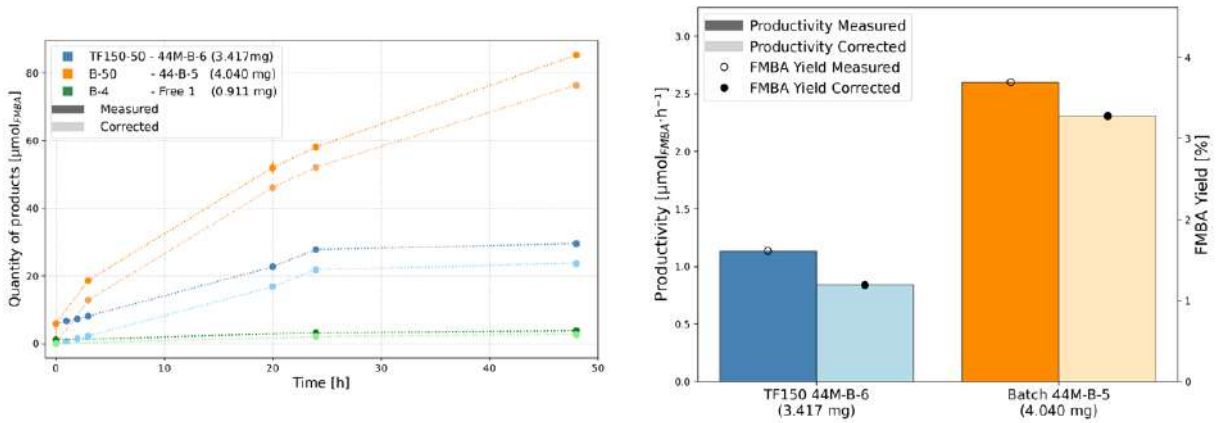

Figs.V.15 – (Left) Quantity of FMBA produced over 48 h, measured in batch and tangential flow modes. For the batch catalytic tests, membrane 44M-B-5 (4.040 mg) and free enzymes (0.910 mg) were immersed in 50 mL and 4 mL of reaction mixture (250 mM ISO, 25 mM FAP in HEPES, PLP, pH = 8) maintained at 35 °C, respectively. For the recirculating tangential flow mode, membrane 44M-B-6 (3.417 mg) was fixed in setup 2, where 50 mL of the same reaction mixture was recirculated at 150 mL/min and maintained at 35 °C. Both measured and corrected values are shown. (Right) Productivity and FMBA yield obtained after 20 h of catalytic test for membranes 44M-B-5 (4.040 mg) and 44M-B-6 (3.417 mg), investigated in batch and tangential flow modes, respectively. Indicators based on directly measured and corrected values are represented by dark and light colors, respectively, for productivity, and by empty and filled circle for FMBA yield.

The results obtained for the flow catalytic test in Figs.V.15 (left) appear more reliable compared to those in Fig.V.13, as the FMBA yield increase progressively—and linearly during the first 24 h—in accordance with expectations for such a recirculating setup[29]–except for the value obtained after 48 h, which shows a lower than expected FMBA concentration[30].

[28] Set-up 2, which employs pump B, is less efficient and can not reach 300 mL/min. At 50 mL/min, a discontinuous flow was observed, while 150 and 300 mL/min flow rates provided a fluent, constant stream. Thus, the intermediate flow rate of 150 mL/min was selected for this longer time-scale investigation.

[29] Batch catalytic tests involving 44M-B-5 also exhibit expected behavior.

[30] The value obtained for the TF catalytic test at 48 h is less reliable than the results obtained at 20 or 24 h. In fact, this value does not strictly correspond to a point measured precisely at 48 h of recirculation, as the flow was interrupted for several hours due to a power outage. This is clearly visible in Figs.V.15 (left), where

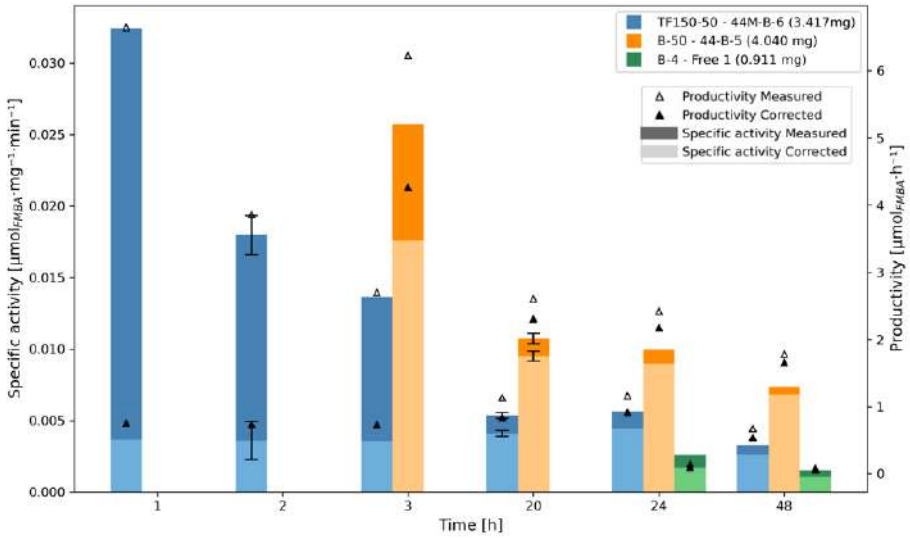

Fig.V.16 - Specific activity and productivity measured in batch and tangential flow modes over 48h of catalytic test. For the batch catalytic tests, membrane 44M-B-5 (4.040 mg) and free enzymes (0.910 mg) were immersed in 50 mL and 4 mL of reaction mixture (250 mM ISO, 25 mM FAP in HEPES, PLP, pH = 8) maintained at 35 °C, respectively. For the recirculating tangential flow mode, membrane 44M-B-6 (3.417 mg) was fixed in setup 2, where 50 mL of the same reaction mixture was recirculated at 150 mL/min and maintained at 35 °C. Measured and corrected values are plotted together, both starting from the baseline value. Error bars indicate standard deviation when triplicate extractions were performed on the same sample.

To effectively compare both immobilized system, the value after 20 h appears to be the most relevant, as it corresponds to the classical time typically considered for catalytic tests, and variability considerations are taken into account at this point (whereas only one sample was collected at 24 h and 48 h). The productivity and yield obtained for immobilized enzymes (44M-B-5 and -6) after 20 h are therefore presented in Figs.V.15 (right).

Considering Figs.V.15 (right), batch processes appear to be more productive than flow process. 44M-B-5 (batch test) and 44M-B-6 (flow test) exhibit a productivity (corrected value) of 2.31 and 0.84 µmol/h, respectively, after 20 h. Similarly to the productivity values, the FMBA yield obtained for the batch experiment is almost three times higher than that obtained with the flow set-up, reaching a conversion after 20 h of 3.28% and 1.19% (corrected values) for the batch and flow catalytic tests, respectively. This higher productivity in batch cannot be solely attributed to the greater amount of immobilized enzyme, as 44M-B-5 contains only 20% more enzyme. Specific activity appears however to be the most relevant parameter to effectively compare catalytic test experiments. While the results demonstrate that flow processes involving immobilized enzymes outperform the free form in batch mode (as already suggested in Fig.V.14), the comparative observations of process performance involving immobilized enzymes—whether in flow or batch—obtained in Fig.V.16 differ from the previous results.

---

the value appears lower than expected based on the overall trend (disruption of the expected increasing pattern). Additionally, it should be noted that after 48 h, the FAP concentration in the RM began to fall below the minimum level required for optimal enzyme activity due to significant FAP loss.

Considering the specific activity calculated at 20 h (Fig.V.16), the enzymes immobilized on the membrane used in batch mode (44M-B-5) exhibit a specific activity approximately twice as high as in tangential flow (44M-B-6). Contrary to value obtained in Fig.V.14, this observation is consistent with the experimental context, where it can be assumed that approximately only half of the total immobilized enzymes is actually exposed to the reaction mixture in the case of tangential flow. Indeed, during immobilization in batch mode, there is no control over the side on which the enzymes bind, as the membrane is entirely immersed in the immobilization solution. Thus, assuming homogeneous immobilization on both sides of the membrane, only half of the enzymes should be exposed to the RM during tangential flow catalytic testing[31]. Since only approximately half on the immobilized enzymes works, the specific activity represented in Fig.V.16 must be multiply by factor 2 to estimated the real enzymatic activity. Based on this, it can be assumed that the enzymes investigated in the batch and flow catalytic tests are comparable. While no improvement was observed, as suggested in Fig.V.14 and as might have been desired, these more robust values obtained confirm that a flow rate of 150 mL/min does not appear to limit enzymatic performance through potential substrate availability issues (i.e., no significant mass transfer limitations).

V.3.2.3 Evaluation of Leaching

Leaching tests were also performed to evaluate the robustness of the biocatalytic membrane. As shown in Fig.V.17 and Figs.V.S14, all three flow rates (50, 150, and 300 mL/min) were investigated, and no leaching was observed in any case.

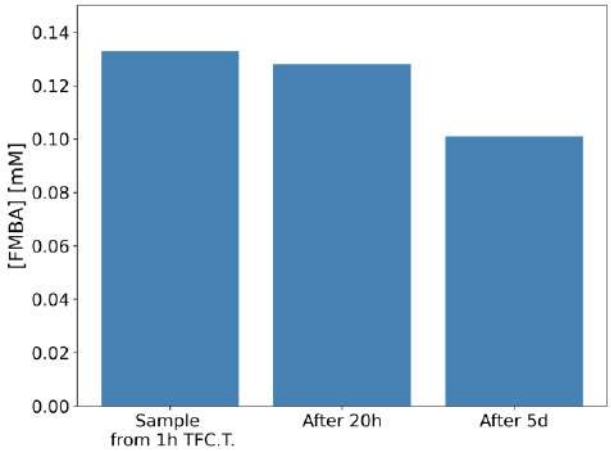

Fig.V.17 - Leaching test inspired by the "hot filtration test," applied to the sample solution from the tangential flow catalytic test performed on membrane 44M-B-6 (3.417 mg) in set-up 2 at 150 mL/min. The sample, harvested after 1 h from the recirculating reaction mixture, was maintained at 35 °C under gentle stirring in a round-bottom flask. Samples were analyzed after 20 h and 5 days. Values shown are non-corrected.

Figure 20 investigates potential leaching during a tangential-flow catalytic test performed at 150 mL/min and serves to illustrate this general conclusion. After 1 h of recirculation in

[31] In this reasoning, the activity of enzymes potentially immobilized within the porosity is considered negligible.

the tangential-flow setup used for the catalytic test (44M-B-6), the RM was sampled and transferred to a round-bottom glass flask maintained at 35 °C under magnetic stirring, following the same conditions as in a typical batch catalytic test. Samples were taken over time to determine whether FMBA production occurred, which would indicate the presence and activity of leached free enzyme. Since the FMBA concentration measured at the initial sampling point (after 1 h of catalytic testing) was similar to that measured after 20 h and after 5 days, it can be concluded that no free enzyme (resulting from leaching) was present in the analyzed solution, as the FMBA concentration remained relatively stable[32].

Similarly, the stable FMBA concentration over time observed in the other leaching tests (Figs.V.S14) indicates that no leaching occurred at those flow rates after the catalytic test sampling time. However, there is no guarantee that no leaching occurs later during the catalytic test. Therefore, additional tests with later sampling times after the start of the catalytic test should be performed.

V.3.3 Final remarks

The results obtained in Figs.V.15 and Fig.V.16 suggest that similar performance could be achieved in both batch and flow modes—superior to the free enzyme—while also preventing enzyme leaching. These findings appear promising and open the way to further experimental perspectives. Even though additional experiments are required to properly evaluate the effect of flow (over reaction times longer than 3 h), the implementation of more sophisticated systems appears relevant. Indeed, performing the same experiment in the presence of a crystallizing agent such as 3,3-diphenylpropionic acid (DPPA), as previously demonstrated by Meersseman *et al*. [30], could be the next step to evaluate how the flow system responds.

Additionally, these results, which demonstrated that the biocatalytic membrane is at least as effective in flow as in batch, pave the way for the development of systems in which the membrane could function not only as a support but also as a combined biocatalytic–separator unit. Along this line, a separate experiment evaluating a new membrane composed of PP and PDMS in a pervaporation system—to selectively remove acetone co-product and thereby shift the equilibrium [165]—appears, based on the current results, a particularly relevant direction to investigate.

[32] The slightly lower concentration observed after 5 days is likely due to extraction variability.

VI. Conclusion

Enantiopure amines are essential building blocks of active pharmaceutical ingredients and drug precursors. However, current production strategies are poorly sustainable. They are generally based on multistep syntheses involving poorly selective homogeneous organometallic catalysts, which require subsequent energy-intensive purification steps. Therefore, greener production processes are required.

The first part of this work aimed to demonstrate how biocatalysis can represent a relevant strategy to improve the sustainability of chiral amine production, based on advances of the last decades. Transaminases (TAs) appear particularly promising candidates due to their remarkable enantioselectivity under mild conditions. Nevertheless, their industrial application remains limited because of weak stability and unfavorable reaction equilibria. A review of existing strategies showed that a wide range of approaches—including enzyme engineering, equilibrium shifting, immobilization, and flow process implementation—can be considered to improve biocatalytic processes. Among them, the implementation of TA-immobilized membranes in flow processes, forming so-called "enzymatic membrane reactors (EMRs)," appears especially promising. Immobilization has proven to be an effective strategy to recover and reuse enzymes, and in some cases, to enhance their stability and/or activity. Combining such biocatalytic membranes with continuous flow processes is expected to increase chiral amine production thanks to continuous substrate feeding and product removal. In such systems, membranes can simultaneously exhibit biocatalytic and separation functions, thereby helping to shift reaction equilibria. Despite this high potential, this strategy has so far been scarcely explored. The few studies involving TAs remain largely restricted to batch reactors, and membranes have rarely been employed for separation, limiting their full potential.

To enable optimal use of membranes as both biocatalysts and separation units, flow process implementation is preferred over batch. While highly promising for process intensification, flow processes also pose challenges, as they may create conditions that negatively affect enzyme activity and stability, potentially leading to enzyme leaching. In this work, the implementation of TA-immobilized membranes in flow was investigated in an attempt to evaluate the potential positive effects of flow on both membrane preparation and enzymatic performance, while also assessing the feasibility of future integrated membrane-separation processes. Two flow modes were studied: dead-end flow and recirculating tangential flow.

Dead-end flow mode was first employed to prepare biocatalytic membranes through covalent immobilization on pre-functionalized polypropylene membranes (12M). Compared to batch immobilization, flow immobilization was markedly more efficient, achieving up to four times higher enzyme loading in significantly less time, even under identical immobilization solution concentrations. This improvement, probably due to

better enzyme penetration into the membrane porosity, was more pronounced at lower flow rates (0.5mL/h). Following preparation, the asymmetric synthesis of (R)-2-fluoromethylbenzylamine (R-FMBA) was performed to evaluate the effect of flow on enzymatic performance. Although membranes prepared in batch appeared more active than those prepared under flow (0.5–4 mL/h) at similar loadings, conclusive interpretation was hindered by large variability in the results and by non-negligible temperature differences between processes. Nevertheless, the membrane obtained through the most effective flow immobilization exhibited a 56% increase in R-FMBA production compared to the best-performing batch membranes, despite its lower specific activity. This result highlights the strong potential of dead-end flow, especially when high enzyme loadings are achieved.

In the second process investigated, recirculating tangential flow was used to evaluate the same asymmetric synthesis reaction. In this case, membranes prepared in batch (44M) were tested under much higher flow rates than those studied in dead-end mode. Results suggested that membranes used at 150 mL/min exhibited similar activity to those employed in batch. While improvement would have been expected, this comparable performance is nonetheless promising for future implementation of membrane-separation processes, such as pervaporation, aimed at removing acetone co-product from the reaction mixture and shifting the equilibrium.

In addition to asymmetric synthesis, membrane robustness was assessed in both flow modes through leaching tests. In both cases, no detectable enzyme activity was found in the reaction mixtures, indicating that immobilized enzymes did not leach under the tested conditions.

To conclude, this work has largely achieved its objectives by successfully implementing two different flow setups, demonstrating their potential benefits in the preparation of biocatalytic membranes and in maintaining the catalytic activity of the enzymes. Although further experiments are required to definitively assess the impact of flow compared to batch, the results already demonstrate preserved enzymatic activity, which represents a significant advantage over soluble TAs. While additional optimization is still needed, this study highlights that flow processes constitute a promising strategy for improving chiral amine production through biocatalysis.

VII. Future Work

Primarily, beyond additional catalytic tests, it would be valuable to identify an internal standard that could be used in GC analysis to eliminate analytical errors arising from extraction and analysis. Ideally, such a molecule should exhibit properties similar to those of the target product while remaining inert toward both the reaction and the enzyme.

Dead-end flow

Regarding dead-end flow immobilization, significant variability in immobilization efficiency was observed under identical conditions (concentration, flow rate, etc.). This variability suggests that one or more uncontrolled factors, other than flow rate, play an essential role. The time gap between the end of functionalization and the start of immobilization appears to be a key parameter, which was not controlled during the different membrane preparations and varied between two days and two weeks. It would therefore be interesting to test immobilization using membranes with a controlled functionalization–immobilization gap. Experimental investigation of the temperature effect on enzymatic stability and activity would be informative. Two strategies could be considered. The first would consist of performing both immobilization and catalytic tests in batch mode at 20 °C to determine whether a decrease in activity is observed. This approach appears more robust, given that temperature control is easier in batch reactors than in flow setups. Alternatively, immobilization and catalytic tests under dead-end flow could be performed in an oven maintained at 35 °C to evaluate whether activity increases compared to previous results. If a difference is observed, the specific contribution of temperature to deactivation could then be assessed. In addition, performing catalytic tests at different flow rates (for a given membrane), while repeating measurements at the same flow rate to confirm trends, would provide better insight into flow effects. Both slower and faster flow rates could be evaluated. It would also be useful to perform catalytic tests over several days (beyond three) until complete loss of activity, in order to assess the operational lifetime of the biocatalytic membranes. A cross-experiment, in which a membrane immobilized in batch is tested under flow conditions (and vice versa), could also help evaluate the potential influence of enzyme spatial distribution resulting from the immobilization step.

While single-pass dead-end flow has the advantage of continuously renewing the reaction mixture—avoiding progressive substrate limitation inherent to batch processes—the implementation of a recirculating dead-end flow system also appears relevant. For immobilization, such a system would optimize the use of the immobilization solution and minimize enzyme waste. During catalysis, it would allow a more direct comparison of batch and flow processes on identical time scales, while also maximizing reaction mixture utilization and reducing waste.

Tangential flow

To evaluate the real specific activity, future experiments with tangential flow could explore modifications to the immobilization step, such as restricting immobilization to a single side of the membrane, thereby localizing the enzymes primarily on one surface, and then repeating catalytic tests. Alternatively, the experimental setup could be adapted to expose both sides of the membrane to the reaction mixture during catalysis. This could be achieved by modifying the system so that pumps recirculate the reaction mixture on both sides of the membrane. In this case, the configuration would mimic the typical batch immobilization, where the entire membrane is immersed. Recirculating tangential flow should also be extended by investigating a broader range of flow rates and longer reaction durations (up to equilibrium) to fully assess flow effects. In long-term experiments, measurements after approximately 48 h indicated that FAP concentration dropped below the level required for optimal enzymatic activity, likely due to evaporation and adsorption within the system. For catalytic tests exceeding 48 h, periodic renewal of the reaction mixture would therefore be required. Once longer-term experiments and optimal flow rates have been established, equilibrium-shifting strategies could be implemented. For instance, the use of crystallizing agents such as 3,3-diphenylpropionic acid (DPPA)—already shown to be effective in batch—could be tested under flow conditions to determine whether improved conversion can be achieved.

In a longer-term perspective, if the above experiments provide promising results, further setup modifications could be envisaged. After immobilization, the membrane could be partially modified with PDMS and implemented in a pervaporation system, enabling acetone co-product removal from the reaction mixture and potentially shifting the equilibrium toward higher conversion.

VIII. Bibliography

(1) Rockström, J.; Steffen, W.; Noone, K.; Persson, Å.; Chapin, F. S.; Lambin, E. F.; Lenton, T. M.; Scheffer, M.; Folke, C.; Schellnhuber, H. J.; Nykvist, B.; de Wit, C. A.; Hughes, T.; van der Leeuw, S.; Rodhe, H.; Sörlin, S.; Snyder, P. K.; Costanza, R.; Svedin, U.; Falkenmark, M.; Karlberg, L.; Corell, R. W.; Fabry, V. J.; Hansen, J.; Walker, B.; Liverman, D.; Richardson, K.; Crutzen, P.; Foley, J. A. A Safe Operating Space for Humanity. *Nature* **2009**, *461* (7263), 472–475. https://doi.org/10.1038/461472a.

(2) Steffen, W.; Richardson, K.; Rockström, J.; Cornell, S. E.; Fetzer, I.; Bennett, E. M.; Biggs, R.; Carpenter, S. R.; de Vries, W.; de Wit, C. A.; Folke, C.; Gerten, D.; Heinke, J.; Mace, G. M.; Persson, L. M.; Ramanathan, V.; Reyers, B.; Sörlin, S. Planetary Boundaries: Guiding Human Development on a Changing Planet. *Science* **2015**, *347* (6223), 1259855. https://doi.org/10.1126/science.1259855.

(3) United Nations Conference on the Human Environment. *Report of the United Nations Conference on the Human Environment*; United Nations: Stockholm, 1972.

(4) Wang, R.; Hertwich, E. G.; Fishman, T.; Deetman, S.; Behrens, P.; Chen, W.; de Koning, A.; Xu, M.; Matus, K.; Ward, H.; Tukker, A.; Zimmerman, J. B. The Legacy Environmental Footprints of Manufactured Capital. *Proc. Natl. Acad. Sci. U. S. A.* *120* (24), e2218828120. https://doi.org/10.1073/pnas.2218828120.

(5) Carl, S. M.; Lindley, D. J.; Knipp, G. T.; Morris, K. R.; Oliver, E.; Becker, G. W.; Arnold, R. D. Biotechnology-Derived Drug Product Development. In *Pharmaceutical Manufacturing Handbook*; John Wiley & Sons, Ltd, 2008; pp 1–32. https://doi.org/10.1002/9780470259818.ch1.

(6) Truppo, M. D. Biocatalysis in the Pharmaceutical Industry: The Need for Speed. *ACS Med. Chem. Lett.* **2017**, *8* (5), 476–480. https://doi.org/10.1021/acsmedchemlett.7b00114.

(7) Sheldon, R. A.; Woodley, J. M. Role of Biocatalysis in Sustainable Chemistry. *Chem. Rev.* **2018**, *118* (2), 801–838. https://doi.org/10.1021/acs.chemrev.7b00203.

(8) Constable, D. J. C.; Dunn, P. J.; Hayler, J. D.; Humphrey, G. R.; Johnnie L. Leazer, J.; Linderman, R. J.; Lorenz, K.; Manley, J.; Pearlman, B. A.; Wells, A.; Zaks, A.; Zhang, T. Y. Key Green Chemistry Research Areas—a Perspective from Pharmaceutical Manufacturers. *Green Chem.* **2007**, *9* (5), 411–420. https://doi.org/10.1039/B703488C.

(9) Diorazio, L. J.; Richardson, P.; Sneddon, H. F.; Moores, A.; Briddell, C.; Martinez, I. Making Sustainability Assessment Accessible: Tools Developed by the ACS Green Chemistry Institute Pharmaceutical Roundtable. *ACS Sustain. Chem. Eng.* **2021**, *9* (50), 16862–16864. https://doi.org/10.1021/acssuschemeng.1c07651.

(10) D. Patil, M.; Grogan, G.; Bommarius, A.; Yun, H. Recent Advances in ω-Transaminase-Mediated Biocatalysis for the Enantioselective Synthesis of Chiral Amines. *Catalysts* **2018**, *8* (7), 254. https://doi.org/10.3390/catal8070254.

(11) Ghislieri, D.; Turner, N. J. Biocatalytic Approaches to the Synthesis of Enantiomerically Pure Chiral Amines. *Top. Catal.* **2014**, *57* (5), 284–300. https://doi.org/10.1007/s11244-013-0184-1.

(12) Iwao Ojima. Catalytic Asymmetric Synthesis. In *Catalytic Asymmetric Synthesis*; John Wiley & Sons, Ltd, 2010. https://doi.org/10.1002/9780470584248.fmatter.

(13) Ward, J.; Wohlgemuth, R. High-Yield Biocatalytic Amination Reactions in Organic Synthesis. *Curr. Org. Chem.* **2010**, *14* (17), 1914–1927. https://doi.org/10.2174/138527210792927546.

(14) Nugent, T. C.; El-Shazly, M. Chiral Amine Synthesis – Recent Developments and Trends for Enamide Reduction, Reductive Amination, and Imine Reduction. *Adv. Synth. Catal.* **2010**, *352* (5), 753–819. https://doi.org/10.1002/adsc.200900719.

(15) Kelefiotis-Stratidakis, P.; Tyrikos-Ergas, T.; Pavlidis, I. V. The Challenge of Using Isopropylamine as an Amine Donor in Transaminase Catalysed Reactions. *Org. Biomol. Chem.* **2019**, *17* (7), 1634–1642. https://doi.org/10.1039/C8OB02342E.
(16) Anastas, P. T.; Warner, J. C. *Green Chemistry: Theory and Practice*; Oxford University Press, 1998.
(17) Debecker, D. P.; Kuok (Mimi) Hii, K.; Moores, A.; Rossi, L. M.; Sels, B.; Allen, D. T.; Subramaniam, B. Shaping Effective Practices for Incorporating Sustainability Assessment in Manuscripts Submitted to ACS Sustainable Chemistry & Engineering: Catalysis and Catalytic Processes. *ACS Sustain. Chem. Eng.* **2021**, *9* (14), 4936–4940. https://doi.org/10.1021/acssuschemeng.1c02070.
(18) Dunn, P. J.; Wells, A. S.; Williams, M. T. *Green Chemistry in the Pharmaceutical Industry*; Green Chemistry in the Pharmaceutical Industry; 2010. https://doi.org/10.1002/9783527629688.
(19) Hollmann, F.; Opperman, D. J.; Paul, C. E. Biocatalytic Reduction Reactions from a Chemist's Perspective. *Angew. Chem. Int. Ed.* **2021**, *60* (11), 5644–5665. https://doi.org/10.1002/anie.202001876.
(20) Savile, C. K.; Janey, J. M.; Mundorff, E. C.; Moore, J. C.; Tam, S.; Jarvis, W. R.; Colbeck, J. C.; Krebber, A.; Fleitz, F. J.; Brands, J.; Devine, P. N.; Huisman, G. W.; Hughes, G. J. Biocatalytic Asymmetric Synthesis of Chiral Amines from Ketones Applied to Sitagliptin Manufacture. *Science* **2010**, *329* (5989), 305–309. https://doi.org/10.1126/science.1188934.
(21) Slabu, I.; Galman, J. L.; Lloyd, R. C.; Turner, N. J. Discovery, Engineering, and Synthetic Application of Transaminase Biocatalysts. *ACS Catal.* **2017**, *7* (12), 8263–8284. https://doi.org/10.1021/acscatal.7b02686.
(22) Sehl, T.; Hailes, H. C.; Ward, J. M.; Wardenga, R.; von Lieres, E.; Offermann, H.; Westphal, R.; Pohl, M.; Rother, D. Two Steps in One Pot: Enzyme Cascade for the Synthesis of Nor(Pseudo)Ephedrine from Inexpensive Starting Materials. *Angew. Chem. Int. Ed.* **2013**, *52* (26), 6772–6775. https://doi.org/10.1002/anie.201300718.
(23) Nguyen, L. A.; He, H.; Pham-Huy, C. Chiral Drugs: An Overview. *Int. J. Biomed. Sci. IJBS* **2006**, *2* (2), 85–100.
(24) Arango, H. M.; Biggelaar, L. van den; Soumillion, P.; Luis, P.; Leyssens, T.; Paradisi, F.; Debecker, D. P. Continuous Flow-Mode Synthesis of (Chiral) Amines with Transaminase: A Strategic Biocatalytic Approach to Essential Building Blocks. *React. Chem. Eng.* **2023**, *8* (7), 1505–1544. https://doi.org/10.1039/D3RE00210A.
(25) Arango, H. M.; Leyssens, T.; Luis, P.; Debecker, D. Enzyme-Membrane-Reactors: Recent Trends and Applications for the Production of Fine Chemicals and Pharmaceutical Building-Blocks. ChemRxiv January 28, 2025. https://doi.org/10.26434/chemrxiv-2025-6b2mp.
(26) Šketa, B.; Galman, J. L.; Turner, N. J.; Žnidaršič-Plazl, P. Immobilization of His6-Tagged Amine Transaminases in Microreactors Using Functionalized Nonwoven Nanofiber Membranes. *New Biotechnol.* **2024**, *83*, 46–55. https://doi.org/10.1016/j.nbt.2024.06.005.
(27) Montanari, U.; Cocchi, D.; Brugo, T. M.; Pollicino, A.; Taresco, V.; Romero Fernandez, M.; Moore, J. C.; Sagnelli, D.; Paradisi, F.; Zucchelli, A.; Howdle, S. M.; Gualandi, C. Functionalisable Epoxy-Rich Electrospun Fibres Based on Renewable Terpene for Multi-Purpose Applications. *Polymers* **2021**, *13* (11), 1804. https://doi.org/10.3390/polym13111804.
(28) Roura Padrosa, D.; Nisar, Z.; Paradisi, F. Efficient Amino Donor Recycling in Amination Reactions: Development of a New Alanine Dehydrogenase in Continuous Flow and Dialysis Membrane Reactors. *Catalysts* **2021**, *11* (4), 520. https://doi.org/10.3390/catal11040520.

(29) Arango, H. M.; Nguyen, X. D. L.; Luis, P.; Leyssens, T.; Padrosa, D. R.; Paradisi, F.; Debecker, D. P. Membrane-Immobilized Transaminases for the Synthesis of Enantiopure Amines. *RSC Sustain.* **2024**, *2* (10), 3139–3152. https://doi.org/10.1039/D4SU00293H.
(30) Meersseman Arango, H.; Bachus, N.; Nguyen, X. D. L.; Bredun, B.; Luis, P.; Leyssens, T.; Roura Padrosa, D.; Paradisi, F.; Debecker, D. P. Crystallization-Assisted Asymmetric Synthesis of Enantiopure Amines Using Membrane-Immobilized Transaminase. *Chem Bio Eng.* **2025**, *2* (4), 272–282. https://doi.org/10.1021/cbe.4c00186.
(31) Nugent, T. C. *Chiral Amine Synthesis: Methods, Developments and Applications*; Chiral Amine Synthesis: Methods, Developments and Applications; 2010. https://doi.org/10.1002/9783527629541.
(32) Jeschke, P. Current Status of Chirality in Agrochemicals. *Pest Manag. Sci.* **2018**, *74* (11), 2389–2404. https://doi.org/10.1002/ps.5052.
(33) Jeschke, P. The Continuing Significance of Chiral Agrochemicals. *Pest Manag. Sci.* **2025**, *81* (4), 1697–1716. https://doi.org/10.1002/ps.8655.
(34) France, S.; Guerin, D. J.; Miller, S. J.; Lectka, T. Nucleophilic Chiral Amines as Catalysts in Asymmetric Synthesis. *Chem. Rev.* **2003**, *103* (8), 2985–3012. https://doi.org/10.1021/cr020061a.
(35) Cabré, A.; Verdaguer, X.; Riera, A. Recent Advances in the Enantioselective Synthesis of Chiral Amines via Transition Metal-Catalyzed Asymmetric Hydrogenation. *Chem. Rev.* **2022**, *122* (1), 269–339. https://doi.org/10.1021/acs.chemrev.1c00496.
(36) Brooks, W. H.; Guida, W. C.; Daniel, K. G. The Significance of Chirality in Drug Design and Development. *Curr. Top. Med. Chem.* **2011**, *11* (7), 760–770. https://doi.org/10.2174/156802611795165098.
(37) Senkuttuvan, N.; Komarasamy, B.; Krishnamoorthy, R.; Sarkar, S.; Dhanasekaran, S.; Anaikutti, P. The Significance of Chirality in Contemporary Drug Discovery-a Mini Review. *RSC Adv.* **2024**, *14* (45), 33429–33448. https://doi.org/10.1039/D4RA05694A.
(38) Ariëns, E. J. Stereochemistry, a Basis for Sophisticated Nonsense in Pharmacokinetics and Clinical Pharmacology. *Eur. J. Clin. Pharmacol.* **1984**, *26* (6), 663–668. https://doi.org/10.1007/BF00541922.
(39) McVicker, R. U.; O'Boyle, N. M. Chirality of New Drug Approvals (2013–2022): Trends and Perspectives. *J. Med. Chem.* **2024**, *67* (4), 2305–2320. https://doi.org/10.1021/acs.jmedchem.3c02239.
(40) Höhne, M.; Bornscheuer, U. T. Biocatalytic Routes to Optically Active Amines. *ChemCatChem* **2009**, *1* (1), 42–51. https://doi.org/10.1002/cctc.200900110.
(41) Yin, L.; Shan, W.; Jia, X.; Li, X.; Chan, A. S. C. Ru-Catalyzed Enantioselective Preparation of Methyl (*R*)-*o*-Chloromandelate and Its Application in the Synthesis of (*S*)-Clopidogrel. *J. Organomet. Chem.* **2009**, *694* (13), 2092–2095. https://doi.org/10.1016/j.jorganchem.2009.02.008.
(42) Salunke, S.; Paul, A.; Nair, R.; Kintali, R. V. Process for the Preparation of Clopidogrel Bisulphate Form i. WO2009080469A1, July 2, 2009.
(43) Hansen, K. B.; Hsiao, Y.; Xu, F.; Rivera, N.; Clausen, A.; Kubryk, M.; Krska, S.; Rosner, T.; Simmons, B.; Balsells, J.; Ikemoto, N.; Sun, Y.; Spindler, F.; Malan, C.; Grabowski, E. J. J.; Armstrong, J. D. Highly Efficient Asymmetric Synthesis of Sitagliptin. *J. Am. Chem. Soc.* **2009**, *131* (25), 8798–8804. https://doi.org/10.1021/ja902462q.
(44) CHIKKALI, S. H.; KHOPADE, K. V. Highly Efficient Process for the Preparation of Sitagliptin via Rhodium Catalyzed Asymmetric Hydrogenation. WO2020121321A1, June 18, 2020.
(45) Yan, P.-C.; Zhu, G.-L.; Xie, J.-H.; Zhang, X.-D.; Zhou, Q.-L.; Li, Y.-Q.; Shen, W.-H.; Che, D.-Q. Industrial Scale-Up of Enantioselective Hydrogenation for the Asymmetric Synthesis of Rivastigmine. *Org. Process Res. Dev.* **2013**, *17* (2), 307–312. https://doi.org/10.1021/op3003147.

(46) Jaweed, M. S. M.; Upadhye, B. K.; Rai, V. C.; Zia, H. Process for Preparing Rivastigmine. WO2007026373A2, March 8, 2007. https://patents.google.com/patent/WO2007026373A2/en (accessed 2025-05-15).
(47) Breuer, M.; Ditrich, K.; Habicher, T.; Hauer, B.; Keßeler, M.; Stürmer, R.; Zelinski, T. Industrial Methods for the Production of Optically Active Intermediates. *Angew. Chem. Int. Ed.* **2004**, *43* (7), 788–824. https://doi.org/10.1002/anie.200300599.
(48) He, Q.; Rohani, S.; Zhu, J.; Gomaa, H. Resolution of Sertraline with (R)-Mandelic Acid: Chiral Discrimination Mechanism Study. *Chirality* **2012**, *24* (2), 119–128. https://doi.org/10.1002/chir.21033.
(49) Khamar, B. M.; Modi, I. A.; Rajappa, M.; Shashikala, K. N.; Achanath, R.; Chheda, A. Process for the Preparation of Sertraline Hydrochloride Form Ii. WO2006027658A2, March 16, 2006. https://patents.google.com/patent/WO2006027658A2/en (accessed 2025-05-15).
(50) Smejkal, G. B.; and Kakumanu, S. Enzymes and Their Turnover Numbers. *Expert Rev. Proteomics* **2019**, *16* (7), 543–544. https://doi.org/10.1080/14789450.2019.1630275.
(51) Zawodny, W.; Montgomery, S. L. Evolving New Chemistry: Biocatalysis for the Synthesis of Amine-Containing Pharmaceuticals. *Catalysts* **2022**, *12* (6), 595–617. https://doi.org/10.3390/catal12060595.
(52) Aguillón, A. R.; de Miranda, A. S.; Junior, I. I.; de Souza, R. O. M. A. Biocatalysis toward the Synthesis of Chiral Amines. In *Synthetic Approaches to Nonaromatic Nitrogen Heterocycles*; John Wiley & Sons, Ltd, 2020; pp 667–697. https://doi.org/10.1002/9781119708841.ch21.
(53) de María, P. D.; de Gonzalo, G.; Alcántara, A. R. Biocatalysis as Useful Tool in Asymmetric Synthesis: An Assessment of Recently Granted Patents (2014–2019). *Catalysts* **2019**, *9* (10), 802. https://doi.org/10.3390/catal9100802.
(54) Vikhrankar, S. S.; Satbhai, S.; Kulkarni, P.; Ranbhor, R.; Ramakrishnan, V.; Kodgire, P. Enzymatic Routes for Chiral Amine Synthesis: Protein Engineering and Process Optimization. *Biol. Targets Ther.* **2024**, *18*, 165–179.
(55) Lin, B.; Tao, Y. Whole-Cell Biocatalysts by Design. *Microb. Cell Factories* **2017**, *16* (1), 106. https://doi.org/10.1186/s12934-017-0724-7.
(56) Planchestainer, M.; Contente, M. L.; Cassidy, J.; Molinari, F.; Tamborini, L.; Paradisi, F. Continuous Flow Biocatalysis: Production and in-Line Purification of Amines by Immobilised Transaminase from Halomonas Elongata. *Green Chem.* **2017**, *19* (2), 372–375. https://doi.org/10.1039/c6gc01780k.
(57) Han, G.; Ren, W.; Zhang, S.; Zuo, Z.; He, W. Application of Chiral Recyclable Catalysts in Asymmetric Catalysis. *RSC Adv.* **2024**, *14* (23), 16520–16545. https://doi.org/10.1039/D4RA01050G.
(58) Antenucci, A.; Dughera, S.; Renzi, P. Green Chemistry Meets Asymmetric Organocatalysis: A Critical Overview on Catalysts Synthesis. *ChemSusChem* **2021**, *14* (14), 2785–2853. https://doi.org/10.1002/cssc.202100573.
(59) Kohls, H.; Steffen-Munsberg, F.; Höhne, M. Recent Achievements in Developing the Biocatalytic Toolbox for Chiral Amine Synthesis. *Curr. Opin. Chem. Biol.* **2014**, *19*, 180–192. https://doi.org/10.1016/j.cbpa.2014.02.021.
(60) Bell, E. L.; Finnigan, W.; France, S. P.; Green, A. P.; Hayes, M. A.; Hepworth, L. J.; Lovelock, S. L.; Niikura, H.; Osuna, S.; Romero, E.; Ryan, K. S.; Turner, N. J.; Flitsch, S. L. Biocatalysis. *Nat. Rev. Methods Primer* **2021**, *1* (1), 1–21. https://doi.org/10.1038/s43586-021-00044-z.
(61) Rocha, R. A.; Speight, R. E.; Scott, C. Engineering Enzyme Properties for Improved Biocatalytic Processes in Batch and Continuous Flow. *Org. Process Res. Dev.* **2022**, *26* (7), 1914–1924. https://doi.org/10.1021/acs.oprd.1c00424.
(62) Homaei, A. A.; Sariri, R.; Vianello, F.; Stevanato, R. Enzyme Immobilization: An Update. *J. Chem. Biol.* **2013**, *6* (4), 185–205. https://doi.org/10.1007/s12154-013-0102-9.

(63) A. Sheldon, R.; Pelt, S. van. Enzyme Immobilisation in Biocatalysis: Why, What and How. *Chem. Soc. Rev.* **2013**, *42* (15), 6223–6235. https://doi.org/10.1039/C3CS60075K.
(64) Benítez-Mateos, A. I.; Contente, M. L.; Padrosa, D. R.; Paradisi, F. Flow Biocatalysis 101: Design, Development and Applications. *React. Chem. Eng.* **2021**, *6* (4), 599–611. https://doi.org/10.1039/D0RE00483A.
(65) Santis, P. D.; Meyer, L.-E.; Kara, S. The Rise of Continuous Flow Biocatalysis – Fundamentals, Very Recent Developments and Future Perspectives. *React. Chem. Eng.* **2020**, *5* (12), 2155–2184. https://doi.org/10.1039/D0RE00335B.
(66) John, R. A. Pyridoxal Phosphate-Dependent Enzymes. *Biochim. Biophys. Acta* **1995**, *1248* (2), 81–96. https://doi.org/10.1016/0167-4838(95)00025-p.
(67) Fessner, W.-D. Systems Biocatalysis: Development and Engineering of Cell-Free "Artificial Metabolisms" for Preparative Multi-Enzymatic Synthesis. *New Biotechnol.* **2015**, *32* (6), 658–664. https://doi.org/10.1016/j.nbt.2014.11.007.
(68) Guo, F.; Berglund, P. Transaminase Biocatalysis: Optimization and Application. *Green Chem.* **2017**, *19* (2), 333–360. https://doi.org/10.1039/C6GC02328B.
(69) Mathew, S.; Yun, H. ω-Transaminases for the Production of Optically Pure Amines and Unnatural Amino Acids. *ACS Catal.* **2012**, *2* (6), 993–1001. https://doi.org/10.1021/cs300116n.
(70) Shin, J.-S.; Kim, B.-G. Asymmetric Synthesis of Chiral Amines with ω-Transaminase. *Biotechnol. Bioeng.* **1999**, *65* (2), 206–211. https://doi.org/10.1002/(SICI)1097-0290(19991020)65:2%253C206::AID-BIT11%253E3.0.CO;2-9.
(71) Koszelewski, D.; Tauber, K.; Faber, K.; Kroutil, W. ω-Transaminases for the Synthesis of Non-Racemic α-Chiral Primary Amines. *Trends Biotechnol.* **2010**, *28* (6), 324–332. https://doi.org/10.1016/j.tibtech.2010.03.003.
(72) Musa, M. M.; Hollmann, F.; Mutti, F. G. Synthesis of Enantiomerically Pure Alcohols and Amines via Biocatalytic Deracemisation Methods. *Catal. Sci. Technol.* **2019**, *9* (20), 5487–5503. https://doi.org/10.1039/C9CY01539F.
(73) Koszelewski, D.; Clay, D.; Rozzell, D.; Kroutil, W. Deracemisation of α-Chiral Primary Amines by a One-Pot, Two-Step Cascade Reaction Catalysed by ω-Transaminases. *Eur. J. Org. Chem.* **2009**, *2009* (14), 2289–2292. https://doi.org/10.1002/ejoc.200801265.
(74) Börner, T.; Rämisch, S.; Reddem, E. R.; Bartsch, S.; Vogel, A.; Thunnissen, A.-M. W. H.; Adlercreutz, P.; Grey, C. Explaining Operational Instability of Amine Transaminases: Substrate-Induced Inactivation Mechanism and Influence of Quaternary Structure on Enzyme–Cofactor Intermediate Stability. *ACS Catal.* **2017**, *7* (2), 1259–1269. https://doi.org/10.1021/acscatal.6b02100.
(75) Fuchs, M.; Farnberger, J. E.; Kroutil, W. The Industrial Age of Biocatalytic Transamination. *Eur. J. Org. Chem.* **2015**, *2015* (32), 6965–6982. https://doi.org/10.1002/ejoc.201500852.
(76) Bornscheuer, U. T.; Huisman, G. W.; Kazlauskas, R. J.; Lutz, S.; Moore, J. C.; Robins, K. Engineering the Third Wave of Biocatalysis. *Nature* **2012**, *485* (7397), 185–194. https://doi.org/10.1038/nature11117.
(77) Gargiulo, S.; Soumillion, P. Directed Evolution for Enzyme Development in Biocatalysis. *Curr. Opin. Chem. Biol.* **2021**, *61*, 107–113. https://doi.org/10.1016/j.cbpa.2020.11.006.
(78) Yun, H.; Hwang, B.-Y.; Lee, J.-H.; Kim, B.-G. Use of Enrichment Culture for Directed Evolution of the Vibrio Fluvialis JS17 Omega-Transaminase, Which Is Resistant to Product Inhibition by Aliphatic Ketones. *Appl. Environ. Microbiol.* **2005**, *71* (8), 4220–4224. https://doi.org/10.1128/AEM.71.8.4220-4224.2005.
(79) Li, Y.; Cirino, P. C. Recent Advances in Engineering Proteins for Biocatalysis. *Biotechnol. Bioeng.* **2014**, *111* (7), 1273–1287. https://doi.org/10.1002/bit.25240.
(80) Littlechild, J. A. Enzymes from Extreme Environments and Their Industrial Applications. *Front. Bioeng. Biotechnol.* **2015**, *3*. https://doi.org/10.3389/fbioe.2015.00161.
(81) DasSarma, S.; DasSarma, P. Halophiles and Their Enzymes: Negativity Put to Good Use. *Curr. Opin. Microbiol.* **2015**, *25*, 120–126. https://doi.org/10.1016/j.mib.2015.05.009.

(82) Stekhanova, T. N.; Rakitin, A. L.; Mardanov, A. V.; Bezsudnova, E. Y.; Popov, V. O. A Novel Highly Thermostable Branched-Chain Amino Acid Aminotransferase from the Crenarchaeon Vulcanisaeta Moutnovskia. *Enzyme Microb. Technol.* **2017**, *96*, 127–134. https://doi.org/10.1016/j.enzmictec.2016.10.002.
(83) Cerioli, L.; Planchestainer, M.; Cassidy, J.; Tessaro, D.; Paradisi, F. Characterization of a Novel Amine Transaminase from *Halomonas Elongata*. *J. Mol. Catal. B Enzym.* **2015**, *120*, 141–150. https://doi.org/10.1016/j.molcatb.2015.07.009.
(84) Ni, Y.; Holtmann, D.; Hollmann, F. How Green Is Biocatalysis? To Calculate Is To Know. *ChemCatChem* **2014**, *6* (4), 930–943. https://doi.org/10.1002/cctc.201300976.
(85) Abu, R.; Woodley, J. M. Application of Enzyme Coupling Reactions to Shift Thermodynamically Limited Biocatalytic Reactions. *ChemCatChem* **2015**, *7* (19), 3094–3105. https://doi.org/10.1002/cctc.201500603.
(86) Fellechner, O.; Blatkiewicz, M.; Smirnova, I. Reactive Separations for In Situ Product Removal of Enzymatic Reactions: A Review. *Chem. Ing. Tech.* **2019**, *91* (11), 1522–1543. https://doi.org/10.1002/cite.201900027.
(87) Halling, P. J. Solvent Selection for Biocatalysis in Mainly Organic Systems: Predictions of Effects on Equilibrium Position. *Biotechnol. Bioeng.* **1990**, *35* (7), 691–701. https://doi.org/10.1002/bit.260350706.
(88) Lye, G. J.; Woodley, J. M. Application of *in Situ* Product-Removal Techniques to Biocatalytic Processes. *Trends Biotechnol.* **1999**, *17* (10), 395–402. https://doi.org/10.1016/S0167-7799(99)01351-7.
(89) Hülsewede, D.; Tänzler, M.; Süss, P.; Mildner, A.; Menyes, U.; von Langermann, J. Development of an in Situ-Product Crystallization (ISPC)-Concept to Shift the Reaction Equilibria of Selected Amine Transaminase-Catalyzed Reactions. *Eur. J. Org. Chem.* **2018**, *2018* (18), 2130–2133. https://doi.org/10.1002/ejoc.201800323.
(90) Schrittwieser, J. H.; Velikogne, S.; Hall, M.; Kroutil, W. Artificial Biocatalytic Linear Cascades for Preparation of Organic Molecules. *Chem. Rev.* **2018**, *118* (1), 270–348. https://doi.org/10.1021/acs.chemrev.7b00033.
(91) Winkler, C. K.; Schrittwieser, J. H.; Kroutil, W. Power of Biocatalysis for Organic Synthesis. *ACS Cent. Sci.* **2021**, *7* (1), 55–71. https://doi.org/10.1021/acscentsci.0c01496.
(92) Rios-Solis, L.; Morris, P.; Grant, C.; Odeleye, A. O. O.; Hailes, H. C.; Ward, J. M.; Dalby, P. A.; Baganz, F.; Lye, G. J. Modelling and Optimisation of the One-Pot, Multi-Enzymatic Synthesis of Chiral Amino-Alcohols Based on Microscale Kinetic Parameter Determination. *Chem. Eng. Sci.* **2015**, *122*, 360–372. https://doi.org/10.1016/j.ces.2014.09.046.
(93) Truppo, M. D.; Rozzell, J. D.; Moore, J. C.; Turner, N. J. Rapid Screening and Scale-up of Transaminase Catalysed Reactions. *Org. Biomol. Chem.* **2008**, *7* (2), 395–398. https://doi.org/10.1039/B817730A.
(94) Park, E.-S.; Dong, J.-Y.; Shin, J.-S. ω-Transaminase-Catalyzed Asymmetric Synthesis of Unnatural Amino Acids Using Isopropylamine as an Amino Donor. *Org. Biomol. Chem.* **2013**, *11* (40), 6929–6933. https://doi.org/10.1039/C3OB40495A.
(95) Meadows, R. E.; Mulholland, K. R.; Schürmann, M.; Golden, M.; Kierkels, H.; Meulenbroeks, E.; Mink, D.; May, O.; Squire, C.; Straatman, H.; Wells, A. S. Efficient Synthesis of (S)-1-(5-Fluoropyrimidin-2-Yl)Ethylamine Using an ω-Transaminase Biocatalyst in a Two-Phase System. *Org. Process Res. Dev.* **2013**, *17* (9), 1117–1122. https://doi.org/10.1021/op400131h.
(96) Shin, J.-S.; Kim, B.-G.; Shin, D.-H. Kinetic Resolution of Chiral Amines Using Packed-Bed Reactor. *Enzyme Microb. Technol.* **2001**, *29* (4), 232–239. https://doi.org/10.1016/S0141-0229(01)00382-9.
(97) Cho, B.-K.; Cho, H. J.; Park, S.-H.; Yun, H.; Kim, B.-G. Simultaneous Synthesis of Enantiomerically Pure (S)-Amino Acids and (R)-Amines Using Coupled Transaminase Reactions. *Biotechnol. Bioeng.* **2003**, *81* (7), 783–789. https://doi.org/10.1002/bit.10526.

(98) Neuburger, J.; Helmholz, F.; Tiedemann, S.; Lehmann, P.; Süss, P.; Menyes, U.; von Langermann, J. Implementation and Scale-up of a Semi-Continuous Transaminase-Catalyzed Reactive Crystallization for the Preparation of (*S*)-(3-Methoxyphenyl)Ethylamine. *Chem. Eng. Process. - Process Intensif.* **2021**, *168*, 108578. https://doi.org/10.1016/j.cep.2021.108578.
(99) Green, A. P.; Turner, N. J.; O'Reilly, E. Chiral Amine Synthesis Using ω-Transaminases: An Amine Donor That Displaces Equilibria and Enables High-Throughput Screening. *Angew. Chem. Int. Ed.* **2014**, *53* (40), 10714–10717. https://doi.org/10.1002/anie.201406571.
(100) Maghraby, Y. R.; El-Shabasy, R. M.; Ibrahim, A. H.; Azzazy, H. M. E.-S. Enzyme Immobilization Technologies and Industrial Applications. *ACS Omega* **2023**, *8* (6), 5184–5196. https://doi.org/10.1021/acsomega.2c07560.
(101) M. Bolivar, J.; M. Woodley, J.; Fernandez-Lafuente, R. Is Enzyme Immobilization a Mature Discipline? Some Critical Considerations to Capitalize on the Benefits of Immobilization. *Chem. Soc. Rev.* **2022**, *51* (15), 6251–6290. https://doi.org/10.1039/D2CS00083K.
(102) Bornscheuer, U. T. Immobilizing Enzymes: How to Create More Suitable Biocatalysts. *Angew. Chem. Int. Ed.* **2003**, *42* (29), 3336–3337. https://doi.org/10.1002/anie.200301664.
(103) Ye, R.; Zhao, J.; Wickemeyer, B. B.; Toste, F. D.; Somorjai, G. A. Foundations and Strategies of the Construction of Hybrid Catalysts for Optimized Performances. *Nat. Catal.* **2018**, *1* (5), 318–325. https://doi.org/10.1038/s41929-018-0052-2.
(104) Holtze, C.; Boehling, R. Batch or Flow Chemistry? – A Current Industrial Opinion on Process Selection. *Curr. Opin. Chem. Eng.* **2022**, *36*, 100798. https://doi.org/10.1016/j.coche.2022.100798.
(105) I. Benítez-Mateos, A.; L. Contente, M.; Padrosa, D. R.; Paradisi, F. Flow Biocatalysis 101: Design, Development and Applications. *React. Chem. Eng.* **2021**, *6* (4), 599–611. https://doi.org/10.1039/D0RE00483A.
(106) Britton, J.; Majumdar, S.; Weiss, G. A. Continuous Flow Biocatalysis. *Chem. Soc. Rev.* **2018**, *47* (15), 5891–5918. https://doi.org/10.1039/c7cs00906b.
(107) Crotti, M.; Robescu, M. S.; Bolivar, J. M.; Ubiali, D.; Wilson, L.; Contente, M. L. What's New in Flow Biocatalysis? A Snapshot of 2020–2022. *Front. Catal.* **2023**, *3*. https://doi.org/10.3389/fctls.2023.1154452.
(108) Klibanov, A. M. Enzyme Stabilization by Immobilization. *Anal. Biochem.* **1979**, *93*, 1–25. https://doi.org/10.1016/S0003-2697(79)80110-4.
(109) Rodrigues, R. C.; Berenguer-Murcia, Á.; Carballares, D.; Morellon-Sterling, R.; Fernandez-Lafuente, R. Stabilization of Enzymes via Immobilization: Multipoint Covalent Attachment and Other Stabilization Strategies. *Biotechnol. Adv.* **2021**, *52*, 107821. https://doi.org/10.1016/j.biotechadv.2021.107821.
(110) Sheldon, R. A. Enzyme Immobilization: The Quest for Optimum Performance. *Adv. Synth. Catal.* **2007**, *349* (8–9), 1289–1307. https://doi.org/10.1002/adsc.200700082.
(111) Patti, S.; Magrini Alunno, I.; Pedroni, S.; Riva, S.; Ferrandi, E. E.; Monti, D. Advances and Challenges in the Development of Immobilized Enzymes for Batch and Flow Biocatalyzed Processes. *ChemSusChem* **2025**, *18* (8). https://doi.org/10.1002/cssc.202402007.
(112) Reus, B.; Damian, M.; Mutti, F. G. Advances in Cofactor Immobilization for Enhanced Continuous-Flow Biocatalysis. *J. Flow Chem.* **2024**, *14* (1), 219–238. https://doi.org/10.1007/s41981-024-00315-2.
(113) Twala, B. V.; Sewell, B. T.; Jordaan, J. Immobilisation and Characterisation of Biocatalytic Co-Factor Recycling Enzymes, Glucose Dehydrogenase and NADH Oxidase, on Aldehyde Functional ReSyn™ Polymer Microspheres. *Enzyme Microb. Technol.* **2012**, *50* (6), 331–336. https://doi.org/10.1016/j.enzmictec.2012.03.003.
(114) Debecker, D. P.; Smeets, V.; Van der Verren, M.; Meersseman Arango, H.; Kinnaer, M.; Devred, F. Hybrid Chemoenzymatic Heterogeneous Catalysts. *Curr. Opin. Green Sustain. Chem.* **2021**, *28*, 100437. https://doi.org/10.1016/j.cogsc.2020.100437.

(115) Júnior, A. A. da T.; Ladeira, Y. F. X.; França, A. da S.; Souza, R. O. M. A. de; Moraes, A. H.; Wojcieszak, R.; Itabaiana, I.; Miranda, A. S. de. Multicatalytic Hybrid Materials for Biocatalytic and Chemoenzymatic Cascades—Strategies for Multicatalyst (Enzyme) Co-Immobilization. *Catalysts* **2021**, *11* (8), 936. https://doi.org/10.3390/catal11080936.
(116) Hanefeld, U.; Gardossi, L.; Magner, E. Understanding Enzyme Immobilisation. *Chem. Soc. Rev.* **2009**, *38* (2), 453–468. https://doi.org/10.1039/b711564b.
(117) Lee, S.; O'Connor, T.; Yang, X.; Cruz, C.; Chatterjee, S.; Madurawe, R.; Moore, C.; Yu, L.; Woodcock, J. Modernizing Pharmaceutical Manufacturing: From Batch to Continuous Production. *J. Pharm. Innov.* **2015**, *10*. https://doi.org/10.1007/s12247-015-9215-8.
(118) Baumann, M.; Moody, T. S.; Smyth, M.; Wharry, S. A Perspective on Continuous Flow Chemistry in the Pharmaceutical Industry. *Org. Process Res. Dev.* **2020**, *24* (10), 1802–1813. https://doi.org/10.1021/acs.oprd.9b00524.
(119) Porta, R.; Benaglia, M.; Puglisi, A. Flow Chemistry: Recent Developments in the Synthesis of Pharmaceutical Products. *Org. Process Res. Dev.* **2016**, *20* (1), 2–25. https://doi.org/10.1021/acs.oprd.5b00325.
(120) Thompson, M. P.; Peñafiel, I.; Cosgrove, S. C.; Turner, N. J. Biocatalysis Using Immobilized Enzymes in Continuous Flow for the Synthesis of Fine Chemicals. *Org. Process Res. Dev.* **2019**, *23* (1), 9–18. https://doi.org/10.1021/acs.oprd.8b00305.
(121) Santi, M.; Sancineto, L.; Nascimento, V.; Braun Azeredo, J.; Orozco, E. V. M.; Andrade, L. H.; Gröger, H.; Santi, C. Flow Biocatalysis: A Challenging Alternative for the Synthesis of APIs and Natural Compounds. *Int. J. Mol. Sci.* **2021**, *22* (3), 990. https://doi.org/10.3390/ijms22030990.
(122) Tamborini, L.; Fernandes, P.; Paradisi, F.; Molinari, F. Flow Bioreactors as Complementary Tools for Biocatalytic Process Intensification. *Trends Biotechnol.* **2018**, *36* (1), 73–88. https://doi.org/10.1016/j.tibtech.2017.09.005.
(123) Robescu, M. S.; Bavaro, T. A Comprehensive Guide to Enzyme Immobilization: All You Need to Know. *Molecules* **2025**, *30* (4), 939. https://doi.org/10.3390/molecules30040939.
(124) Bié, J.; Sepodes, B.; Fernandes, P. C. B.; Ribeiro, M. H. L. Enzyme Immobilization and Co-Immobilization: Main Framework, Advances and Some Applications. *Processes* **2022**, *10* (3), 494. https://doi.org/10.3390/pr10030494.
(125) Datta, S.; Christena, L. R.; Rajaram, Y. R. S. Enzyme Immobilization: An Overview on Techniques and Support Materials. *3 Biotech* **2013**, *3* (1), 1–9. https://doi.org/10.1007/s13205-012-0071-7.
(126) Hegarty, E.; Paradisi, F. Implementation of Biocatalysis in Continuous Flow for the Synthesis of Small Cyclic Amines. *Chimia* **2020**, *74* (11), 890–894. https://doi.org/10.2533/chimia.2020.890.
(127) Yi, S.-S.; Lee, C.; Kim, J.; Kyung, D.; Kim, B.-G.; Lee, Y.-S. Covalent Immobilization of ω-Transaminase from *Vibrio Fluvialis* JS17 on Chitosan Beads. *Process Biochem.* **2007**, *42* (5), 895–898. https://doi.org/10.1016/j.procbio.2007.01.008.
(128) Mallin, H.; Menyes, U.; Vorhaben, T.; Höhne, M.; Bornscheuer, U. T. Immobilization of Two (R)-Amine Transaminases on an Optimized Chitosan Support for the Enzymatic Synthesis of Optically Pure Amines. *ChemCatChem* **2013**, *5* (2), 588–593. https://doi.org/10.1002/cctc.201200420.
(129) Mallin, H.; Höhne, M.; Bornscheuer, U. T. Immobilization of (*R*)- and (*S*)-Amine Transaminases on Chitosan Support and Their Application for Amine Synthesis Using Isopropylamine as Donor. *J. Biotechnol.* **2014**, *191*, 32–37. https://doi.org/10.1016/j.jbiotec.2014.05.015.
(130) Truppo, M. D.; Strotman, H.; Hughes, G. Development of an Immobilized Transaminase Capable of Operating in Organic Solvent. *ChemCatChem* **2012**, *4* (8), 1071–1074. https://doi.org/10.1002/cctc.201200228.
(131) Cassimjee, K. E.; Kadow, M.; Wikmark, Y.; Humble, M. S.; Rothstein, M. L.; Rothstein, D. M.; Bäckvall, J.-E. A General Protein Purification and Immobilization Method on Controlled

Porosity Glass: Biocatalytic Applications. *Chem. Commun.* **2014**, *50* (65), 9134–9137. https://doi.org/10.1039/C4CC02605E.
(132) Koszelewski, D.; Müller, N.; Schrittwieser, J. H.; Faber, K.; Kroutil, W. Immobilization of ω-Transaminases by Encapsulation in a Sol–Gel/Celite Matrix. *J. Mol. Catal. B Enzym.* **2010**, *63* (1), 39–44. https://doi.org/10.1016/j.molcatb.2009.12.001.
(133) Päiviö, M.; Kanerva, L. T. Reusable ω-Transaminase Sol–Gel Catalyst for the Preparation of Amine Enantiomers. *Process Biochem.* **2013**, *48* (10), 1488–1494. https://doi.org/10.1016/j.procbio.2013.07.021.
(134) Patramani, I.; Katsiri, K.; Pistevou, E.; Kalogerakos, T.; Pavlatos, M.; Evangelopoulos, A. E. Glutamic-Aspartic Transaminase — Antitransaminase Interaction: *Eur. J. Biochem.* **1969**, *11* (1), 28–36. https://doi.org/10.1111/j.1432-1033.1969.tb00734.x.
(135) Benítez-Mateos, A. I.; Paradisi, F. Perspectives on Flow Biocatalysis: The Engine Propelling Enzymatic Reactions. *J. Flow Chem.* **2024**, *14* (1), 211–218. https://doi.org/10.1007/s41981-023-00283-z.
(136) Barros, R. J.; Wehtje, E.; Adlercreutz, P. Effect of Mass-Transfer Limitations on the Selectivity of Immobilized α-Chymotrypsin Biocatalysts Prepared for Use in Organic Medium. *Biotechnol. Bioeng.* **2000**, *67* (3), 319–326. https://doi.org/10.1002/(SICI)1097-0290(20000205)67:3%253C319::AID-BIT8%253E3.0.CO;2-S.
(137) Böhmer, W.; Knaus, T.; Volkov, A.; Slot, T. K.; Shiju, N. R.; Engelmark Cassimjee, K.; Mutti, F. G. Highly Efficient Production of Chiral Amines in Batch and Continuous Flow by Immobilized ω-Transaminases on Controlled Porosity Glass Metal-Ion Affinity Carrier. *J. Biotechnol.* **2019**, *291*, 52–60. https://doi.org/10.1016/j.jbiotec.2018.12.001.
(138) Dawood, A. W. H.; Bassut, J.; de Souza, R. O. M. A.; Bornscheuer, U. T. Combination of the Suzuki–Miyaura Cross-Coupling Reaction with Engineered Transaminases. *Chem. – Eur. J.* **2018**, *24* (60), 16009–16013. https://doi.org/10.1002/chem.201804366.
(139) Mattey, A. P.; Ford, G. J.; Citoler, J.; Baldwin, C.; Marshall, J. R.; Palmer, R. B.; Thompson, M.; Turner, N. J.; Cosgrove, S. C.; Flitsch, S. L. Development of Continuous Flow Systems to Access Secondary Amines Through Previously Incompatible Biocatalytic Cascades. *Angew. Chem. Int. Ed.* **2021**, *60* (34), 18660–18665. https://doi.org/10.1002/anie.202103805.
(140) Heckmann, C. M.; Dominguez, B.; Paradisi, F. Enantio-Complementary Continuous-Flow Synthesis of 2-Aminobutane Using Covalently Immobilized Transaminases. *ACS Sustain. Chem. Eng.* **2021**, *9* (11), 4122–4129. https://doi.org/10.1021/acssuschemeng.0c09075.
(141) Contente, M. L.; Dall'Oglio, F.; Tamborini, L.; Molinari, F.; Paradisi, F. Highly Efficient Oxidation of Amines to Aldehydes with Flow-Based Biocatalysis. *ChemCatChem* **2017**, *9* (20), 3843–3848. https://doi.org/10.1002/cctc.201701570.
(142) Heinks, T.; Merz, L. M.; Liedtke, J.; Höhne, M.; van Langen, L. M.; Bornscheuer, U. T.; Fischer von Mollard, G.; Berglund, P. Biosynthesis of Furfurylamines in Batch and Continuous Flow by Immobilized Amine Transaminases. *Catalysts* **2023**, *13* (5), 875. https://doi.org/10.3390/catal13050875.
(143) Souza, S. P. de; Junior, I. I.; Silva, G. M. A.; Miranda, L. S. M.; Santiago, M. F.; Lam, F. L.-Y.; Dawood, A.; Bornscheuer, U. T.; Souza, R. O. M. A. de. Cellulose as an Efficient Matrix for Lipase and Transaminase Immobilization. *RSC Adv.* **2016**, *6* (8), 6665–6671. https://doi.org/10.1039/C5RA24976G.
(144) Biggelaar, L. van den; Soumillion, P.; Debecker, D. P. Biocatalytic Transamination in a Monolithic Flow Reactor: Improving Enzyme Grafting for Enhanced Performance. *RSC Adv.* **2019**, *9* (32), 18538–18546. https://doi.org/10.1039/C9RA02433F.
(145) Contente, M. L.; Paradisi, F. Self-Sustaining Closed-Loop Multienzyme-Mediated Conversion of Amines into Alcohols in Continuous Reactions. *Nat. Catal.* **2018**, *1* (6), 452–459. https://doi.org/10.1038/s41929-018-0082-9.

(146) Peris, E.; Okafor, O.; Kulcinskaja, E.; Goodridge, R.; Luis, S. V.; Garcia-Verdugo, E.; O'Reilly, E.; Sans, V. Tuneable 3D Printed Bioreactors for Transaminations under Continuous-Flow. *Green Chem.* **2017**, *19* (22), 5345–5349. https://doi.org/10.1039/C7GC02421E.
(147) Wang, X.; Xie, Y.; Wang, Z.; Zhang, K.; Wang, H.; Wei, D. Efficient Synthesis of (S)-1-Boc-3-Aminopiperidine in a Continuous Flow System Using ω-Transaminase-Immobilized Amino-Ethylenediamine-Modified Epoxide Supports. *Org. Process Res. Dev.* **2022**, *26* (5), 1351–1359. https://doi.org/10.1021/acs.oprd.1c00217.
(148) Abaházi, E.; Sátorhelyi, P.; Erdélyi, B.; Vértessy, B. G.; Land, H.; Paizs, C.; Berglund, P.; Poppe, L. Covalently Immobilized Trp60Cys Mutant of ω-Transaminase from *Chromobacterium Violaceum* for Kinetic Resolution of Racemic Amines in Batch and Continuous-Flow Modes. *Biochem. Eng. J.* **2018**, *132*, 270–278. https://doi.org/10.1016/j.bej.2018.01.022.
(149) Bajić, M.; Plazl, I.; Stloukal, R.; Žnidaršič-Plazl, P. Development of a Miniaturized Packed Bed Reactor with *ω*-Transaminase Immobilized in LentiKats®. *Process Biochem.* **2017**, *52*, 63–72. https://doi.org/10.1016/j.procbio.2016.09.021.
(150) Menegatti, T.; Žnidaršič-Plazl, P. Hydrogel-Based Enzyme and Cofactor Co-Immobilization for Efficient Continuous Transamination in a Microbioreactor. *Front. Bioeng. Biotechnol.* **2021**, *9*. https://doi.org/10.3389/fbioe.2021.752064.
(151) Benítez-Mateos, A. I.; Contente, M. L.; Velasco-Lozano, S.; Paradisi, F.; López-Gallego, F. Self-Sufficient Flow-Biocatalysis by Coimmobilization of Pyridoxal 5'-Phosphate and ω-Transaminases onto Porous Carriers. *ACS Sustain. Chem. Eng.* **2018**, *6* (10), 13151–13159. https://doi.org/10.1021/acssuschemeng.8b02672.
(152) Contente, M. L.; Paradisi, F. Transaminase-Catalyzed Continuous Synthesis of Biogenic Aldehydes. *ChemBioChem* **2019**, *20* (22), 2830–2833. https://doi.org/10.1002/cbic.201900356.
(153) Andrade, L. H.; Kroutil, W.; Jamison, T. F. Continuous Flow Synthesis of Chiral Amines in Organic Solvents: Immobilization of E. Coli Cells Containing Both ω-Transaminase and PLP. *Org. Lett.* **2014**, *16* (23), 6092–6095. https://doi.org/10.1021/ol502712v.
(154) Miložič, N.; Stojkovič, G.; Vogel, A.; Bouwes, D.; Žnidaršič-Plazl, P. Development of Microreactors with Surface-Immobilized Biocatalysts for Continuous Transamination. *New Biotechnol.* **2018**, *47*, 18–24. https://doi.org/10.1016/j.nbt.2018.05.004.
(155) Molnár, Z.; Farkas, E.; Lakó, Á.; Erdélyi, B.; Kroutil, W.; Vértessy, B. G.; Paizs, C.; Poppe, L. Immobilized Whole-Cell Transaminase Biocatalysts for Continuous-Flow Kinetic Resolution of Amines. *Catalysts* **2019**, *9* (5), 438. https://doi.org/10.3390/catal9050438.
(156) Rehn, G.; Adlercreutz, P.; Grey, C. Supported Liquid Membrane as a Novel Tool for Driving the Equilibrium of ω-Transaminase Catalyzed Asymmetric Synthesis. *J. Biotechnol.* **2014**, *179*, 50–55. https://doi.org/10.1016/j.jbiotec.2014.03.022.
(157) Romero-Fernandez, M.; Heckmann, C. M.; Paradisi, F. Biocatalytic Production of a Nylon 6 Precursor from Caprolactone in Continuous Flow. *ChemSusChem* **2022**, *15* (16), e202200811. https://doi.org/10.1002/cssc.202200811.
(158) Romero-Fernandez, M.; Paradisi, F. Biocatalytic Access to Betazole Using a One-Pot Multienzymatic System in Continuous Flow. *Green Chem.* **2021**, *23* (12), 4594–4603. https://doi.org/10.1039/D1GC01095F.
(159) Yang, L.; Shi, J.; Chen, C.; Wang, S.; Zhu, L.; Xie, W.; Guo, L. Dual-Enzyme, Co-Immobilized Capillary Microreactor Combined with Substrate Recycling for High-Sensitive Glutamate Determination Based on CE. *ELECTROPHORESIS* **2009**, *30* (20), 3527–3533. https://doi.org/10.1002/elps.200900195.
(160) Shin, J.-S.; Kim, B.-G.; Liese, A.; Wandrey, C. Kinetic Resolution of Chiral Amines with ω-Transaminase Using an Enzyme-Membrane Reactor. *Biotechnol. Bioeng.* **2001**, *73* (3), 179–187. https://doi.org/10.1002/bit.1050.

(161) Abdul Halim, A.; Szita, N.; Baganz, F. Characterization and Multi-Step Transketolase-ω-Transaminase Bioconversions in an Immobilized Enzyme Microreactor (IEMR) with Packed Tube. *J. Biotechnol.* **2013**, *168* (4), 567–575. https://doi.org/10.1016/j.jbiotec.2013.09.001.
(162) Van den Biggelaar, L.; Soumillion, P.; Debecker, D. P. Enantioselective Transamination in Continuous Flow Mode with Transaminase Immobilized in a Macrocellular Silica Monolith. *Catalysts* **2017**, *7* (2), 54. https://doi.org/10.3390/catal7020054.
(163) Börner, T.; Rehn, G.; Grey, C.; Adlercreutz, P. A Process Concept for High-Purity Production of Amines by Transaminase-Catalyzed Asymmetric Synthesis: Combining Enzyme Cascade and Membrane-Assisted ISPR. *Org. Process Res. Dev.* **2015**, *19* (7), 793–799. https://doi.org/10.1021/acs.oprd.5b00055.
(164) Satyawali, Y.; del Pozo, D. F.; Vandezande, P.; Nopens, I.; Dejonghe, W. Investigating Pervaporation for In Situ Acetone Removal as Process Intensification Tool in ω-Transaminase Catalyzed Chiral Amine Synthesis. *Biotechnol. Prog.* **2019**, *35* (1), e2731. https://doi.org/10.1002/btpr.2731.
(165) Satyawali, Y.; Ehimen, E.; Cauwenberghs, L.; Maesen, M.; Vandezande, P.; Dejonghe, W. Asymmetric Synthesis of Chiral Amine in Organic Solvent and *in-Situ* Product Recovery for Process Intensification: A Case Study. *Biochem. Eng. J.* **2017**, *117*, 97–104. https://doi.org/10.1016/j.bej.2016.11.006.
(166) Sitanggang, A. B.; Drews, A.; Kraume, M. Enzymatic Membrane Reactors: Designs, Applications, Limitations and Outlook. *Chem. Eng. Process. - Process Intensif.* **2022**, *180*, 108729. https://doi.org/10.1016/j.cep.2021.108729.
(167) Luis, P. *Fundamental Modeling of Membrane Systems*; 2018. https://doi.org/10.1016/B978-0-12-813483-2.00001-0.
(168) Li, W.; Estager, J.; Monbaliu, J.-C. M.; Debecker, D. P.; Luis, P. Separation of Bio-Based Chemicals Using Pervaporation. *J. Chem. Technol. Biotechnol.* **2020**, *95* (9), 2311–2334. https://doi.org/10.1002/jctb.6434.
(169) *Membrane Processes in Separation and Purification*; Crespo, J. G., Böddeker, K. W., Eds.; Springer Netherlands: Dordrecht, 1994. https://doi.org/10.1007/978-94-015-8340-4.
(170) Jochems, P.; Satyawali, Y.; Diels, L.; Dejonghe, W. Enzyme Immobilization on/in Polymeric Membranes: Status, Challenges and Perspectives in Biocatalytic Membrane Reactors (BMRs). *Green Chem.* **2011**, *13* (7), 1609–1623. https://doi.org/10.1039/C1GC15178A.
(171) Pinelo, M.; Jonsson, G.; Meyer, A. S. Membrane Technology for Purification of Enzymatically Produced Oligosaccharides: Molecular and Operational Features Affecting Performance. *Sep. Purif. Technol.* **2009**, *70* (1), 1–11. https://doi.org/10.1016/j.seppur.2009.08.010.
(172) Ameur, S. B.; Luminiţa Gîjiu, C.; Belleville, M.-P.; Sanchez, J.; Paolucci-Jeanjean, D. Development of a Multichannel Monolith Large-Scale Enzymatic Membrane and Application in an Immobilized Enzymatic Membrane Reactor. *J. Membr. Sci.* **2014**, *455*, 330–340. https://doi.org/10.1016/j.memsci.2013.12.026.
(173) Luo, J.; Song, S.; Zhang, H.; Zhang, H.; Zhang, J.; Wan, Y. Biocatalytic Membrane: Go Far beyond Enzyme Immobilization. *Eng. Life Sci.* **2020**, *20* (11), 441–450. https://doi.org/10.1002/elsc.202000018.
(174) Giorno, L.; Drioli, E. Biocatalytic Membrane Reactors: Applications and Perspectives. *Trends Biotechnol.* **2000**, *18* (8), 339–349. https://doi.org/10.1016/S0167-7799(00)01472-4.
(175) Prazeres, D. M. F.; Cabral, J. M. S. Enzymatic Membrane Bioreactors and Their Applications. *Enzyme Microb. Technol.* **1994**, *16* (9), 738–750. https://doi.org/10.1016/0141-0229(94)90030-2.
(176) Agustian, J.; Kamaruddin, A. H.; Bhatia, S. Enzymatic Membrane Reactors: The Determining Factors in Two Separate Phase Operations. *J. Chem. Technol. Biotechnol.* **2011**, *86* (8), 1032–1048. https://doi.org/10.1002/jctb.2575.

(177) Giorno, L.; Mazzei, R.; Drioli, E. Biochemical Membrane Reactors in Industrial Processes. In *Membrane Operations*; John Wiley & Sons, Ltd, 2009; pp 397–409. https://doi.org/10.1002/9783527626779.ch17.
(178) Sigurdardóttir, S. B.; Lehmann, J.; Ovtar, S.; Grivel, J.-C.; Negra, M. D.; Kaiser, A.; Pinelo, M. Enzyme Immobilization on Inorganic Surfaces for Membrane Reactor Applications: Mass Transfer Challenges, Enzyme Leakage and Reuse of Materials. *Adv. Synth. Catal.* **2018**, *360* (14), 2578–2607. https://doi.org/10.1002/adsc.201800307.
(179) Kayvani Fard, A.; McKay, G.; Buekenhoudt, A.; Al Sulaiti, H.; Motmans, F.; Khraisheh, M.; Atieh, M. Inorganic Membranes: Preparation and Application for Water Treatment and Desalination. *Materials* **2018**, *11* (1), 74. https://doi.org/10.3390/ma11010074.
(180) Ranieri, G.; Mazzei, R.; Wu, Z.; Li, K.; Giorno, L. Use of a Ceramic Membrane to Improve the Performance of Two-Separate-Phase Biocatalytic Membrane Reactor. *Molecules* **2016**, *21* (3), 345. https://doi.org/10.3390/molecules21030345.
(181) Chakraborty, S.; Rusli ,Handajaya; Nath ,Arijit; Sikder ,Jaya; Bhattacharjee ,Chiranjib; Curcio ,Stefano; and Drioli, E. Immobilized Biocatalytic Process Development and Potential Application in Membrane Separation: A Review. *Crit. Rev. Biotechnol.* **2016**, *36* (1), 43–58. https://doi.org/10.3109/07388551.2014.923373.
(182) Qing, W.; Li, X.; Shao, S.; Shi, X.; Wang, J.; Feng, Y.; Zhang, W.; Zhang, W. Polymeric Catalytically Active Membranes for Reaction-Separation Coupling: A Review. *J. Membr. Sci.* **2019**, *583*, 118–138. https://doi.org/10.1016/j.memsci.2019.04.053.
(183) Yang, H.-C.; Luo, J.; Lv, Y.; Shen, P.; Xu, Z.-K. Surface Engineering of Polymer Membranes via Mussel-Inspired Chemistry. *J. Membr. Sci.* **2015**, *483*, 42–59. https://doi.org/10.1016/j.memsci.2015.02.027.
(184) Bouwer, S. T.; Cuperus, F. P.; Derksen, J. T. P. The Performance of Enzyme-Membrane Reactors with Immobilized Lipase. *Enzyme Microb. Technol.* **1997**, *21* (4), 291–296. https://doi.org/10.1016/S0141-0229(97)00044-6.
(185) Belfort, G. Membrane Modules: Comparison of Different Configurations Using Fluid Mechanics. *J. Membr. Sci.* **1988**, *35* (3), 245–270. https://doi.org/10.1016/S0376-7388(00)80299-9.
(186) Crowder, M. L.; Gooding, C. H. Spiral Wound, Hollow Fiber Membrane Modules: A New Approach to Higher Mass Transfer Efficiency. *J. Membr. Sci.* **1997**, *137* (1), 17–29. https://doi.org/10.1016/S0376-7388(97)00174-9.
(187) Vasileva, N.; Ivanov, Y.; Damyanova, S.; Kostova, I.; Godjevargova, T. Hydrolysis of Whey Lactose by Immobilized β-Galactosidase in a Bioreactor with a Spirally Wound Membrane. *Int. J. Biol. Macromol.* **2016**, *82*, 339–346. https://doi.org/10.1016/j.ijbiomac.2015.11.025.
(188) Othman, M. H. D.; Adam, M. R.; Pauzan, M. A. B.; Hubadillah, S. K.; Rahman, M. A.; Jaafar, J. Ultrafiltration Membrane for Water Treatment. In *Self-standing Substrates: Materials and Applications*; Inamuddin, Boddula, R., Asiri, A. M., Eds.; Springer International Publishing: Cham, 2020; pp 119–145. https://doi.org/10.1007/978-3-030-29522-6_4.
(189) Lindeque, R. M.; Woodley, J. M. Reactor Selection for Effective Continuous Biocatalytic Production of Pharmaceuticals. *Catalysts* **2019**, *9* (3), 262. https://doi.org/10.3390/catal9030262.
(190) Eş, I.; Vieira, J. D. G.; Amaral, A. C. Principles, Techniques, and Applications of Biocatalyst Immobilization for Industrial Application. *Appl. Microbiol. Biotechnol.* **2015**, *99* (5), 2065–2082. https://doi.org/10.1007/s00253-015-6390-y.
(191) Luo, J.; Meyer, A. S.; Jonsson, G.; Pinelo, M. Fouling-Induced Enzyme Immobilization for Membrane Reactors. *Bioresour. Technol.* **2013**, *147*, 260–268. https://doi.org/10.1016/j.biortech.2013.08.019.
(192) Chiang, C.-L.; Tsai, S.-W. Application of a Recycle Dialysis System in a Reversed Micellar Reactor. *J. Chem. Technol. Biotechnol.* **1992**, *54* (1), 27–32. https://doi.org/10.1002/jctb.280540106.

(193) Cen, Y.-K.; Liu, Y.-X.; Xue, Y.-P.; Zheng, Y.-G. Immobilization of Enzymes in/on Membranes and Their Applications. *Adv. Synth. Catal.* **2019**, *361* (24), 5500–5515. https://doi.org/10.1002/adsc.201900439.
(194) Vladisavljević, G. T. Biocatalytic Membrane Reactors (BMR). *Phys. Sci. Rev.* **2016**, *1* (1). https://doi.org/10.1515/psr-2015-0015.
(195) Yang, J.; Stuart, M. A. C.; Kamperman, M. Jack of All Trades: Versatile Catechol Crosslinking Mechanisms. *Chem. Soc. Rev.* **2014**, *43*, 8271–8298. https://doi.org/10.1039/C4CS00185K.
(196) Zhang, H.; Luo, J.; Li, S.; Wei, Y.; Wan, Y. Biocatalytic Membrane Based on Polydopamine Coating: A Platform for Studying Immobilization Mechanisms. *Langmuir* **2018**, *34* (8), 2585–2594. https://doi.org/10.1021/acs.langmuir.7b02860.
(197) Bahulekar, R.; Ayyangar, N. R.; Ponrathnam, S. Polyethyleneimine in Immobilization of Biocatalysts. *Enzyme Microb. Technol.* **1991**, *13* (11), 858–868. https://doi.org/10.1016/0141-0229(91)90101-F.
(198) Popkov, A.; Malankowska, M.; Simon De Martini, M.; Singh, S.; Su, Z.; Pinelo, M. Opting for Polyamines with Specific Structural Traits as a Strategy to Boost Performance of Enzymatic Membrane Reactors. *Chem. Eng. J.* **2024**, *494*, 153115. https://doi.org/10.1016/j.cej.2024.153115.
(199) Verma, M. L.; Kumar, S.; Das, A.; Randhawa, J. S.; Chamundeeswari, M. Chitin and Chitosan-Based Support Materials for Enzyme Immobilization and Biotechnological Applications. *Environ. Chem. Lett.* **2020**, *18* (2), 315–323. https://doi.org/10.1007/s10311-019-00942-5.
(200) Vander Straeten, A.; Lefèvre, D.; Demoustier-Champagne, S.; Dupont-Gillain, C. Protein-Based Polyelectrolyte Multilayers. *Adv. Colloid Interface Sci.* **2020**, *280*, 102161. https://doi.org/10.1016/j.cis.2020.102161.
(201) Yuan, Y.; Shen, J.; Salmon, S. Developing Enzyme Immobilization with Fibrous Membranes: Longevity and Characterization Considerations. *Membranes* **2023**, *13* (5), 532. https://doi.org/10.3390/membranes13050532.
(202) Ebrahimi, M.; Placido, L.; Engel, L.; Ashaghi, K. S.; Czermak, P. A Novel Ceramic Membrane Reactor System for the Continuous Enzymatic Synthesis of Oligosaccharides. *Desalination* **2010**, *250* (3), 1105–1108. https://doi.org/10.1016/j.desal.2009.09.118.
(203) Wang, Y.; Hsieh, Y.-L. Immobilization of Lipase Enzyme in Polyvinyl Alcohol (PVA) Nanofibrous Membranes. *J. Membr. Sci.* **2008**, *309* (1), 73–81. https://doi.org/10.1016/j.memsci.2007.10.008.
(204) Luo, J.; Meyer, A. S.; Jonsson, G.; Pinelo, M. Enzyme Immobilization by Fouling in Ultrafiltration Membranes: Impact of Membrane Configuration and Type on Flux Behavior and Biocatalytic Conversion Efficacy. *Biochem. Eng. J.* **2014**, *83*, 79–89. https://doi.org/10.1016/j.bej.2013.12.007.
(205) Luo, J.; Marpani, F.; Brites, R.; Frederiksen, L.; Meyer, A. S.; Jonsson, G.; Pinelo, M. Directing Filtration to Optimize Enzyme Immobilization in Reactive Membranes. *J. Membr. Sci.* **2014**, *459*, 1–11. https://doi.org/10.1016/j.memsci.2014.01.065.
(206) Luo, J.; Meyer, A. S.; Mateiu, R. V.; Kalyani, D.; Pinelo, M. Functionalization of a Membrane Sublayer Using Reverse Filtration of Enzymes and Dopamine Coating. *ACS Appl. Mater. Interfaces* **2014**, *6* (24), 22894–22904. https://doi.org/10.1021/am507308k.
(207) Tang, C. Y.; Chong, T. H.; Fane, A. G. Colloidal Interactions and Fouling of NF and RO Membranes: A Review. *Adv. Colloid Interface Sci.* **2011**, *164* (1), 126–143. https://doi.org/10.1016/j.cis.2010.10.007.
(208) Drews, A. Membrane Fouling in Membrane Bioreactors—Characterisation, Contradictions, Cause and Cures. *J. Membr. Sci.* **2010**, *363* (1), 1–28. https://doi.org/10.1016/j.memsci.2010.06.046.

(209) Meng, F.; Zhang, S.; Oh, Y.; Zhou, Z.; Shin, H.-S.; Chae, S.-R. Fouling in Membrane Bioreactors: An Updated Review. *Water Res.* **2017**, *114*, 151–180. https://doi.org/10.1016/j.watres.2017.02.006.
(210) Thomas, C. R.; Geer, D. Effects of Shear on Proteins in Solution. *Biotechnol. Lett.* **2011**, *33* (3), 443–456. https://doi.org/10.1007/s10529-010-0469-4.
(211) Bekard, I. B.; Asimakis, P.; Bertolini, J.; Dunstan, D. E. The Effects of Shear Flow on Protein Structure and Function. *Biopolymers* **2011**, *95* (11), 733–745. https://doi.org/10.1002/bip.21646.
(212) Elias, C. B.; Joshi, J. B. Role of Hydrodynamic Shear on Activity and Structure of Proteins. In *Bioprocess and Algae Reactor Technology, Apoptosis*; Springer: Berlin, Heidelberg, 1998; pp 47–71. https://doi.org/10.1007/BFb0102296.
(213) Yang, J.; Buekenhoudt, A.; Dael, M. V.; Luis, P.; Satyawali, Y.; Malina, R.; Lizin, S. A Techno-Economic Assessment of a Biocatalytic Chiral Amine Production Process Integrated with In Situ Membrane Extraction. *Org. Process Res. Dev.* **2022**, *26* (7), 2052–2066. https://doi.org/10.1021/acs.oprd.1c00464.
(214) Niu, Z.; Zhao, Y.; Sun, W.; Shi, S.; Gong, Y. Biomimetic Surface Modification of Polypropylene by Surface Chain Transfer Reaction Based on Mussel-Inspired Adhesion Technology and Thiol Chemistry. *Appl. Surf. Sci.* **2016**, *386*, 41–50. https://doi.org/10.1016/j.apsusc.2016.06.006.
(215) Souza, S. P. de; Junior, I. I.; Silva, G. M. A.; Miranda, L. S. M.; Santiago, M. F.; Lam, F. L.-Y.; Dawood, A.; Bornscheuer, U. T.; Souza, R. O. M. A. de. Cellulose as an Efficient Matrix for Lipase and Transaminase Immobilization. *RSC Adv.* **2016**, *6* (8), 6665–6671. https://doi.org/10.1039/C5RA24976G.
(216) Mateo, C.; Grazú, V.; Pessela, B. C. C.; Montes, T.; Palomo, J. M.; Torres, R.; López-Gallego, F.; Fernández-Lafuente, R.; Guisán, J. M. Advances in the Design of New Epoxy Supports for Enzyme Immobilization–Stabilization. *Biochem. Soc. Trans.* **2007**, *35* (6), 1593–1601. https://doi.org/10.1042/BST0351593.
(217) Rozicka, A.; Niemistö, J.; Keiski, R. L.; Kujawski, W. Apparent and Intrinsic Properties of Commercial PDMS Based Membranes in Pervaporative Removal of Acetone, Butanol and Ethanol from Binary Aqueous Mixtures. *J. Membr. Sci.* **2014**, *453*, 108–118. https://doi.org/10.1016/j.memsci.2013.10.065.
(218) Heckmann, C. M.; Gourlay, L. J.; Dominguez, B.; Paradisi, F. An (R)-Selective Transaminase From Thermomyces Stellatus: Stabilizing the Tetrameric Form. *Front. Bioeng. Biotechnol.* **2020**, *8*, 1–13. https://doi.org/10.3389/fbioe.2020.00707.
(219) Cerioli, L.; Planchestainer, M.; Cassidy, J.; Tessaro, D.; Paradisi, F. Characterization of a Novel Amine Transaminase from *Halomonas Elongata*. *J. Mol. Catal. B Enzym.* **2015**, *120*, 141–150. https://doi.org/10.1016/j.molcatb.2015.07.009.
(220) Velasco-Lozano, S.; Jackson, E.; Ripoll, M.; López-Gallego, F.; Betancor, L. Stabilization of ω-Transaminase from *Pseudomonas Fluorescens* by Immobilization Techniques. *Int. J. Biol. Macromol.* **2020**, *164*, 4318–4328. https://doi.org/10.1016/j.ijbiomac.2020.09.003.
(221) Chen, S.; Land, H.; Berglund, P.; Humble, M. S. Stabilization of an Amine Transaminase for Biocatalysis. *J. Mol. Catal. B Enzym.* **2016**, *124*, 20–28. https://doi.org/10.1016/j.molcatb.2015.11.022.
(222) Gomm, A.; O'Reilly, E. Transaminases for Chiral Amine Synthesis. *Curr. Opin. Chem. Biol.* **2018**, *43*, 106–112. https://doi.org/10.1016/j.cbpa.2017.12.007.
(223) Cosgrove, S. C.; Ramsden, J. I.; Mangas-Sanchez, J.; Turner, N. J. Biocatalytic Synthesis of Chiral Amines Using Oxidoreductases. In *Methodologies in Amine Synthesis*; John Wiley & Sons, Ltd, 2021; pp 243–283. https://doi.org/10.1002/9783527826186.ch7.
(224) Schmid, A.; Dordick, J. S.; Hauer, B.; Kiener, A.; Wubbolts, M.; Witholt, B. Industrial Biocatalysis Today and Tomorrow. *Nature* **2001**, *409* (6817), 258–268. https://doi.org/10.1038/35051736.

(225) Khanra, M.; Ravichandiran, V.; Swain, S. P. Lipase Enzymes for Sustainable Synthesis of Pharmaceuticals and Chiral Organic Building Blocks. *Adv. Sustain. Syst.* **2025**, *9* (1), 2400495. https://doi.org/10.1002/adsu.202400495.
(226) Clapés, P.; Fessner, W.-D.; Sprenger, G. A.; Samland, A. K. Recent Progress in Stereoselective Synthesis with Aldolases. *Curr. Opin. Chem. Biol.* **2010**, *14* (2), 154–167. https://doi.org/10.1016/j.cbpa.2009.11.029.
(227) Mathipa-Mdakane, M. G.; Steenkamp, L. Aldolase: A Desirable Biocatalytic Candidate for Biotechnological Applications. *Catalysts* **2024**, *14* (2), 114. https://doi.org/10.3390/catal14020114.
(228) Yang, L.-C.; Deng, H.; Renata, H. Recent Progress and Developments in Chemoenzymatic and Biocatalytic Dynamic Kinetic Resolution. *Org. Process Res. Dev.* **2022**, *26* (7), 1925–1943. https://doi.org/10.1021/acs.oprd.1c00463.
(229) Cassimjee, K. E.; Humble, M. S.; Miceli, V.; Colomina, C. G.; Berglund, P. Active Site Quantification of an ω-Transaminase by Performing a Half Transamination Reaction. *ACS Catal.* **2011**, *1* (9), 1051–1055. https://doi.org/10.1021/cs200315h.
(230) Cassimjee, K. E.; Manta, B.; Himo, F. A Quantum Chemical Study of the ω-Transaminase Reaction Mechanism. *Org. Biomol. Chem.* **2015**, *13* (31), 8453–8464. https://doi.org/10.1039/C5OB00690B.
(231) Koszelewski, D.; Tauber, K.; Faber, K.; Kroutil, W. ω-Transaminases for the Synthesis of Non-Racemic α-Chiral Primary Amines. *Trends Biotechnol.* **2010**, *28* (6), 324–332. https://doi.org/10.1016/j.tibtech.2010.03.003.
(232) US EPA, O. *Presidential Green Chemistry Challenge: 2010 Greener Reaction Conditions Award*. https://www.epa.gov/greenchemistry/presidential-green-chemistry-challenge-2010-greener-reaction-conditions-award.
(233) Desai, A. A. Sitagliptin Manufacture: A Compelling Tale of Green Chemistry, Process Intensification, and Industrial Asymmetric Catalysis. *Angew. Chem. Int. Ed.* **2011**, *50* (9), 1974–1976. https://doi.org/10.1002/anie.201007051.
(234) Mangion, I. K.; Sherry, B. D.; Yin, J.; Fleitz, F. J. Enantioselective Synthesis of a Dual Orexin Receptor Antagonist. *Org. Lett.* **2012**, *14* (13), 3458–3461. https://doi.org/10.1021/ol3014123.
(235) Wallace, D. J.; Mangion, I.; Coleman, P. Discovery and Chemical Development of Suvorexant - A Dual Orexin Antagonist for Sleep Disorder. In *Comprehensive Accounts of Pharmaceutical Research and Development: From Discovery to Late-Stage Process Development Volume 1*; ACS Symposium Series; American Chemical Society, 2016; Vol. 1239, pp 1–36. https://doi.org/10.1021/bk-2016-1239.ch001.
(236) Chung, J. Y. L.; Zhong, Y.-L.; Maloney, K. M.; Reamer, R. A.; Moore, J. C.; Strotman, H.; Kalinin, A.; Feng, R.; Strotman, N. A.; Xiang, B.; Yasuda, N. Unusual Pyrimidine Participation: Efficient Stereoselective Synthesis of Potent Dual Orexin Receptor Antagonist MK-6096. *Org. Lett.* **2014**, *16* (22), 5890–5893. https://doi.org/10.1021/ol5028249.
(237) Chung, J. Y. L.; Marcune, B.; Strotman, H. R.; Petrova, R. I.; Moore, J. C.; Dormer, P. G. Synthesis of ((3R,6R)-6-Methylpiperidin-3-Yl)Methanol via Biocatalytic Transamination and Crystallization-Induced Dynamic Resolution. *Org. Process Res. Dev.* **2015**, *19* (10), 1418–1423. https://doi.org/10.1021/acs.oprd.5b00259.
(238) Frodsham, L.; Golden, M.; Hard, S.; Kenworthy, M. N.; Klauber, D. J.; Leslie, K.; Macleod, C.; Meadows, R. E.; Mulholland, K. R.; Reilly, J.; Squire, C.; Tomasi, S.; Watt, D.; Wells, A. S. Use of ω-Transaminase Enzyme Chemistry in the Synthesis of a JAK2 Kinase Inhibitor. *Org. Process Res. Dev.* **2013**, *17* (9), 1123–1130. https://doi.org/10.1021/op400133d.
(239) Ferrandi, E. E.; Monti, D. Amine Transaminases in Chiral Amines Synthesis: Recent Advances and Challenges. *World J. Microbiol. Biotechnol.* **2017**, *34* (1), 13. https://doi.org/10.1007/s11274-017-2395-2.

(240) Burns, M.; Martinez, C. A.; Vanderplas, B.; Wisdom, R.; Yu, S.; Singer, R. A. A Chemoenzymatic Route to Chiral Intermediates Used in the Multikilogram Synthesis of a Gamma Secretase Inhibitor. *Org. Process Res. Dev.* **2017**, *21* (6), 871–877. https://doi.org/10.1021/acs.oprd.7b00096.
(241) Novick, S. J.; Dellas, N.; Garcia, R.; Ching, C.; Bautista, A.; Homan, D.; Alvizo, O.; Entwistle, D.; Kleinbeck, F.; Schlama, T.; Ruch, T. Engineering an Amine Transaminase for the Efficient Production of a Chiral Sacubitril Precursor. *ACS Catal.* **2021**, *11* (6), 3762–3770. https://doi.org/10.1021/acscatal.0c05450.
(242) Molinaro, C.; Bulger, P. G.; Lee, E. E.; Kosjek, B.; Lau, S.; Gauvreau, D.; Howard, M. E.; Wallace, D. J.; O'Shea, P. D. CRTH2 Antagonist MK-7246: A Synthetic Evolution from Discovery through Development. *J. Org. Chem.* **2012**, *77* (5), 2299–2309. https://doi.org/10.1021/jo202620r.
(243) Midelfort, K. S.; Kumar, R.; Han, S.; Karmilowicz, M. J.; McConnell, K.; Gehlhaar, D. K.; Mistry, A.; Chang, J. S.; Anderson, M.; Villalobos, A.; Minshull, J.; Govindarajan, S.; Wong, J. W. Redesigning and Characterizing the Substrate Specificity and Activity of Vibrio Fluvialis Aminotransferase for the Synthesis of Imagabalin. *Protein Eng. Des. Sel. PEDS* **2013**, *26* (1), 25–33. https://doi.org/10.1093/protein/gzs065.
(244) Busto, E.; Simon, R. C.; Grischek, B.; Gotor-Fernández, V.; Kroutil, W. Cover Picture: Cutting Short the Asymmetric Synthesis of the Ramatroban Precursor by Employing ω-Transaminases (Adv. Synth. Catal. 9/2014). *Adv. Synth. Catal.* **2014**, *356* (9), 1889–1889. https://doi.org/10.1002/adsc.201400458.
(245) Kohrt, J. T.; Dorff, P. H.; Burns, M.; Lee, C.; O'Neil, S. V.; Maguire, R. J.; Kumar, R.; Wagenaar, M.; Price, L.; Lall, M. S. Application of Flow and Biocatalytic Transaminase Technology for the Synthesis of a 1-Oxa-8-Azaspiro[4.5]Decan-3-Amine. *Org. Process Res. Dev.* **2022**, *26* (3), 616–623. https://doi.org/10.1021/acs.oprd.1c00075.
(246) Matosevic, S.; Lye, G. J.; Baganz, F. Immobilised Enzyme Microreactor for Screening of Multi-Step Bioconversions: Characterisation of a *de Novo* Transketolase-ω-Transaminase Pathway to Synthesise Chiral Amino Alcohols. *J. Biotechnol.* **2011**, *155* (3), 320–329. https://doi.org/10.1016/j.jbiotec.2011.07.017.
(247) Semproli, R.; Vaccaro, G.; Ferrandi, E. E.; Vanoni, M.; Bavaro, T.; Marrubini, G.; Annunziata, F.; Conti, P.; Speranza, G.; Monti, D.; Tamborini, L.; Ubiali, D. Use of Immobilized Amine Transaminase from Vibrio Fluvialis under Flow Conditions for the Synthesis of (S)-1-(5-Fluoropyrimidin-2-Yl)-Ethanamine. *ChemCatChem* **2020**, *12* (5), 1359–1367. https://doi.org/10.1002/cctc.201902080.
(248) Truppo, M. D.; Journet, M.; Strotman, H.; Mcmullen, J. P.; Grosser, S. T. Immobilized Transaminases and Process for Making and Using Immobilized Transaminase. WO2014133928A1, September 4, 2014. https://patents.google.com/patent/WO2014133928A1/en (accessed 2025-05-27).
(249) Benítez-Mateos, A. I.; Bertella, S.; Behaghel de Bueren, J.; Luterbacher, J. S.; Paradisi, F. Dual Valorization of Lignin as a Versatile and Renewable Matrix for Enzyme Immobilization and (Flow) Bioprocess Engineering. *ChemSusChem* **2021**, *14* (15), 3198–3207. https://doi.org/10.1002/cssc.202100926.
(250) Bank, R. P. D. *RCSB PDB - 6XWB: Crystal structure of an R-selective transaminase from Thermomyces stellatus*. https://www.rcsb.org/structure/6XWB.

IX. Annexes

IX.1 Annex I – Introduction

Annex I.S1 - Biocatalysis for Chiral Amine Compounds Production

Types of enzymes

Tab.I.S1 - List of most currently employed enzymes for production of chiral amine compounds distinguishing by their primary metabolic functions inspired from 31

Enzyme category	Enzyme type	Main metabolic function	Ref.
Transferases	Transaminases	Transfer of amine groups	70,71,223
Oxidoreductases	Monoamine oxidases, Amine oxidases, Imine reductases, Amino acid dehydrogenases, Lactate dehydrogenase, Glucose dehydrogenase	Oxidation of amines ; Reduction of imines or ketones ; Cofactor recycling	10,224
Hydrolases	Lipases Amidases Proteases	Hydrolysis of esters or amides	225,226
Lyases/-Decarboxylases	Decarboxylase Aldolase	Decarboxylation and carbon–carbon bond formation (Aldol)	227,228

Types of reactional strategies

Biocatalytic strategies for the synthesis of chiral amines encompass three main approaches: KR, AS and Deracemization, each involving specific enzyme classes Tab.I.S2 [11,31,40,51].

KR relies on enantioselective enzymes such as lipases, amidases, or transaminases to selectively convert one enantiomer from a racemic mixture. However, this method is inherently constrained by a maximum theoretical yield of 50% [31,40]. To overcome this limitation, the hybrid approach known as Dynamic Kinetic Resolution (DKR) integrates a racemization catalyst—typically a transition metal complex—that continuously interconverts the enantiomers. This mechanism allows the reaction to approach theoretical yields of 100%, significantly enhancing its efficiency [31,40,229].

In contrast, AS enables the direct construction of chiral amines from prochiral ketones or imines. This method employs enzymes such as transaminases, imine reductases, amino acid dehydrogenases, or decarboxylases to achieve complete theoretical conversion with high enantioselectivity. Recent advances in enzyme engineering have further enhanced its industrial applicability, making it a preferred strategy for large-scale production [11,31,51].

Finally, Deracemization represents a powerful biocatalytic approach capable of reaching 100% yield. This process typically involves the selective oxidation of one enantiomer through monoamine oxidases, followed by stereoselective reduction. This dual-step strategy is particularly well-suited for the synthesis of complex amine targets, offering a viable pathway to high-purity chiral amines [31,40].

Tab.I.S2 - Main reactional strategies associated with types of enzymes currently used when biocatalysis route are employed for production of chiral amine compounds inspired from 31

Strategy	Enzymes Involved
Kinetic & Dynamic Kinetic Resolution	Transaminases, Lipases, Amidases, Proteases
Asymmetric Synthesis	Transaminases, Imine reductases, Amino acid dehydrogenases, Decarboxylase, Aldolase
Deracemization	Transaminase, Monoamine oxidases, Amine oxidases

Annex I.S2 - Structure, Specificity and Mechanism of ATA

To elucidate the structural and functional specificity of ATAs, we selected ATA-117, a commercially available and well-characterized R-selective ATA, as the reference enzyme for the following analysis.

ATA enzymes function as homodimers, with each monomer contributing half of the active site. Proper dimerization is essential for optimal catalytic activity (Fig.I.S1, left).

Each active site consists of three distinct pockets: one for binding the PLP cofactor—anchored via a conserved lysine residue forming a reversible imine linkage (Fig.I.S2) —and two for substrate binding (Fig.I.S1, right). The small substrate pocket accommodates minimal substituents (e.g., methyl groups), while the large pocket is more permissive, tolerating bulkier groups such as alkyl chains, carboxylic acids, ethers, and aromatic rings. Consequently, ATA-117 efficiently catalyzes the transformation of amines bearing a small substituent on one side and a larger functional group on the other.

These enzymes follow a ping-pong bi–bi kinetic mechanism Fig.I.S2, involving two successive bimolecular reactions in which the enzyme alternates between an intermediate and a regenerated state after each half-reaction [230–232].

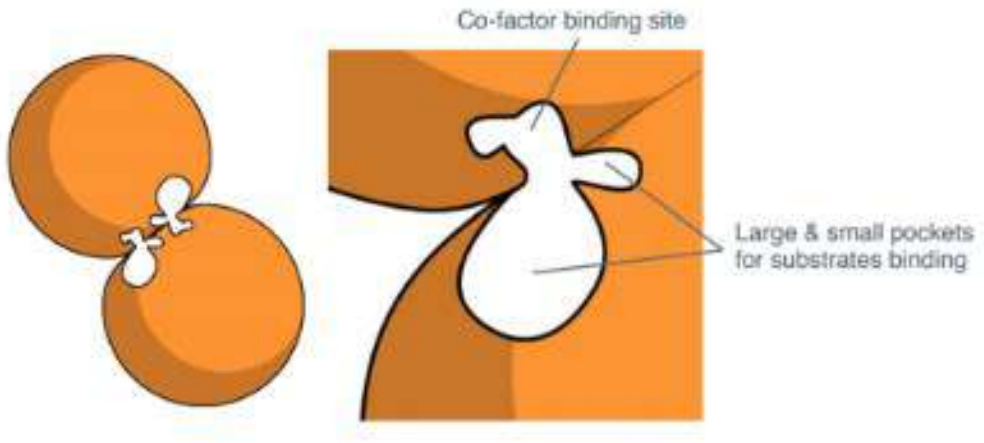

Fig.I.S1 - Schematic representation of ATA enzymes. (Left) Scheme of ATA homo-dimers. (Right) Schematic representation of an active site [24].

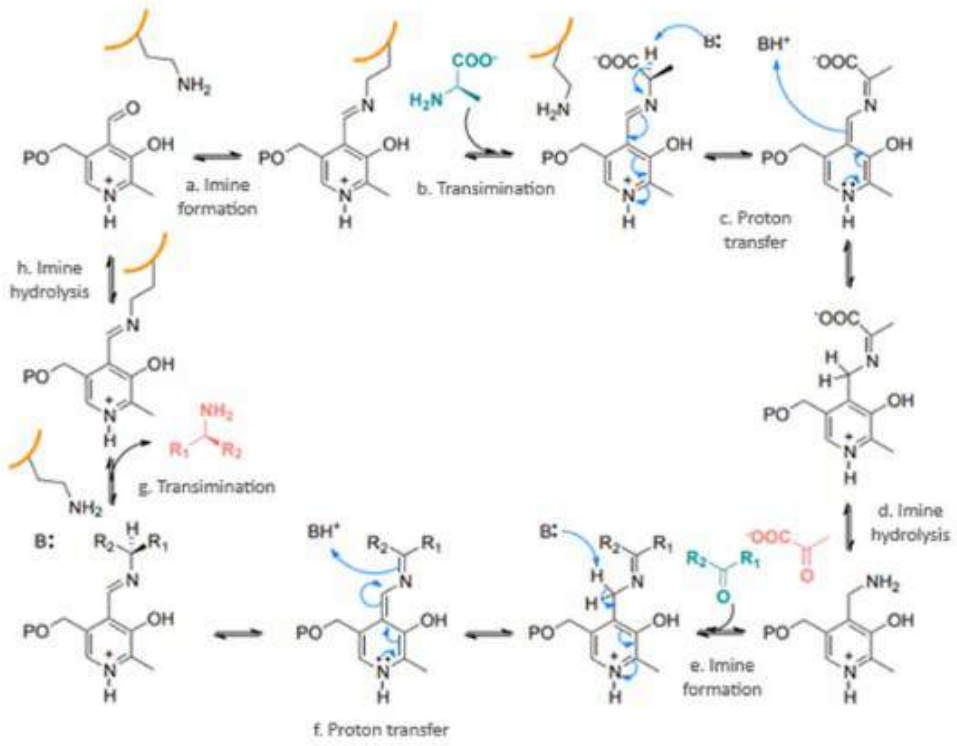

Fig.I.S2 - Transamination mechanism. Substrates and products of the reaction are depicted in green and red respectively. Two half-reactions execute the ping-pong bi–bi mechanism [71,230,231].

Annex I.S3 - Industrial Applications Using TAs for Chiral Amine Production

Tab.I.S3 - Non exhaustive list of relevance of industrial-scale production of chiral amine compounds (APIs or key intermediates) via transaminase-catalyzed processes from g to hundred kg scale. All presented processes employed asymmetric synthesis as reactional strategy. Inspired from Meersseman et al. [24]

Transaminase Type & Firm	Reaction Strategy	Process Description	Production Efficiency	Product & Function	Ref.
Pilot to pre-industrial scale (kg scale)					
ATA-117-11Rd Codexis/Merck	Asymmetric synthesis	IPA as amino donor; 50% DMSO; 50°C; high substrate concentration	250 g/L; pilot scale; 53% increased productivity	R-Sitagliptin – Anti-diabetic drug, DPP-4 inhibitor for type 2 diabetes treatment	20,76,233
ATA-117 Codexis	Asymmetric synthesis	IPA as amino donor; 4-step synthesis for suvorexant	kg scale; 43% overall yield	Suvorexant – Orexin receptor antagonist for insomnia treatment	234,235
CDX-010 (engineered from ATA-117)	Asymmetric synthesis	IPA as amino donor; integrated in 4-step chemoenzymatic route	40% overall yield; 100 L scale	Filorexant intermediate – Candidate for insomnia therapy	236,237
Vf-ATA from *Vibrio fluvialis* AstraZeneca	Asymmetric synthesis	S-MBA as donor; biphasic extraction with toluene	68% yield; 99% ee; 100 L scale	AZD1480 intermediate – Kinase inhibitor for idiopathic myelofibrosis treatment	70,238,239

ATA-47 from LCeta Pfizer	Asymmetric synthesis	Large library screening; substituted tetralone substrate	40 kg product; 94% isolated yield	γ-Secretase inhibitor intermediate – Alzheimer's disease and cancer therapy research	240
CDX-043 (engineered from ATA-217) Codexis	Asymmetric synthesis	IPA as donor; acetone evaporation; 58°C	90% conversion; 200 kg enzyme; 20 kg product	Sacubitril precursor – Heart failure drug (Entresto component)	241
CDX-017	Asymmetric synthesis	IPA as donor; 8-step synthesis of MK-7246	>100 kg scale; improved productivity	MK-7246 intermediate – Drug for respiratory diseases	242
Smaller scale (>100 mg to g scale)					
Vf-TA r414 (engineered)	Asymmetric synthesis	Oxooctanoate substrate; imagabalin production	277 mg; 95% de	Imagabalin – Analgesic for neuropathic pain and anxiety disorders	243
ATA purchased from Codexis	Asymmetric synthesis	4-step synthesis for S-ivabradine	50% yield; excellent ee	S-Ivabradine – Heart rate-reducing agent for angina and heart failure	21
Cv-ATA from *Chromobacterium violaceum*	Asymmetric synthesis	Intermediate for ramatroban	500 mg scale; 96% yield; enantiopure	Ramatroban intermediate – Antiallergic agent targeting thromboxane receptors	244
Sp-ATA from *Silicibacter pomeroyi*	Asymmetric synthesis	In situ crystallization; vacuum evaporation of acetone	g scale >1 M concentration	S-(3-methoxyphenyl)ethylamine – Rivastigmine intermediate for Alzheimer's treatment	99
ATA-200 purchased from Codexis	Asymmetric synthesis	Chiral spirocyclic amine synthesis	580 g; 82% yield; ee 97.8%	Chiral spirocyclic amine – Intermediate in pharmaceutical synthesis (enhanced safety)	245

IPA = Isopropylamine ; DMSO = Dimethyl sulfoxide ; S-MBA = (S)-α-methylbenzylamine

Annex I.S4 - Strengths and Weaknesses of Immobilization Strategies

The choice of immobilization strategy significantly impacts the performance, stability, and reusability of enzymes in industrial biocatalysis. This section provides an overview of the main immobilization approaches—surface binding, entrapment, and cross-linking—and discusses their associated advantages and limitations Tab.I.S4.

1. Surface Binding to Carriers or Materials

This category includes physical adsorption, site-specific affinity binding, and covalent grafting, all of which involve anchoring the enzyme on the surface of a solid support [101,111].

- **Adsorption**

Enzymes are immobilized via weak, reversible interactions such as van der Waals forces, hydrogen bonding, or electrostatic interactions. This cost-effective method typically preserves

enzyme conformation and catalytic activity due to minimal structural alteration [63]. However, the weak nature of the interactions can lead to enzyme leaching under operational conditions. Moreover, enzymes immobilized via adsorption remain susceptible to pH, temperature, and ionic strength fluctuations due to retained conformational flexibility [111].

- **Affinity Binding**

Site-specific immobilization using engineered tags (e.g., His-tag) enables precise orientation of the enzyme on functionalized supports (e.g., metal-chelated surfaces). This facilitates a one-step immobilization and purification process while maintaining the accessibility of the active site [101]. However, genetic modification may impact enzyme folding and function. Additionally, the cost and environmental sensitivity of affinity ligands can be limiting [63].

- **Covalent Grafting**

Covalent immobilization forms strong and stable bonds between enzyme and support, often via single-point or multi-point attachment. This method provides excellent resistance to enzyme leaching and can improve thermal and operational stability by restricting conformational mobility [111]. However, the required chemical activation steps can complicate the process and increase cost. Furthermore, if the active site is affected during bonding, catalytic activity may decrease [101].

2. Entrapment and Encapsulation

In this approach, enzymes are confined within the pores of a polymer or sol–gel matrix.

Entrapment offers a favorable microenvironment that enhances enzyme stability and protects it from harsh reaction conditions (e.g., extreme pH or organic solvents) [63]. It is compatible with a wide range of enzymes and generally maintains catalytic activity. However, diffusion limitations within the matrix can impair substrate accessibility and product release. Enzyme leaching may also occur, especially under continuous flow conditions [106].

3. Cross-Linking (Carrier-Free)

Cross-linked enzyme aggregates or crystals (CLEAs or CLECs) provide a carrier-free immobilization method that results in highly concentrated and dense biocatalyst formulations. These systems exhibit outstanding thermal and operational stability and are produced via cost-effective processes [111]. Nonetheless, cross-linking generally requires purified enzymes and may induce activity loss if active sites are affected. In some cases, diffusional limitations due to the dense aggregate structure can reduce performance. Importantly, cross-linking can also be combined with other strategies (e.g., entrapment) to minimize enzyme leaching and further enhance stability [63,101].

Tab.I.S4 - Summary of enzyme immobilization strategies and some of their main features adapted from Meersseman et al. [24] and supplemented by [62,63,101,111].

	Surface biding			**Entrapment**	**Cross-linking (CLEAs or CLECs)**
	Adsorption	**Site-specific affinity attachment**	**Covalent grafting**		
Type of interactions involved	Reversible (electrostatic or hydrophobic interactions)	Reversible	Reversible or irreversible	Reversible (van der Waals, H-bonds)	Reversible or irreversible
Enzymes localization	Carrier surface			Carrier porosity	Carrier-free

Strengths	Mild enzyme distorsions Enzyme immobilization is tuneable (adapting carrier hydrophobicity or pH and pI during adsorption)	Mild enzyme distorsions Possibly combined with enzyme purification Controlled enzyme orientation (site specific)	Enzyme leaching prevention (strong interactions) Possible stability and activity enhancement Potentially site specific	Mild enzyme distorsions Enzyme protection by the carrier (improvement of stability)	No need of material support High catalyst productivity and stability Enzyme leaching prevention (strong interactions)
Weaknesses	Enzyme leaching (low stability) Non-site specific	Enzyme leaching (low stability) Expensive strategy Possible perturbation of tagged enzyme	Possible rigidification of the enzyme structure (stability activity loss) Possible challenging and costly process	Enzyme leaching (low stability) Possible diffusional limitations	Possible diffusional limitations Possible rigidification of the enzyme structure (activity loss)
Typical immobilized enzymes formulations	Encapsulation into a polymer or a sol–gel matrix	His-tag binding onto metal-derivatized carriers	Covalent grafting onto epoxy-resins Covalent grafting onto glutaraldehyde functionalized carriers	Encapsulation into a polymer or a sol–gel matrix	Enzymes aggregates cross-linked with glutaraldehyde

Annex I.S5 - Main Types of Flow Processes : Characteristics and Applications

Tab.I.S5 - Main features of different types of flow processes and reactors involving enzymes

	Reactor Type	Strengths	Weaknesses	Typical Applications	Ref.
	Lab scale				
Free or immobilized enzymes	**Microreactor And Mesoreactor**	High surface-to-volume ratio, Excellent control over mass/heat transfer, Fast optimization	Low throughput, potential clogging, Scale-up limitations	Screening, Reaction optimization, Small-scale synthesis of complex intermediates	106,123
	Lab to industrial scale				
Free or immobilized enzymes	**Continuous Stirred-Tank Reactor (CSTR)**	Flexible operation, homogeneous mixing, scalable from lab to industrial scale	Back-mixing reduces conversion, lower residence time control	Early-phase process development	65
	Membrane Reactor	Selective retention of enzymes, facilitates downstream processing	Membrane fouling, limited mass transfer for large molecules	Selective biotransformations (simultaneous separation and catalyst activity)	123
Only immobi	**Packed-Bed Reactor (PBR)**	High catalyst loading, easy product separation, suitable for long-term use	Pressure drop, clogging with viscous or particulate streams	Well-established continuous API production using immobilized enzymes (e.g., amide/ester synthesis)	107,121

	Wall-Coated / Monolithic Reactor	Low mass transfer resistance, good for gas or photochemical reactions	Limited enzyme loading, surface immobilization challenges	Gas-phase or photobiocatalysis for oxidative transformations	65

Annex I.S6 - Applications of Immobilized Transaminases in Flow Processes

Tab.I.S6 - Overview of the reported examples of transamination in continuous flow applied to purified-immobilized TAs. Adapted from Meersseman et al.24

Immobilization	Materials	TA	Type of flow reactor	Reaction	Ref.
Biding to the carrier					
His-tag immobilization	EziG™ supports + Fe^{3+} derivatization	ω-TAs	Packed-bed flow reactor	Kinetic resolution	138
His-tag immobilization	Derivatized EziG™ supports	*Aspergillus fumigatus* ω-TA mutant	One-pot batch-to-flow	Asymmetric synthesis (following a Suzuki–Miyaura reaction)	139
His-tag immobilization	EziG™ supports + Fe^{3+} derivatization	ω-TAs	Compartmentalized packed-bed flow	Amination (in multi-enzymatic cascade reactions)	140
His-tag immobilization	Silica capillary + Ni^{2+} derivatization	Immobilized ω-TA and transketolase	Dual capillary microreactor	Asymmetric synthesis (following formation of chiral ketone)	246
His-tag immobilization	Agarose beads + Ni^{2+} derivatization	Immobilized ω-TA and transketolase	Microreactor (packed tube flow)	Asymmetric synthesis (following formation of chiral ketone)	162
Covalent grafting (and His-tag driving)	Sepabeads® + Co2+ derivatization	*Halomonas elongata* ω-TA	Packed-bed flow reactor	Amination	56
Covalent grafting (and His-tag driving)	Sepabeads® + Co^{2+} derivatization	*Halomonas elongata* ω-TA	Packed-bed flow reactor	Amination	127
Covalent grafting (and His-tag driving)	Sepabeads® + Co^{2+} derivatization	*Halomonas elongata* ω-TA	Dual packed-bed flow reactor	Asymmetric synthesis of cyclic chiral amines	141
Covalent grafting (and His-tag driving)	Sepabeads® + Co^{2+} derivatization	*Halomonas elongata* ω-TA	Packed-bed flow reactor	Asymmetric synthesis of 2-aminobutane	142
Covalent grafting (and His-tag driving)	Sepabeads® + Co^{2+} derivatization	*Halomonas elongata* ω-TA and horse liver alcohol dehydrogenase	Closed-loop packed-bed flow reactor	Deamination or kinetic resolution (followed by aldehyde reduction into alcohol)	146
Covalent grafting (and ionic driving)	Epoxy resin 107s (Xi'an Lan Xiao Technology Co. Ltd) + ethylenediamine derivatization	*Caulobacter sp.* ω-TA	Packed-bed flow reactor	Asymmetric synthesis of S-1-Boc-3-aminopiperidine	148
Covalent grafting	Aminoalkyl-functionalized resins (ReliZyme™ EA) + bisepoxides	*Chromobacterium violaceum* ω-TA mutant	Packed-bed flow reactor	Kinetic resolution	149
Covalent grafting	Glyoxyl-agarose beads	*Vibrio fluvialis* ω-TA	Packed-bed flow reactor	Asymmetric synthesis of AZD1480 intermediate	247
Covalent grafting	Amine-functionalized beads (ReliZyme™ HA 403) + glutaraldehyde	*Silicibacter pomeroyi* ω-TA	Packed-bed flow reactor	Amination of furan aldehydes	143

Covalent grafting	Cellulose (+ APTES + glutaraldehyde) or (+ GLYMO)	*Vibrio fluvialis* ω-TA	Packed-bed flow reactor	Asymmetric synthesis (using LDH and GDH)	144
Covalent grafting	Silica monolith + APTES + glutaraldehyde	ATA-117	Silica monolith continuous flow reactor	Kinetic resolution	145,163
Covalent grafting	3D-printed nylon matrix (Taulman) + glutaraldehyde + PEI	ω-TAs	D-printed nylon microreactor	Kinetic resolution	147
Hydrophilic interactions	DIAION HP2MG resin (Mitsubishi)	ω-TA mutant	/	Asymmetric synthesis of R-sitagliptin (in wet isopropylacetate, acetone evaporation by N_2 sparging)	248
Electrostatic interactions	Derivatized lignin + PEI	*Halomonas elongata* ω-TA	Packed-bed flow reactor	Amination (of cinnamaldehyde) and deamination (of S-MBA)	249
Entrapment					
Encapsulation	Lentikats® (polyvinyl alcohol gel)	ω-TA	Miniaturized packed-bed reactor	Deamination	150

PEI = polyethyleneimine. APTES = (3-aminopropyl)triethoxysilane, GLYMO = 3-glycidoxypropyltrimethoxysilane.

Annex I.S7 - TsRTA – Main Characteristics and Properties

TsRTA is an RTA derived from *Thermomyces stellatus*. It is a homodimeric enzyme in which each monomer (chains A (Fig.S3 (a)) and B) consists of 363 amino acids (Fig.S3 (b)). The overall structure corresponds to a molecular weight of approximately 80 kDa. While predominantly present in its dimeric form, the enzyme can also exist as a tetramer (Fig.S3 (c)), which has been identified as responsible for the high thermostability of TsRTA compared to homologous enzymes (40% of activity is retained after 7 days of exposure at 40 °C).

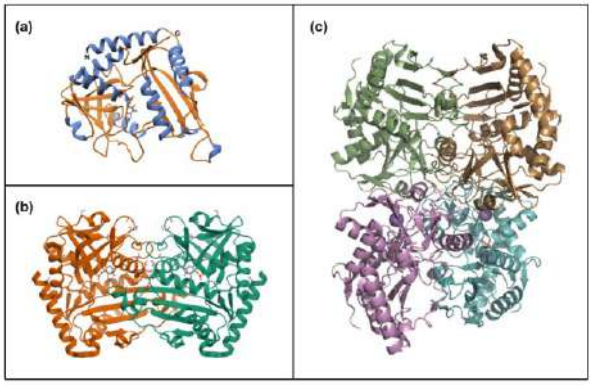

Fig.I.S3 - The 3D structure of TsRTA (secondary structure shown as ribbons) bound to its PLP cofactor (shown as sticks). (a) Representation of one monomer (chain A). (b) Representation of the dimeric structure: chain A (orange) and chain B (green). (c) Tetrameric structure of TsRTA obtained by applying the symmetry operation (–x, y, –z) to the asymmetric unit dimer[215, 250].

Additionally, engineering strategies have been explored to enhance tetramer formation—and thereby improve protein thermostability—through the introduction of disulfide bonds at the dimer–dimer interface.

Regarding substrate specificity, TsRTA exhibits a profile similar to other RTAs, commonly accepting typical amine donors such as (R)-methylbenzylamine, isopropylamine, and D-alanine, as well as various aromatic and aliphatic ketones and aldehydes [215,250].

Annex I.S8 - Application of Crystallization Strategy to Shift Equilibrium

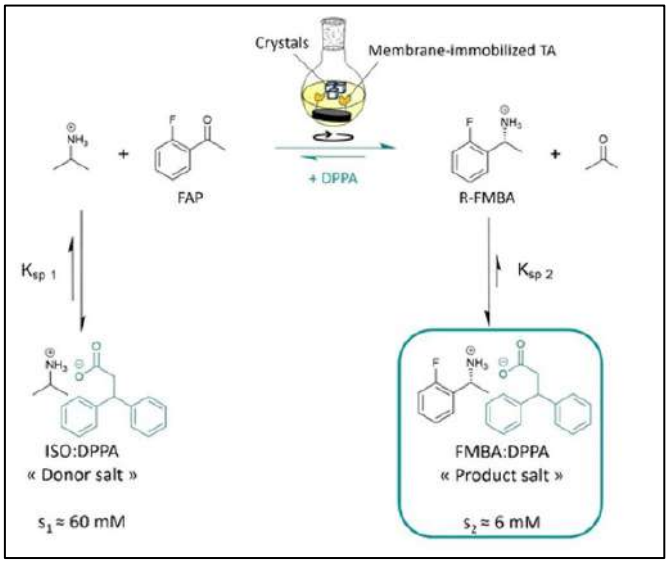

Fig.I.S4 - Reaction strategy involving diphenylpropionic acid (DPPA) as a crystallizing agent to mitigate thermodynamic limitations. By forming a crystalline salt with the amine compounds (FAP and FMBA), DPPA enables a shift of the unfavorable equilibrium by decreasing the concentration of the product (FMBA) in the reaction medium. From Meersseman et al.30.

IX.2 Annex II – Objective

No appendices were required for this section

IX.3 Annex III – Strategy

No appendices were required for this section

IX.4 Annex IV – Experimental

Annex IV.S1 - Expression and Preparation of Cell-Free TsRTA Extract

pCH93b containing the synthetic gene was transformed into BL21 STAR (DE3) E. coli cells. TB-medium (amp 100µg/mL) (300 mL) supplemented with lactose (5 g/L) were inoculated with a single colony and incubated at 37°C, with shaking (180 rpm) for 4 h followed by 25°C with shaking (180 rpm) for 20 h. Cells were harvested by centrifugation (4500 g, 15min, 4°C) and stored at −20°C either as pellets. The pellet was thawed and resuspended in the lysis buffer containing potassium phosphate buffer pH 8.0 (100mM) employing Ultrasonic Processor 75022 VibraCell™, Sonics® 20mL per pellet. Cells were disrupted by sonication at 0°C by (4 min: 30''ON, 30''OFF). After centrifugation (4000×g, 4 ◦C, 30 min), the supernatant was clarified by filtration (0.22 µm). Filtrate is collected and ultra- filtered in 50 mL tubes (Centrifugal Filter Units, Amicon® Ultra-15

10K, Merck Millipore Ltd) by centrifugation at 4 °C at 4000 rpm. Enzyme is aliquoted in 1.5 mL tubes and flash-frozen and stored at – 80°C.

Annex IV.S2 - Structural Characteristics of Polypropylene Membranes

Tab.IV.S1- Structural characteristics of membrane used for TsRTA immobilization. Membranes with diameters of 12 mm (12M) and 44 mm (44M) were shaped using a cookie cutter. Volumes were calculated assuming uniform thickness.

Membrane	Diameter	Rounded Cross-section	Thickness	Membrane volume	
	[m]	[m^2]	[m]	[m^3]	[mL]
12M	0,012	0,00011	0,00012	0,000000014	0,014
44M	0,044	0,00152	0,00012	0,000000182	0,182

Annex IV.S3 – Polydopamine Coating

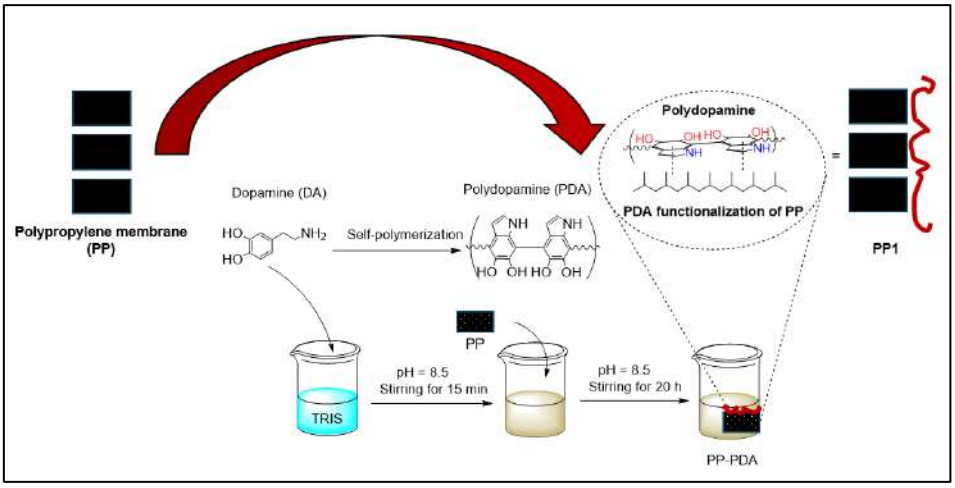

Fig.IV.S1- Schematic representation of the PDA deposition on PP membrane surface from Meersseman et al. [29]

Annex IV.S4 - Preparation of Buffer Solution (HEPES 0.1M /PLP 1mM, pH = 8)

All solutions involving TsRTA, including immobilization solutions and reaction mixtures, were prepared using a HEPES buffer (pKa = 7.2) containing PLP as a cofactor and adjusted to pH 8, which corresponds to the optimal conditions for enzyme stability. Typically, 500 mL of 0.1 M HEPES stock buffer was prepared by separately dissolving HEPES and HEPES sodium salt in distilled water, in appropriate proportions such that the final mixture reached pH 8 upon combination. PLP was then added to a final concentration of 1 mM. After complete dissolution, the two solutions were mixed under gentle stirring for 15 minutes. The final buffer solution was then stored at 6 °C until use.

Annex IV.S5 - Determination of Flash-frozen Enzyme Solution Concentration and Preparation of Immobilization Solution.

After allowing a 1.5 mL tube containing flash-frozen enzyme to thaw at room temperature for 10 minutes, the resulting solution was diluted using various dilution factors (2×, 4×, 10×, 20×, 50×, 80×, and 100×) in buffer solution (HEPES 0.1 M buffer, PLP 1 mM). The resulting solutions of varying concentrations were analyzed using the Bradford protein assay (Annex IV.S6). The protein

concentration of the cell-free extract was estimated as the average of the values falling within the linear range of the calibration curve (C_0 ≈ 8.89 mg/mL). This concentration was assumed to be constant across all frozen aliquots, as they originated from the same preparation batch. It was therefore used as the reference concentration for preparing immobilization solutions at defined target concentrations.

Based on the determined stock concentration and the desired final concentration for immobilization, a specific volume of the thawed enzyme solution was transferred into a glass vessel and diluted in HEPES buffer (0.1 M, pH 8, with 1 mM PLP) under gentle stirring. Typical target concentrations included 0.2, 0.25, and 0.5 mg/mL.

Annex IV.S6 - Soluble Enzymes Quantification : Bradford assay

Similarly to Meersseman Arango *et al* procedure [29], soluble enzyme concentrations is assessed through the Bradford titration method. Calibration is performed by mixing 250 µL of standard solutions of TsRTA cell-free extracts in HEPES 0.1M buffer pH 8, PLP 1 mM (within 0–0.25 mg.mL-1 concentration range) with 750 µL of Bradford reagent. After 5 minutes incubation at room temperature, absorbances is read at 595 nm with a ThermoScientific Genesys 10S-Vis spectrophotometer, and values of A595 is plotted against TA concentration. A conversion factor of 3.736 mL/mg_{TsRTA} was obtained.

Annex IV.S7 - Relatie Frequency Drive Setting – Flow Rate of Pumps Employed in Recirculating Tangential Flow Set-up

Frequency drive setting (/)	Flow rate (mL/min)
10	119
20	234
30	338
40	452
50	550

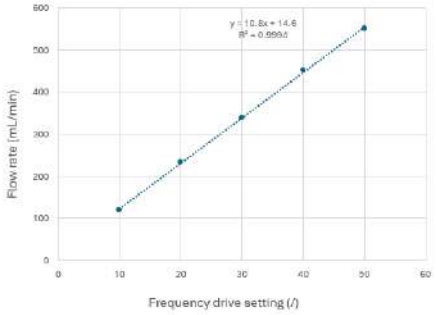

Fig.IV.S2 - Relative frequency drive settings versus flow rate for Pump A. The total tubing length is 535–545 cm, corresponding to a recirculating volume (i.e., the system volume under steady-state flow conditions) of approximately 55–65 mL.

Frequency drive setting (/)	Flow rate (mL/min)
25	96
30	122
35	151
40	178

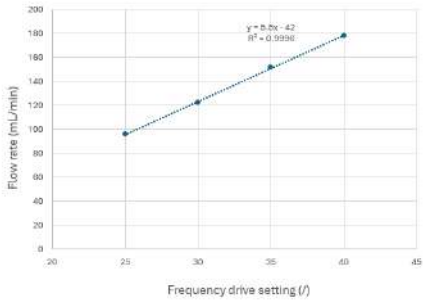

Fig.IV.S3 - Relative frequency drive settings versus flow rate for Pump B. The total tubing length is 310-320 cm, corresponding to a recirculating volume (i.e., the system volume under steady-state flow conditions) of approximately 30–40 mL.

Annex IV.S8 - Gas Chromatography (GC) Analysis

Gas Chromatography (GC) analysis After extraction of the analytes into dichloromethane, the analysis was performed on a Bruker Scion 456-GC with a WCOT fused silica BR-5 column (30 m x 0.32 mm ID x 1.0 µm) and helium as carrier gas (25 mL.min-1), oven temperature at 150 °C, split ratio of 80, injector temperature at 250 °C, flame ionization detector temperature at 300 °C (air flow 300 mL.min1, H2 flow 30 mL.min-1).

Annex IV.S9 - Determination of Component Concentration via Calibration Curve

To determine the concentrations of the various components (ISO, FAP, and FMBA), calibration curves were established (Figs.IV.S4 and Fig.IV.S5) by injecting standard solutions of known concentrations spanning the expected range encountered in the catalytic tests. Each solution was extracted according to the protocol described in Section IV.2.3.2 prior to GC analysis.

- **Calibration curve of reagents (FAP, ISO)**

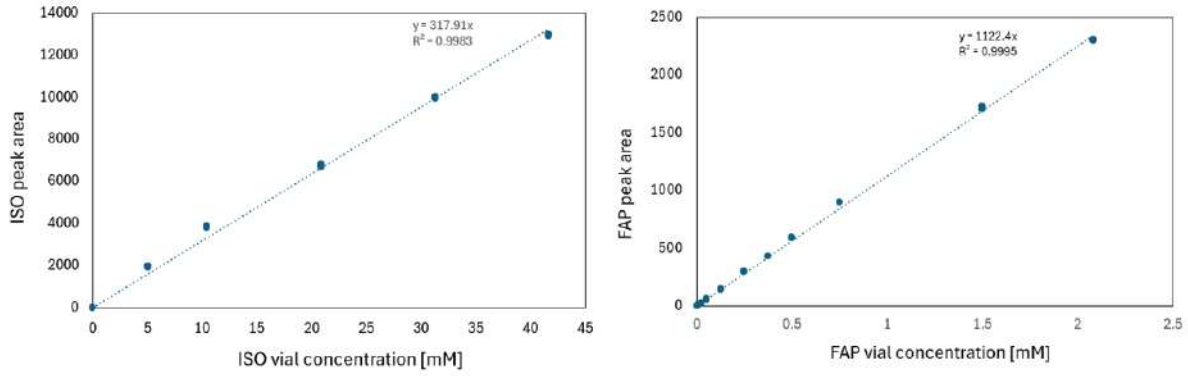

Figs.IV.S4 – (Left) Calibration curves for ISO concentration (mM), obtained by performing triple extractions of standard solutions with 400 µL of DCM. Initial ISO concentrations prior to extraction: 0, 60, 125, and 250 mM. (Right) Calibration curves for FAP concentration (mM), obtained by performing triple extractions of standard solutions with 400 µL of DCM. Initial FAP concentrations prior to extraction: 0, 0.15, 0.3, 0.6, 1.5, 3, 4.5, 6, 9, 18, and 25 mM.

- **Calibration curves of product (FMBA)**

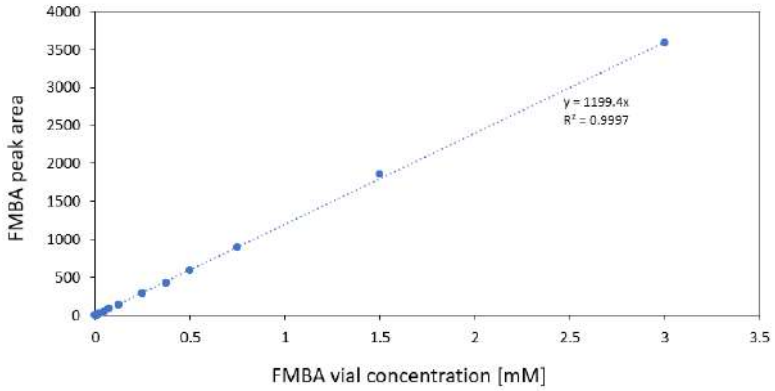

Fig.IV.S5 - Calibration curves for FMBA concentration (mM), obtained by performing triple extractions of standard solutions with 400 µL of DCM. Initial FMBA concentrations prior to extraction: 0, 0.09, 0.15, 0.3, 0.6, 0.9, 1.5, 3, 4.5, 6, 9, 18, and 36 mM.

The surface area (S) of solutions with unknown concentration, obtained by GC analysis, was converted into concentration using previously established calibration curves (Figs.IV.S4 and Fig.IV.S5) and applying Eq.IV.S1.

$$[A]_{RM} = [A]_{vial} \times DF = \frac{S}{\varepsilon} \times DF\ [mM]$$

Eq.IV.S1- Equation used to determine the concentration of component A (mM) in the reaction mixture (RM) after GC analysis. A corresponds to ISO, FAP, or FMBA. S is the surface area obtained by GC analysis, ε is the calibration factor relating surface area to concentration in the GC vial ($\varepsilon_{(ISO)}$ = 317.91, $\varepsilon_{(FAP)}$ = 1122.4, $\varepsilon_{(FMBA)}$ = 1199.4), and DF is the dilution factor resulting from the extraction procedure (DF = $V_{(extraction)}$ / $V_{(harvested)}$ = 1.2 / 0.1 = 12).

Annex IV.S10 - Equation used to Determine Conversion, Yield and STY.

$$(A)\ FAP\ Conversion\ (t) = \frac{FAP_0 - FAP_t}{FAP_0} \times 100\ [\%] \qquad (B)\ FMBA\ yield\ (t) = \frac{FMBA_t}{FAP_0} \times 100\ [\%]$$

Eq.IV.S2 – (A) Equation used to determine the conversion. FAP_0 and FAP_t correspond to the initial concentration of FAP and the concentration of unreacted FAP at the time of measurement, respectively. (B) Equation used to determine the yield of the reaction. FAP_0 and $FMBA_t$ correspond to the initial concentration of FAP and the concentration of formed FMBA at the time of measurement, respectively.

Space-time yield (STY) is also used to evaluate the catalytic performance of the biocatalytic membrane (Eq.IV.S3). STY is defined as the number of micromoles of FMBA produced per hour per milliliter of effective reactor volume (V_m).

$$Space\ time\ yield\ (t) = \frac{[FMBA]_t \times F}{V_m}\ [\mu mol_{FMBA}.mL^{-1}.h^{-1}]$$

Eq.IV.S3 - Equation used to determine the space-time yield (STY) in the dead-end flow system. [FMBA]t is the concentration of FMBA at a given time (in µmol/mL), F is the flow rate set on the syringe pump (in mL/h), and V_m is the effective reactor volume (in mL), corresponding to the volume occupied by the immobilized enzyme (i.e., the membrane volume).

IX.5 Annex V - Results and Discussion

IX.5.1 Batch Investigations

Annex V.S1 – Batch Immobilization Investigation

Typical batch immobilization was performed for both membrane sizes using different concentration. Comparing results obtained for 12M and 44M presented in Tab.V.S1, 44M enable logically to immobilized more enzymes than 12M due to it's higher biding site availability.

Tab.V.S1 - Table summarizing the immobilizations performed in batch mode on 12 mm (1.13 cm^2) and 44mm (15.21 cm^2) membranes. C_0 represents the initial concentration of the immobilization solution (before immobilization), as determined by the Bradford assay.

Membrane	Immobilization Time [h]	C_0 [mg_{TsRTA}/mL]	Volume [mL]	Loading/Surface area [mg_{TsRTA}/ cm^2]	Immobilization yield [%]
12M Membrane (Diameter 12mm – Surface area : 1.13 cm^2)					
12M-B-1	18	0.230	4	0.063	8
12M-B-2	18	0.242	4	0.130	15
12M-B-3	18	0.442	5	0.038	2
12M-B-4	5	0.376	5	0.1	6
12M-B-5	18	0.386	5	0.147	9

44M Membrane (Diameter 44mm – Surface area : 15.21 cm^2)					
44M-B-1	18	0.478	25	0.188	24
44M-B-2	18	0.192	20	0.088	35
44M-B-3	18	0.199	20	0.082	31
44M-B-4	18	0.18	20	0.092	39
44M-B-5	18	0.543	20	0.266	37
44M-B-6	18	0.513	20	0.225	33

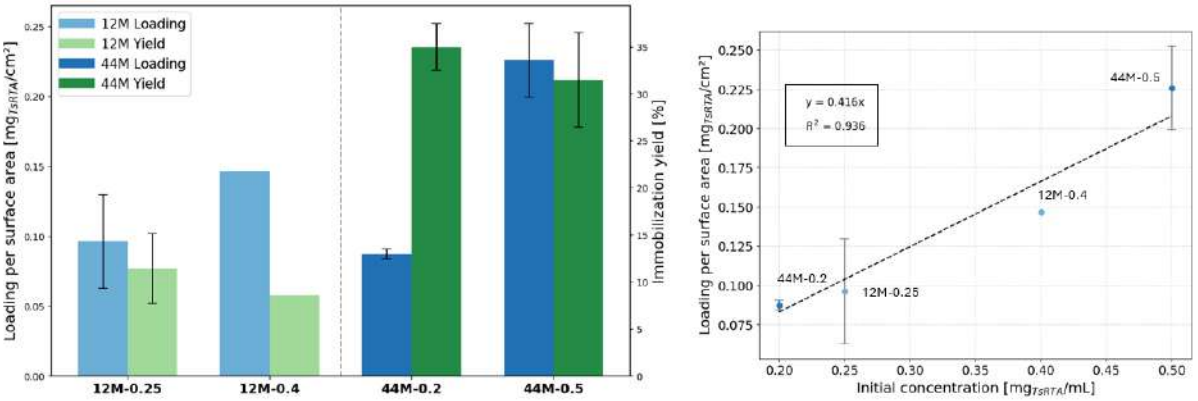

Figs.V.S1 – (Left) Enzyme loading per surface area and immobilization yield of membranes immobilized in batch mode for 18 h using TsRTA solutions (HEPES 0.1 M, PLP 1 mM, pH 8) at different concentrations. For the 12M membrane, two immobilizations were performed at 0.25 mg/mL (4 mL) — 12M-0.25 (12M-B-1 and 12M-B-2) — and one at 0.4 mg/mL (5 mL) — 12M-0.5 (12M-B-5). For the 44M membrane, three immobilizations were performed at 0.2 mg/mL — 44M-0.2 (44M-B-2, 44M-B-3, and 44M-B-4) — and three at 0.5 mg/mL — 44M-0.5 (44M-B-1, 44M-B-5, and 44M-B-6) — using 20 mL of solution. Error bars represent the standard deviation from replicate experiments. (Right) Enzyme loading per surface area as a function of the initial immobilization solution concentration (0.2, 0.25, 0.4 and 0.5 mgTsRTA/mL). Two membrane sizes are represented: 12M (light blue) and 44M (dark blue). A linear regression forced through the origin is shown as a dashed line, with the corresponding equation and R^2 value to illustrate proportionality. Error bars represent the standard deviation from replicate experiments.

For a given membrane size, the immobilization yield appears relatively consistent regardless of the concentrations used for immobilization (at least within the investigated range), falling between 10% and 30% for the 12M and 44M membranes, respectively (Figs.V.S1 (left)). This observation suggests that, for this specific immobilization time (18 h) and membrane area, immobilization is not limited by the number of reactive sites present on the membrane—otherwise, a decrease in immobilization yield would have been expected with increasing concentration. In addition, an increase in enzyme loading appears to be proportional to the initial immobilization solution concentration.

Considering the loading per surface area, it can be assumed that the immobilization step is relatively scalable. Even though immobilizations at identical concentrations were not performed for both membrane sizes, the amount of enzyme immobilized per unit surface area appears to be relatively proportional to the concentration of the immobilization solution, as illustrated in Figs.V.S1 (right), within the investigated concentration range. Thus, it can be assumed that if similar concentrations had been used for both membrane sizes, a similar loading per surface area would have been obtained.

These results suggest that a potential increase in enzyme concentration could enhance membrane loading (and thus potentially yield a more catalytically active biocatalytic membrane), independently of membrane size. However, immobilization increase (i.e., higher TsRTA loading)

would not necessarily result in greater overall activity. Indeed, enzyme overloading could lead to several issues, such as reduced enzyme flexibility—and consequently, decreased catalytic activity—and/or diffusion limitations that restrict substrate access to certain immobilized enzymes [63,112,117]. Furthermore, it can be assumed that some of the additional immobilized enzymes (resulting from increased concentration) may localize in less accessible regions (e.g., deeper within the membrane porosity), limiting their catalytic contribution. Therefore, evaluating the catalytic activity is essential to assess the effect of enzyme loading.

Annex V.S2 – Batch Catalytic Tests Investigations

Typical batch catalytic tests was performed on membrane resulting from batch immobilization (measurements was performed after 20). The results was presented in Figs.V.S2.

Loading – Productivity dynamics

Before consider scalability, a first comment about the loading-productivity dynamics observed for 12M membranes appear relevant (Figs.V.S2 (left)).

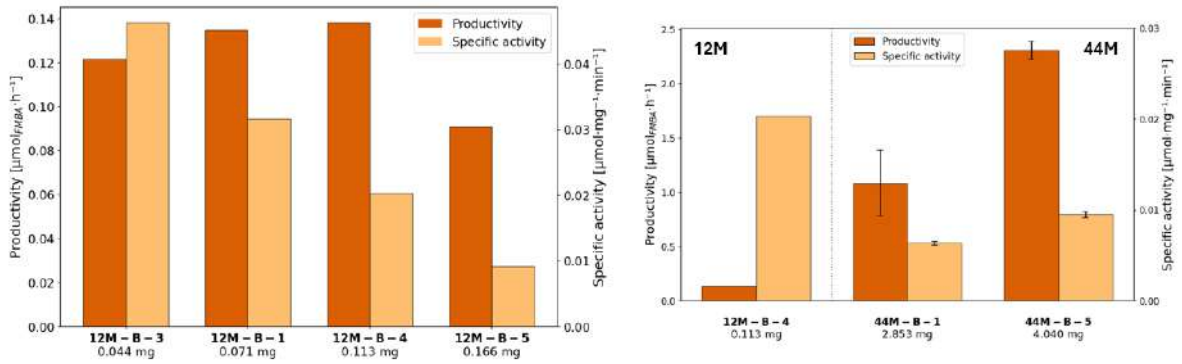

Figs.V.S2 - (Left) Productivity and specific activity of biocatalytic membranes of 12 mm of diameter (12M-B-1, 12M-B-3, 12M-B-4, and 12M-B-5 from 18 h batch immobilization) exhibiting different loadings, obtained from batch catalytic tests. Catalytic tests were performed using a standard reaction mixture (250 mM ISO / 25 mM FAP in 0.1 M HEPES / 1 mM PLP, pH 8), over 20 h in batch mode. (Right) Productivity and specific activity obtained for biocatalytic membranes of different sizes (12mm of diameter (12M-B-4, the most productive of 12M) and 44 mm diameter (44M-B-1 and 44M-B-5)). Catalytic tests were performed using a standard reaction mixture (250 mM ISO / 25 mM FAP in 0.1 M HEPES / 1 mM PLP, pH 8), over 20 h in batch mode.

A increasing the amount of immobilized enzyme appears to improve FMBA production, but not as much as expected (Figs.V.S2 (left). This productivity enhancement is clearly not proportional to the enzyme loading, as one might anticipate. For example, 12M-B-4 (0.113 mg) performs better than 12M-B-5 (0.166 mg) even though less enzyme was immobilized on it. This observation may be explained by a progressive decrease in the enzyme's specific activity with increasing loading, in a relatively proportional manner, as shown in Fig.V.S3. This decline could be explained a crowding phenomenon or a accessibility decrease of the substrate [63,112,117]. For example, 12M-B-3 (0.044 mg) demonstrates higher productivity than 12M-B-5 (0.166 mg)—33% more productive—despite having nearly four times less immobilized enzyme. This is explained by its specific activity, which is five times higher than that of 12M-B-5 (Figs.V.S2 (left)).

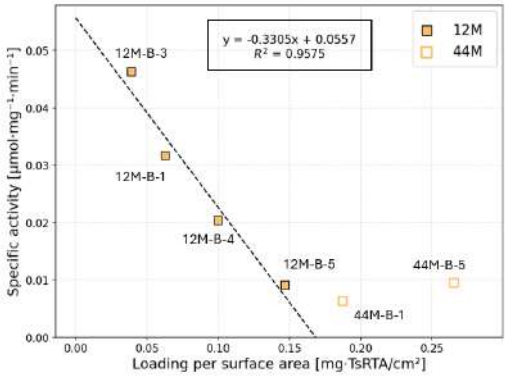

Fig.V.S3 - Specific activity of immobilized enzymes, obtained after 20h of batch catalytic test, as a function of enzyme loading per surface area. Two different membrane areas were investigated: 12M (12M-B-1, 12M-B-3, 12M-B-4 and 12M-B-5) and 44M (44M-B-1 and 44M-B-5). A linear regression based solely on the results from 12M membranes is shown.

According to the results, the drop in specific activity can be compensated by higher enzyme loading, as seen with membranes 12M-B-3, 12M-B-1, and 12M-B-4 (Figs.V.S2 (left)). However, a threshold appears to exist beyond which productivity begins to decline despite further increases in immobilized enzyme quantity. This critical point seems to lie between 0.113 mg and 0.166 mg of immobilized TsRTA for 12M membranes. In this context, a compromise between enzyme loading and specific activity must be achieved to obtain the most efficient biocatalytic membrane possible. This balance is particularly important for developing a cost-effective process.

Comparison of Different Membrane Sizes

Compare the catalytic performance of biocatalytic membranes of different sizes is also essential to evaluate the potential impact of scale-up on biocatalytic efficiency. The productivity and specific activity obtained for best productive 12M (12M-B-4) and both 44M investigated in batch (44M-B-1 and 44M-B-5) are presented in Figs.V.S2 (right).

As expected, the 44M membranes, which contain a higher quantity of immobilized enzymes, show significantly greater FMBA production compared to the 12M membranes, despite exhibiting lower specific activity. Whereas a decrease in productivity was observed for 12M membranes beyond a certain enzyme loading, an increase in productivity was observed with increasing loading for the 44M membranes considered. However, direct comparison remains difficult, as scale-up was not considered. Among the 44M membranes, the result obtained for 44M-B-5 appears particularly relevant, as it shows a productivity more than twice that of 44M-B-1, despite only a 40% increase in immobilized enzyme quantity. Additional catalytic tests using 44M membranes with a broader range of enzyme loadings are required to draw more robust conclusions.

To consider scalability and effectively compare the efficiency of biocatalytic membranes exhibiting different sizes, the specific activity of different immobilized enzymes was plotted as a function of enzyme loading per surface area in Fig.V.S3. While the results obtained for 12M membranes appear to follow a linear trend, the specific activity obtained for the two 44M membranes appears relatively stable across the experimental loading range investigated, particularly when accounting for variability due to analytical error. Although a direct comparison between 12M and 44M biocatalytic membranes is difficult—since no overlapping loading per surface area was investigated—it is noteworthy that the values obtained for 44M membranes do not appear inconsistent. Indeed, when comparing membranes of different dimensions with the most similar loading per surface area (12M-B-5 and 44M-B-1), their specific activities fall within a

similar range. However, 44M-B-5, which contains nearly 40% more immobilized enzyme, exhibits a slightly higher SA than 44M-B-1—while a decrease would have been expected based on the trend observed for 12M membranes. If one assumes that this slightly higher activity is due to experimental variability, one could hypothesize that above a certain loading, the specific activity of immobilized enzymes investigated in batch becomes relatively stable despite additional enzyme immobilization. This could be particularly relevant for the large-scale production of chiral amines.

Further experiments are, however, required to confirm this behavior—especially by increasing the amount of immobilized enzyme further to determine whether specific activity remains stable or eventually decreases. If a decline is observed, an optimal enzyme loading would need to be identified to maximize the efficiency of the biocatalytic membrane.

Annex V.S3 – FAP Conversion Profile

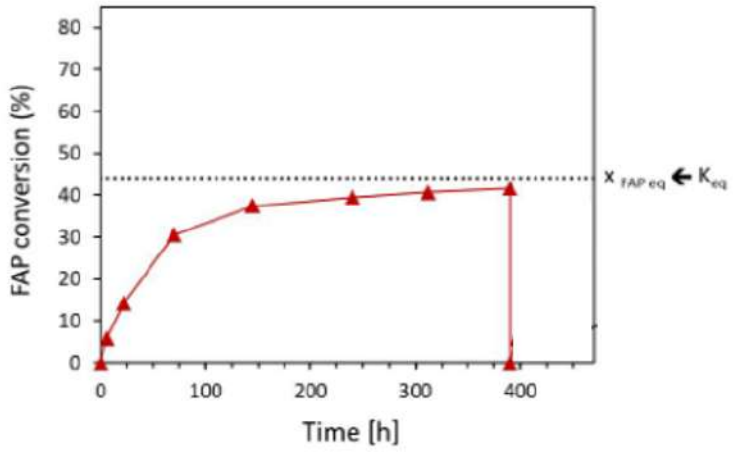

Fig.V.S4 - Reaction profile obtained for biocatalytic membrane (PP_PDA-GDE-PEI_TsRTA) investigated in batch mode. Reaction conditions were: 25 mM FAP, 250 mM ISO, 0 mM DPPA, 10 % v/v MeOH, 1 mM PLP in 0.1 M HEPES buffer pH 8, 35 °C. From Meersseman et al. [30]

IX.5.2 Dead-end Flow investigation

Annex V.S4 – Dead-end Flow mode : Technical Challenges and Resolutions

A preliminary immobilization test was first conducted using an immobilization solution at 0.5 mg/mL, pushed through the pre-functionalized membrane at a controlled flow rate of 1 mL/h. Unfortunately, these initial tests, performed with unsuitable plastic syringes, revealed several operational and technical issues. Significant syringe deformation was observed during the immobilization process, likely due to a substantial pressure drop—particularly pronounced in dead-end flow systems. Additionally, solution loss occurred during the process, not only due to syringe deformation but also because of an improper seal between the syringe tip and the Whatman cell. In addition to causing major reproducibility issues—due to unreliable flow rate control—the loss of immobilization solution made accurate quantification of immobilized enzyme via Bradford-based mass balance impossible.

To address this issue, new syringes equipped with appropriate Luer-lock fittings were tested (one glass and one plastic), using a more diluted immobilization solution (2× dilution, C_0 = 0.25

mg/mL), with the aim of developing a more robust process. While the Luer-lock fitting of both syringes resolved the issue of solution loss at the syringe–Whatman cell connection, the glass syringe—although not subject to deformation—exhibited leakage at the piston side (less tightly sealed than the plastic syringes), despite the diluted immobilization solution. In contrast, the Luer-lock plastic syringe (Omnifix) was successfully used without any deformation or solution loss.

This strategy, employing plastic syringes, was therefore adopted to investigate different flow rates (0.5 mL/h, 1 mL/h, and 1.5 mL/h), which were maintained constant throughout the immobilization process.

Annex V.S5 – Additional Results Obtained for Dead-end Flow Immobilization

Tab.V.S2 - Summary of the immobilization conditions (initial solution concentration and volume) used in the dead-end flow immobilization setup with 12M-PP membranes, along with the main characteristics of the membranes after immobilization (Experimental loading, loading-to-surface area ratio and immobilization yield). Note: A membrane surface area of 1.13 cm^2 (corresponding to a 12 mm diameter) was used to calculate the loading-to-surface area ratio.

	N°	C_0 [mg_{TsRTA}/mL]	Volume [mL]	Exp. Loading [mg_{TsRTA}]	Loading/Surface area [mg_{TsRTA}/ cm^2]	Immobilization yield [%]
12M-DF0.5	1	0.238	3.50	0.480	0.425	58
	2	0.258	3.50	0.169	0.150	19
	3	0.250	3.60	0.112	0.099	12
	4	0.269	3.60	0.296	0.262	31
12M-DF1	1	0.224	4.00	0.202	0.178	22
	2	0.235	4.20	0.176	0.156	18
	3	0.263	3.60	0.153	0.135	16
12M-DF1.5	1	0.235	4.50	0.093	0.082	9

The immobilization yield allows evaluation of the proportion of enzyme that was effectively immobilized relative to the amount initially exposed to the membrane. As it is calculated based on the exact volume and concentration of the immobilization solution used in each experiment, it serves as a reliable indicator for comparison between different conditions.

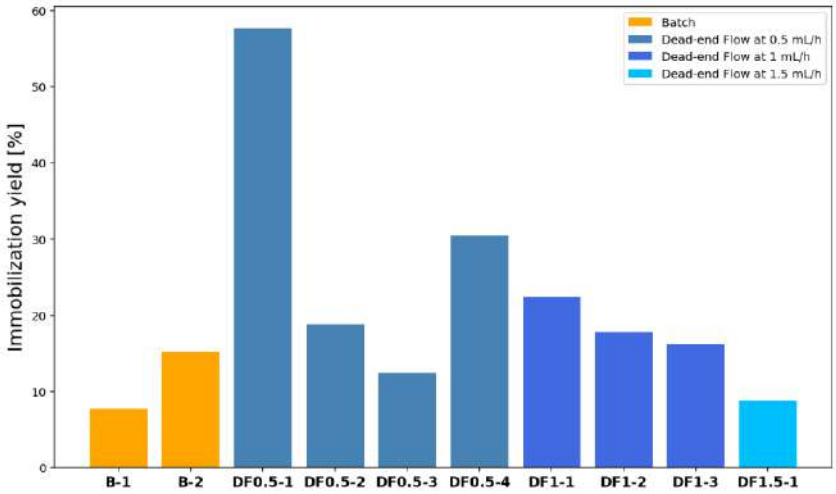

Fig.V.S5 - Immobilization yields obtained following batch and dead-end flow immobilization. All immobilizations were performed on 12 mm diameter membranes (pre-functionalized), using a TsRTA solution prepared in HEPES buffer (0.1 M, PLP 1 mM, pH 8) at a fixed concentration of 0.25 mg/mL. For flow-based immobilization, the solution volume ranged from 3.5 to 4 mL and was contained in Luer-lock plastic syringes (Omnifix). Three flow rates were investigated: 0.5 mL/h

(4 replicates), 1 mL/h (3 replicates), and 1.5 mL/h (1 replicate), referred to as 12M-DF0.5, 12M-DF1, and 12M-DF1.5, respectively. Error bars represent standard deviations, where applicable.

Tab.V.S3 - Loading per unit volume and per unit time obtained using batch and dead-endl flow immobilization strategies. All immobilizations were performed on 12 mm diameter membranes (pre-functionalized), using a TsRTA solution prepared in HEPES buffer (0.1 M, PLP 1 mM, pH 8) at a fixed concentration of 0.25 mg/mL. For flow-based immobilization, the solution volume ranged from 3.5 to 4 mL and was contained in Luer-lock plastic syringes (Omnifix). Three flow rates were investigated: 0.5 mL/h (4 replicates), 1 mL/h (3 replicates), and 1.5 mL/h (1 replicate), referred to as 12M-DF0.5, 12M-DF1, and 12M-DF1.5, respectively.

Membrane		Loading per unit of volume [mg/mL]	Loading per unit of time [mg/h]
Type of immobilization	N°		
12M-B	1	0.018	0.004
	2	0.037	0.008
12M-DF0.5	1	0.137	0.069
	2	0.048	0.024
	3	0.031	0.016
	4	0.082	0.041
12M-DF1	1	0.050	0.050
	2	0.042	0.042
	3	0.042	0.042
12M-DF1.5	1	0.021	0.031

Annex V.S6 - Evaluation of Compounds Loss and Mitigation Attempts

Adsorption tests : Evaluation and Mitigation

To evaluate whether FAP and FMBA could be subject to adsorption phenomena, the evolution of their concentrations was monitored over time under conditions similar to those of the catalytic test, but without a biocatalytic membrane and in a closed system to limit potential evaporation (i.e., a restricted gaseous environment). The syringe was used directly without pre-saturation. The results are presented in Fig.V.S6 (Left). Although this test was not conducted over a period as long as a typical catalytic experiment, a decrease in FAP concentration (blue) measured in the residual solution was observed, while FMBA concentration appeared to remain relatively stable over time. This progressive decrease in FAP concentration suggests adsorption of FAP from the aqueous solution onto the internal surface of the plastic syringe. As no stable FAP concentration was reached during the test, it can be assumed that - if the experiment been extended over a longer period - the FAP concentration would have continued to decline until reaching a potential adsorbed–soluble equilibrium.

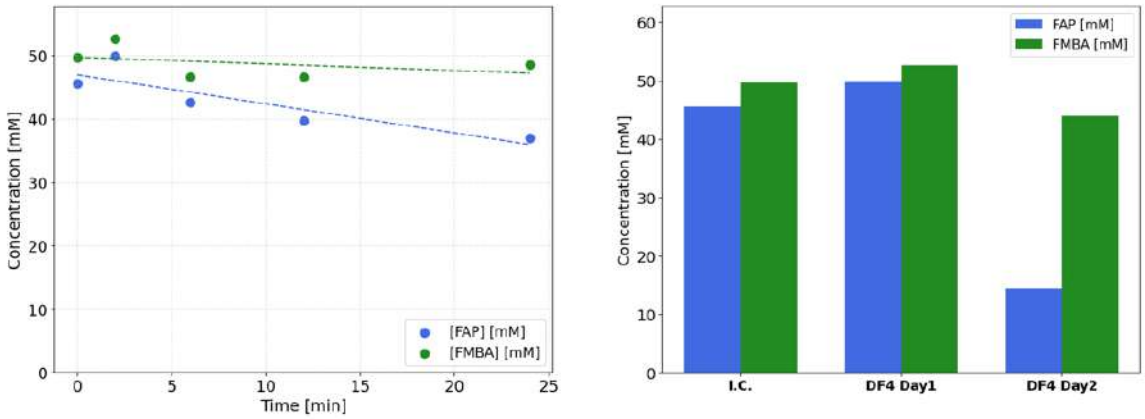

Fig.V.S6 – (Left) FAP (45 mM) and FMBA (50 mM) concentrations in a typical reaction mixture (in HEPES 0.1 M / PLP 1 mM, pH 8) over time. The experiment was performed using a non-saturated syringe at a flow rate of 4 mL/h, and residual solutions were collected in a closed tube. The concentration indicated at time 0 corresponds to the initial concentration (I.C.) of each compound, measured before starting the test, and represents the expected reference value. (Right) FAP (45 mM) and FMBA (50 mM) concentrations after 24 h in a typical reaction mixture (in HEPES 0.1 M / PLP 1 mM, pH 8). The experiment was performed using a non-saturated syringe at a flow rate of 4 mL/h, and residual solutions were collected in a closed tube. I.C. corresponds to the initial concentration measured before starting the test, representing the expected reference value.

To gain insight over a longer timescale, FAP and FMBA concentrations (in RM left in contact with the internal surface of a plastic syringe overnight) were measured after 24 h (Fig.V.S6 (right)). As expected, the FAP concentration continued to decrease, reaching a value approximately three times lower than the initial concentration. In contrast, FMBA concentration showed only a slight decrease. As dead-flow catalytic tests are performed over a timescale of a few hours, it can be reasonably assumed that FMBA adsorption is negligible—especially since FMBA is not expected to be significantly exposed to the internal surface of the plastic syringe. Therefore, the focus will be placed on solving FAP concentration decrease.

Syringe saturation with pure FAP was performed in an attempt to limit this decrease (observed after just a few minutes). To achieve this, the syringe was filled with FAP and left to rest overnight. The results are presented in Fig.V.S7. As this strategy appeared effective, it was subsequently chosen to perform syringe saturation prior to each catalytic test[33].

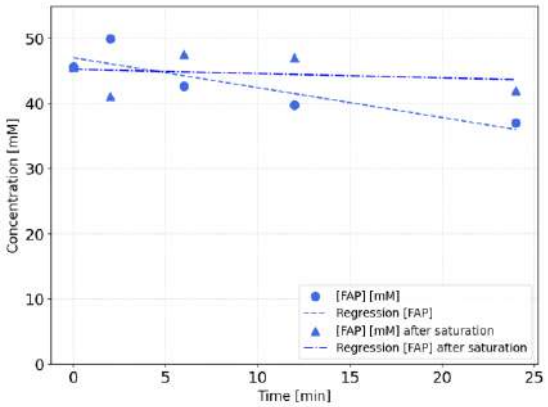

Fig.V.S7 - FAP (45 mM) concentrations with and without saturation in a typical reaction mixture (in HEPES 0.1 M / PLP 1 mM, pH 8) over time. The experiment was performed using a non-saturated syringe at a flow rate of 4 mL/h, and residual

[33] It should be noted, however, that this test was conducted over a shorter duration than a typical catalytic experiment.

solutions were collected in a closed tube. The concentration indicated at time 0 corresponds to the initial concentration (I.C.) of each compound, measured before starting the test, and represents the expected reference value.

Evaporation tests : Evaluation

In preliminary evaporation tests, the evaporation of FAP and FMBA was evaluated by comparing the concentrations of both compounds measured by GC with and without sample extraction (Tab.V.S4). The sample analyzed with GC extraction corresponds to the initial solution extracted into DCM, while the one analyzed without GC extraction corresponds to the same initial solution left in the aqueous phase. The results obtained without extraction suggest that FAP is more prone to evaporation than FMBA, whose evaporation appears negligible. The FAP concentration measured without sampling indicates that a portion of FAP in the aqueous phase evaporates according to the liquid–vapor equilibrium established between the aqueous solution and the dead-air volume in the vial. While this test supports the hypothesis that part of the FAP evaporates, it does not account for the specific experimental conditions associated with the actual catalytic test setup.

Tab.V.S4 - Concentrations of FAP and FMBA measured with and without GC sampling. The sample analyzed with GC sampling corresponds to the initial solution extracted into DCM, while the sample analyzed without GC sampling corresponds to the same initial solution left in the aqueous phase (not extracted). The target concentrations were 45 mM for FAP and 50 mM for FMBA, respectively.

	[FAP] [mM]	[FMBA] [mM]
With sampling	45.599	49.715
Without sampling	0.372	0.084

To evaluate whether the disappearance of FAP during catalytic tests truly results from evaporation, a secondary test was performed under conditions similar to the standard catalytic test but without the biocatalytic membrane. A syringe pre-saturated with FAP overnight was used to eliminate potential adsorption phenomena. In this test, two conditions were evaluated at different flow rates: the residual RM was either collected in an open tube (open system), as done in the catalytic test, or in a closed tube to reduce the gaseous environment and limit it to the dead-air volume of the tube (closed system). The results are presented in Fig.V.S8 (left). While FAP concentrations in the closed system appeared relatively stable, concentrations measured in the open system samples decreased proportionally with the selected flow rate.

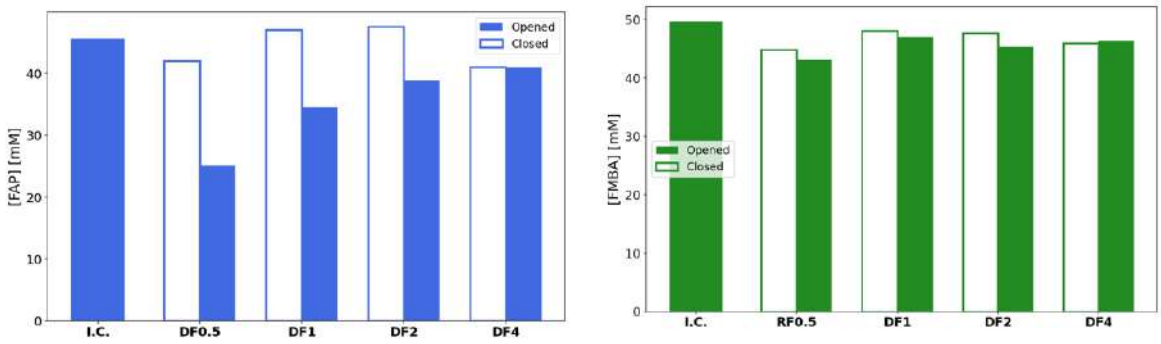

Fig.V.S8 - Evaporation test performed on RM containing 45 mM FAP (left) and 50 mM FMBA (right) (in HEPES 0.1 M / PLP 0.1 mM, pH 8), using a syringe pre-saturated with FAP overnight, following the same conditions as the catalytic test. Different flow rates were tested (0.5, 1, 2, and 4 mL/h) under two conditions: residual RM was collected either in an open tube (exposed to ambient air, as in the catalytic test) or in a closed tube (exposed only to the tube's internal dead-air volume). I.C. corresponds to the initial concentration measured before the start of the test, representing the expected reference value.

The decrease in FAP concentration in the open system suggests that a non-negligible fraction of FAP in the aqueous phase evaporated, with the liquid–vapor equilibrium likely shifting toward the vapor phase due to the significantly larger surrounding gas volume (room atmosphere) compared to the closed system. Additionally, the results suggest that FAP evaporation is more pronounced at lower flow rates, which is consistent with the evaporation hypothesis. Indeed, this observation is reasonable, the droplet forming at the syringe tip—particularly susceptible to evaporation due to its large liquid–air interface— takes longer to fall into the collection tube at lower flow rates (Tab.V.S5). Consequently, volatile FAP molecules in the aqueous phase have more time to evaporate before collection.

Tab.V.S5 - Time required for a droplet to form before falling into the tube as a function of the selected radial flow rate.

Flow rate [mL/h]	Drop forming time [s]
0.5	100
1	50
2	25
4	12

A similar test was performed to determine whether FMBA (the desired product) is also subject to evaporation and to ensure that the amount measured during catalytic tests accurately reflects the total FMBA produced by enzymatic activity. To do this, a defined concentration of 50 mM (contained in the standard RM) was analyzed using the same approach as for FAP. The results are presented in Fig.V.S8 (right). Since the concentrations obtained in both the open and closed systems were comparable to those of the initial solution across all investigated flow rates, it can be concluded that FMBA evaporation is negligible.

Annex V.S7 - Determination of Minimal Loading for Flow become Better Alternative to Batch Catalytic Test

Assuming that specific activity remains constant with respect to enzyme loading (at least within the experimental range) for flow processes, flow-based catalytic testing becomes more advantageous than batch processing when a sufficiently large quantity of enzyme is immobilized—the lower activity being offset by the higher enzyme amount. In this context, the theoretical determination of the minimum enzyme loading required for the flow process to outperform the batch catalytic test appears to be a relevant and meaningful approach.

A first approach, based on a regression line forced through the origin, provided an approximate value of 0.314 mg of TsRTA. In a second strategy, the theoretical quantity was directly determined from the experimental data using uncertainty propagation. This yielded a value of 0.367 ± 0.041 mg, which also falls within the range estimated by the calibration line. A average loading of 0.340 mg appear required to obtained a more efficient processes employing flow.

Theoretical Threshold Determination via Linear Regression

The constant specific activity suggests that the productivity of the catalyst investigated under flow conditions is linearly proportional to the amount of immobilized enzyme (Fig.V.S9).

Considering the most efficient membrane in the batch process (12M-B-4), and based on the linear regression determined using the experimental data from membranes 12M-DF0.5-1, 12M-DF0.5-2, and 12M-DF0.5-3 (Fig.V.S9), it can be estimated that a catalytic test under radial flow would

become more efficient than batch processes once the immobilized enzyme quantity exceeds approximately 0.314 mg.

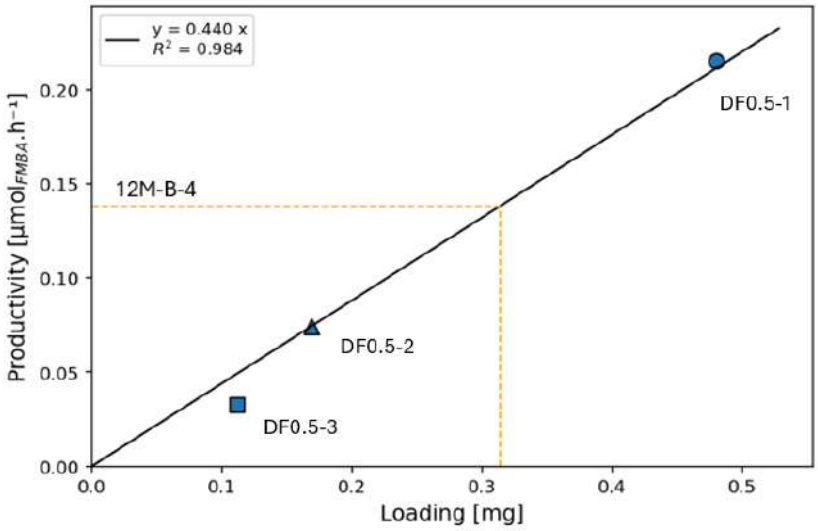

Fig.V.S9 - Productivity of three different membranes – expressed in in µmol/h- as a function of enzyme loading, obtained during catalytic tests performed in dead-end flow mode at 0.5 mL/h with classical RM (250 mM ISO, 25 mM FAP in HEPES buffer 0.1M, 1 mM PLP, pH 8). A linear regression constrained through the origin was used to estimate the minimum enzyme loading required for dead-end flow processes to outperform batch processes. The horizontal orange dashed line indicates the experimental productivity obtained from the most efficient batch catalytic test (12M-B-4). The vertical orange dashed line marks the theoretical amount of immobilized enzyme required for flow tests to exceed batch performance (for a 12 mm diameter membrane and a 0.5 mL/h radial flow). In this case, the theoretical value is 0.314 mg of TsRTA. Note: The slope of the linear curve corresponds to the specific activity.

Theoretical Threshold Determination Based on Average Enzyme Activity

By determining an average specific activity from the three membranes investigated under DF0.5 catalytic tests, the minimum amount of enzyme required to be immobilized for the flow process to become more productive than batch processes can be estimated using the productivity of the most efficient membrane in batch mode (12M-B-4). A minimum theoretical quantity of 0.367 mg (S.D. = 0.042 mg) was determined. The used formula and obtained data are presented in Eq.V.S1 and Tab.V.S6, respectively.

$$\bar{x} = \frac{x_{RF0.5-1} + x_{RF0.5-2} + x_{RF0.5-3}}{3} \quad with\ \sigma_x = \frac{\sqrt{\sigma_{RF0.5-1} + \sigma_{RF0.5-2} + \sigma_{RF0.5-3}}}{3}$$

$$y = \frac{P_B}{\bar{x}} \quad with\ \sigma_y = \frac{P_B \times \sigma_x}{\bar{x}^2}$$

Eq.V.S1 - Formula used to determine the theoretical minimum loading required for flow catalytic tests to outperform batch processes. $x_{RF0.5-i}$ and $\sigma_{RF0.5-i}$ correspond to the average and standard deviation, respectively, of the specific activity of the three membranes investigated in flow catalytic tests. P_B refers to the productivity of the most efficient membrane in the batch process (12M-B-4).

Tab.V.S6 - Recapitulative table of the various data used and results obtained to determine the theoretical minimum enzyme loading required for flow catalytic tests to outperform batch processes.

	Specific activity [µmol/(mg.min)]				Immobilized enzymes [mg]	
	Mean $(x_{RF0.5-i})$	S.D. $(\sigma_{RF0.5-i})$	Mean $(\bar{x})$	S.D. (σ_x)	Mean (y)	S.D. (σ_y)

12M-DF0.5-1 (0.480 mg)	0.0075	0.000231	0.0063	0.000708	0.3669	0.041387
12M-DF0.5-2 (0.169 mg)	0.0073	0.000049				
12M-DF0.5-3 (0.112 mg)	0.0041	0.002112				

Annex V.S8 – Specific Activity Obtained at Variable Flow Rates

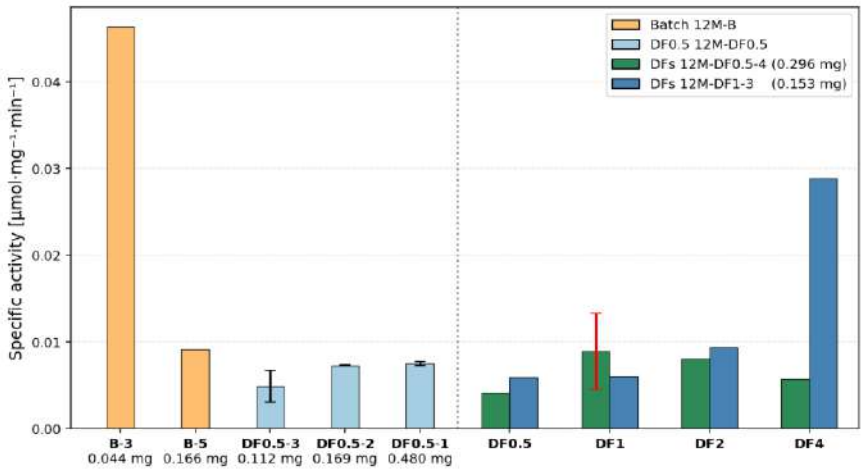

Fig.V.S10 - Specific activity obtained for 12M-DF0.5-4 and 12M-DF1-3 membranes investigated under different flow rates (0.5, 1, 2, and 4 mL/h) during catalytic tests. These values are compared to membranes used in batch mode that exhibited the highest and lowest specific activity (12M-B-3 and 12M-B-5, respectively), as well as membranes tested under a 0.5 mL/h flow rate (12M-DF0.5-1, 12M-DF0.5 -2, 12M-DF0.5 -3). Dark error bars represent the standard deviation from multiple samples collected at the same flow rate. Red error bars indicate the variability from triplicate extractions of a single sample, reflecting experimental error associated with the extraction process.

Annex V.S9 – Transaminase Deactivation at Room Temperature

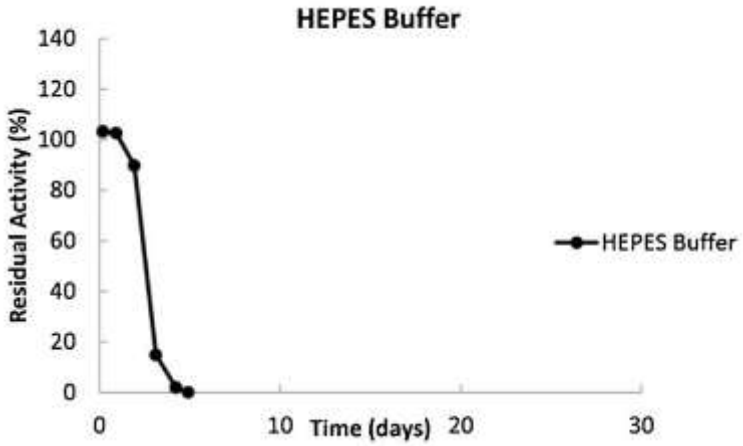

Fig.V.S11 - The storage stability at room temperature of Cv-ATA in HEPES buffer (50 mM, pH 8.2). From Chen et al.[222]

IX.5.3 Tangential Flow Processes Investigation

Annex V.S10 - Evaluation of FAP Evaporation and Adsorption Phenomenon

Evaluation of FAP Evaporation

While no experiments could be carried out to demonstrate that a significant part of the FAP loss was due to evaporation, it can be reasonably assumed given the results demonstrated in the dead-end flow experiments (Annex V.S6), particularly at 35 °C, the temperature of the catalytic tests.

Experimental Evaluation of Adsorption

While avoiding evaporation phenomena remains difficult—hindering the ability to exclusively evaluate potential FAP losses due to adsorption—one experiment highlighted that a portion of the FAP decrease was nevertheless attributable to adsorption within the system. Indeed, sample analyses taken at the inlet and outlet of the set-up at a given time revealed a difference in FAP concentration, at least during the first hour of RM recirculation (as it can be observed in saturation part of Fig.V.S12). As the only difference between the two samples lies in the path traveled through the system (with no contact with the gaseous environment), the lower FAP concentration measured at the end of the set-up (before returning to the RM reservoir) can thus be attributed to adsorption phenomena.

Strategy to Prevent FAP Depletion in Flow catalytic system

The rapid and significant disappearance of FAP can be problematic if its concentration drops below the threshold required for optimal enzymatic activity (~ 10 mM FAP). While preventing evaporation appears challenging, a saturation of the system is performed prior to catalytic testing in an attempt to at least limit adsorption phenomena. During the saturation step, a reaction mixture (RM) containing an excess of FAP (250 mM ISO and ~125 mM FAP) is recirculated through the system—equipped with a non-immobilized membrane—for 90 to 180 minutes. After this saturation phase, the solution is replaced with the typical RM used during catalytic tests (250 mM ISO, 25 mM FAP in HEPES/PLP buffer). The corresponding results are shown in Fig.V.S12.

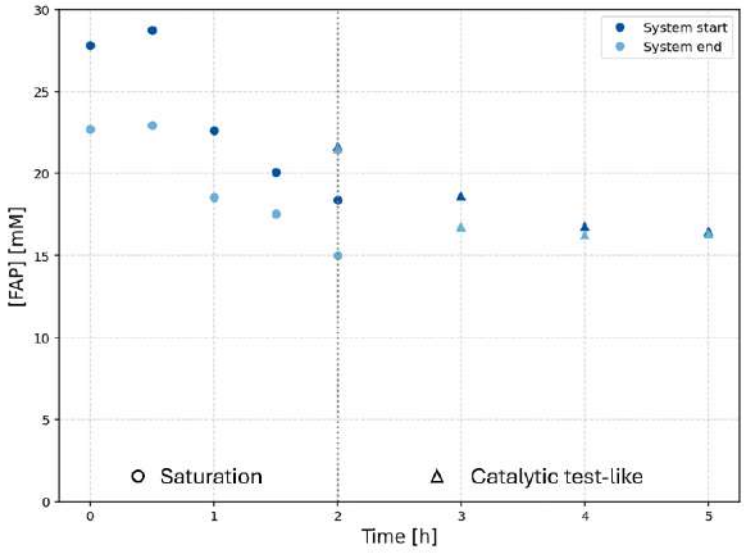

Fig.V.S12 - FAP concentration over time when a saturation mitigation strategy is applied prior to the catalytic test. During the saturation step, 100 mL of RM containing approximately 125 mM of FAP was recirculated for 2 hours in Set-up 1 containing a non-functionalized membrane (at 150 mL/min). A catalytic test-like procedure was then performed by recirculating a typical RM (250 mM ISO, 25 mM FAP in HEPES/PLP) under the same conditions as the catalytic test for 3 hours.

By performing such a strategy, the FAP concentration appears to stabilize at approximately 15 mM—at least during the first 3 hours following the saturation step. Accordingly, the same

approach will be applied in subsequent catalytic test experiments; however, the non-functionalized membrane used during the saturation step will be replaced by a membrane with immobilized enzymes simultaneously with the RM replacement. In this approach, it will be assumed that the FAP concentration remains above the minimum threshold required for optimal enzymatic activity throughout the catalytic test.

Annex V.S11 - Evaluation of the Flow Rates on Catalytic Performance : Specific Activity Over Time

Concerning the non-corrected values shown in Fig.V.S13, the observed decrease in SA at 50 and 300 mL/min does not accurately reflect enzymatic activity, as a measurable FMBA concentration is already present before recirculation begins. The apparent decrease thus results from the passage of time while FMBA concentration remains relatively stable. Only SA values calculated from corrected FMBA concentrations are therefore relevant, as they account for product formation truly attributable to enzymatic activity. Considering the corrected values, SA appears relatively stable over the first hours of the catalytic test for 44M-B-3 (50 mL/min)—considering only values obtained after 3 hours. In the case of TF300, neither corrected SA could be determined, as the FMBA concentration in the initial RM (used as a blank) was higher than that measured during the first 3 hours of the catalytic test. However, even the corrected values remain difficult to exploit, as analyses were conducted over a short time frame, resulting in limited conversion and product formation. Consequently, the calculations are highly dependent on the initial solution concentration, which itself is subject to considerable variability.

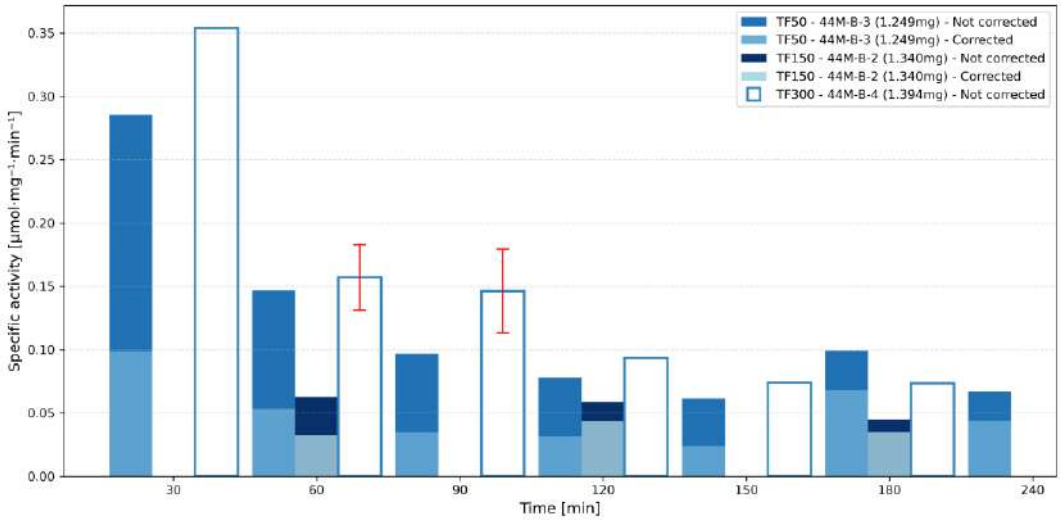

Fig.V.S13 - Specific activity obtained when different flow rates was investigated during the first hours of catalytic tests. 100 mL of RM (maintained at 35 °C) was recirculated at various flow rates: 50 mL/min (4 h), 150 mL/min (3 h), and 300 mL/min (4 h). Dark bars represent values directly calculated from GC measurements, while lighter bars indicate corrected values obtained by subtracting the concentration measured under initial conditions. When available for a given process, measured and corrected values are plotted together, both starting from the baseline value. Red error bars correspond to the standard deviation from multiple extractions of the same sample. Note: Triplicate GC analyses of the same sample were also performed to assess GC variability; in this case, the average value was reported.

Annex V.S12 - Additional Leaching Tests

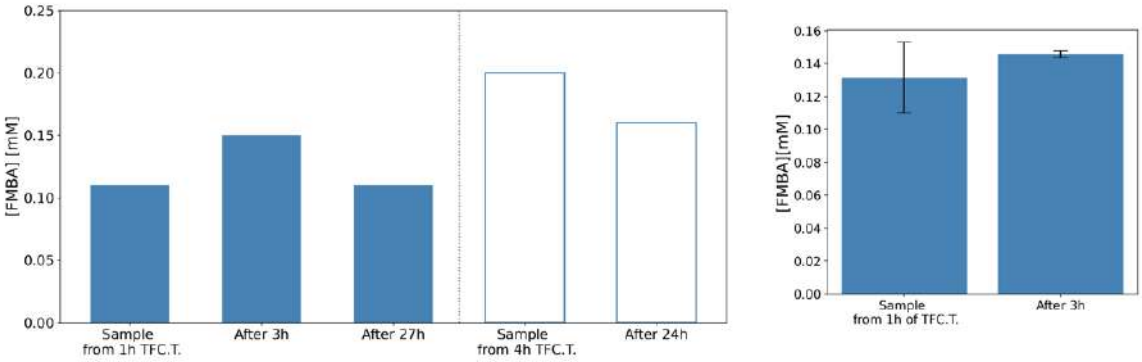

Figs.V.S14 – (Left) Leaching test inspired by the "hot filtration test" applied to sample solutions from the tangential flow catalytic test performed on 44M-B-3 (1.249 mg) (in set-up 1 at 50 mL/min), harvested after 1 h and 4 h of RM recirculation. Sample solutions were maintained at 35 °C under gentle stirring in a round-bottom flask. In the case of the sample taken after 1 h, analyses were performed after 3 h and 27 h of incubation. For the sample collected after 4 h, analysis was conducted after 24 h. Values shown are non-corrected. (Right) Leaching test inspired by the "hot filtration test" applied to a sample solution from the tangential flow catalytic test performed on 44M-B-4 (1.394 mg) (in set-up 1 at 300 mL/min), harvested after 1 h of RM recirculation. The sample solution was maintained at 35 °C under gentle stirring in a round-bottom flask. Analysis was performed after 3 h of incubation. Values shown are non-corrected.

IX.5.4 Variability due to Analytical Error

Annex VI.S1 - Variability due to Extraction and GC Analysis

A non-negligible analytical error arises from both extraction and GC analysis variability. Fig.VI.S1 shows a relatively large variation in the measured (non-corrected) values. While it is difficult to identify a clear pattern explaining this variation, it can be confidently stated that a significant portion of the variability is primarily due to the extraction step, which can exhibit considerable error (up to a 22% coefficient of variation). Indeed, for a single identical sample, the coefficient of variation resulting from three extractions is consistently higher than that observed from triplicate GC analyses. Excluding the results obtained for 44M-B-6, it can be estimated that GC analysis alone contributes a maximum variability of approximately 3% (coefficient of variation).

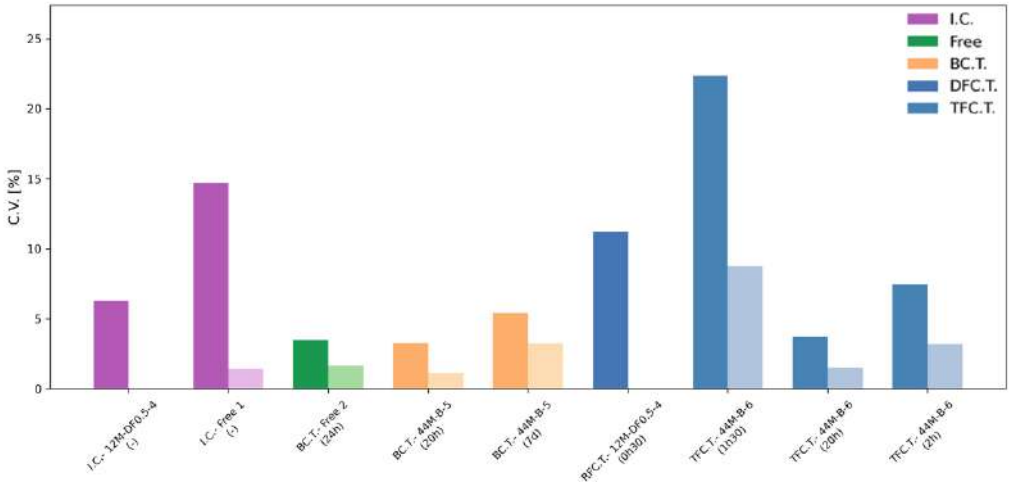

Fig.VI.S1- Evaluation of variability (expressed as coefficient of variation) due to extraction and GC analysis on the measured concentration of FMBA. Dark and light colors correspond to the coefficient of variation for extraction and GC

analysis, respectively. BC.T., DFC.T., and TFC.T. refer to batch, dead-end flow, and tangential-flow catalytic tests, respectively.

Annex VI.S2 - Variability of Initial Condition and Corrected Value

While the FMBA concentration measured in the initial RM should be null—given that the reaction is very slow and no catalyst is yet present—a variable amount is consistently detected by GC analysis. This value ranges from 0.024 to 0.860 mM, with an average measured concentration of 0.160 mM. [34]

To estimate the amount of chiral product (FMBA) that can be genuinely attributed to enzymatic activity, the FMBA concentration measured in the initial RM is typically subtracted from the values obtained during the catalytic test. However, applying this correction can introduce significant variability due to error propagation. Indeed, FMBA concentrations measured after a specific catalytic time already exhibit variability caused by both the extraction and GC analysis steps (the latter being itself influenced by extraction efficiency (see Annex VI.S*1*). By subtracting an initial value that is also subject to such variability (Annex VI.S2Fig.VI.S2 illustrates the potential magnitude of this variability, specifically due to the extraction and GC analysis of FMBA in the initial RM), the propagated error can become substantial.

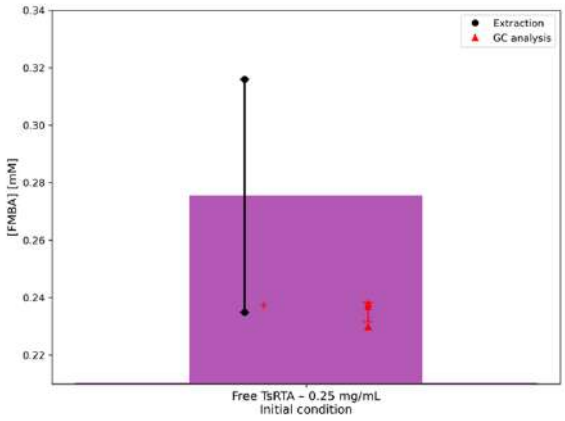

Fig.VI.S2 - Representation of variability in FMBA concentration [mM] measured in the initial RM (before starting the catalytic test), due to extraction (indicated by dark error bars) and GC analysis (indicated by red error bars).

While corrected values are scientifically more accurate, they are subject to greater variability—particularly problematic when low FMBA concentrations are analyzed (early stages of the catalytic test). Therefore, to obtain more robust, interpretable, and exploitable results, it is recommended to consider performance indicators (SA, productivity, STY, FMBA yield, etc.) based on corrected values from long-term sampling—when FMBA concentrations are higher.

[34] Several tests were conducted to determine whether this initial detection could result from contaminated vessels or magnetic stir bars. However, none of these tests—performed using only HEPES buffer—showed any detectable FMBA.

Transaminases Immobilized on a Membrane Reactor for the Production of Chiral Amine

By Basile Bredun

Compared to conventional chemical routes, biocatalysis appears to be a more sustainable approach for producing enantiopure chiral amines, essential components of active pharmaceutical ingredients (APIs). Enzymes, particularly transaminases (TAs), are attractive catalysts as they offer several promising pathways for the synthesis of chiral amines with excellent enantioselectivity under mild conditions. Asymmetric synthesis is especially relevant, enabling the production of chiral amines from keto precursors using inexpensive and readily available amino donors. However, challenges such as unfavorable reaction equilibria and poor enzyme stability still limit the development of this strategy into a truly productive industrial alternative. Thus, strategies are required to mitigate these two major issues. Among them, TA immobilization on membranes appears promising, as it can enhance enzyme stability while simultaneously allowing the membrane to act as a one-pot biocatalytic and separation unit—a powerful approach to address thermodynamic limitations. In particular, integrating such biocatalytic membranes with continuous flow processes has the potential to intensify the process and thereby improve chiral amine production. Continuous substrate feeding and product removal can further enhance enzymatic performance. In this context, this work aims to demonstrate the influence of flow process implementation on (i) biocatalytic membrane preparation, (ii) catalytic performance, and (iii) membrane robustness compared to a conventional batch reactor, as a first step toward more advanced processes involving membrane-based separations. Specifically, the effect of flow rate on membrane preparation and enzymatic performance was investigated.

Dead-end flow mode was employed to optimize biocatalytic membrane preparation via covalent immobilization on functionalized polypropylene membranes. Dead-end flow demonstrated improved TA immobilization compared to batch methods, particularly at lower flow rates. Following membrane preparation, asymmetric synthesis targeting the conversion of 2'-fluoroacetophenone (FAP) into (R)-fluoromethylbenzylamine (R-FMBA) using isopropylamine as the amino donor was evaluated under both dead-end and recirculating tangential-flow conditions. In dead-end mode, FMBA production was improved relative to batch when high enzyme loadings were immobilized. Catalytic tests under tangential flow showed similar performance to batch, confirming the relevance of this configuration for integration with membrane separation processes. Finally, the robustness of TA-immobilized membranes under both dead-end and tangential flow conditions was successfully demonstrated through leaching tests.

Building on these results, the successful implementation of flow processes paves the way for more sophisticated membrane–separator systems, which could further enhance chiral amine production.

UNIVERSITÉ CATHOLIQUE DE LOUVAIN
Faculté des bioingénieurs
Croix du Sud, 2 bte L7.05.01, 1348 Louvain-la-Neuve, Belgique | **www.uclouvain.be/agro**